

ornl

**OAK
RIDGE
NATIONAL
LABORATORY**

**UNION
CARBIDE**

NUREG/CR-2525, Vol. 4
ORNL/NUREG/TM-407/V4

ORNL Rod Bundle Heat Transfer Test Data

**Volume 4. ORNL Small Break LOCA
Heat Transfer Test Series II:
Experimental Data Report**

T. M. Anklam

D. F. Hunt	A. G. Sutton
D. K. Felde	S. S. Gould
M. S. Thompson	C. R. Hyman

Prepared for the U.S. Nuclear Regulatory Commission
Office of Nuclear Regulatory Research
Under Interagency Agreements DOE 40-551-75 and 40-552-75

8208260087 820731
PDR NUREC
CR-2525 R PDR

**OPERATED BY
UNION CARBIDE CORPORATION
FOR THE UNITED STATES
DEPARTMENT OF ENERGY**

Printed in the United States of America. Available from
National Technical Information Service
U.S. Department of Commerce
5285 Port Royal Road, Springfield, Virginia 22161

Available from
GPO Sales Program
Division of Technical Information and Document Control
U.S. Nuclear Regulatory Commission
Washington, D.C. 20555

This report was prepared as an account of work sponsored by an agency of the United States Government. Neither the United States Government nor any agency thereof, nor any of their employees, makes any warranty, express or implied, or assumes any legal liability or responsibility for the accuracy, completeness, or usefulness of any information, apparatus, product, or process disclosed, or represents that its use would not infringe privately owned rights. Reference herein to any specific commercial product, process, or service by trade name, trademark, manufacturer, or otherwise, does not necessarily constitute or imply its endorsement, recommendation, or favoring by the United States Government or any agency thereof. The views and opinions of authors expressed herein do not necessarily state or reflect those of the United States Government or any agency thereof.

NUREG/CR-2525, Vol. 4
ORNL/NUREG/TM-407/V4
Dist. Category R2

Contract No. W-7405-eng-26

Engineering Technology Division

ORNL ROD BUNDLE HEAT TRANSFER TEST DATA

VOLUME 4. ORNL SMALL BREAK LOCA HEAT TRANSFER
TEST SERIES II: EXPERIMENTAL DATA REPORT

T. M. Anklam M. S. Thompson
D. F. Hunt A. G. Sutton
D. K. Felde S. S. Gould
 C. R. Hyman

Manuscript Completed - May 26, 1982
Date Published - June 1982

Prepared for the
U.S. Nuclear Regulatory Commission
Office of Nuclear Regulatory Research
Under Interagency Agreements 40-551-75 and 40-552-75

NRC Fin No. B0125

Prepared by
OAK RIDGE NATIONAL LABORATORY
Oak Ridge, Tennessee 37830
operated by
UNION CARBIDE CORPORATION
for the
DEPARTMENT OF ENERGY

CONTENTS

	<u>Page</u>
ACKNOWLEDGMENTS	v
ABSTRACT	1
1. INTRODUCTION	1
2. FACILITY DESCRIPTION	6
2.1 Flow Circuit Description	6
2.2 Bundle Description	11
2.3 Differential Pressure Instrumentation	15
2.4 Summary	15
3. EXPERIMENTAL PROCEDURES	19
3.1 Quasi-Steady-State Heat Transfer and Mixture Level Swell Testing	19
3.2 High-Pressure Reflood Testing	19
3.3 Bundle Boiloff Testing	20
4. PRESENTATION OF DATA	21
4.1 Instrument Description and Status	21
4.2 Quasi-Steady-State Data	22
4.3 Transient Reflood and Boiloff Data	22
4.4 Instrument Uncertainty	22
REFERENCES	27
APPENDIX A. INSTRUMENT UNCERTAINTY ANALYSIS FOR THE THTF LOOP ...	29
APPENDIX B. CALCULATED MASS FLOWS	87
APPENDIX C. CALCULATED FUEL ROD SIMULATOR POWER LEVELS (appears on microfiche at the end of this report)	
APPENDIX D. QUASI-STEADY-STATE DATA IN ENGLISH ENGINEERING UNITS (appears on microfiche at the end of this report)	

ACKNOWLEDGMENTS

In the conduct of a large experimental and analytical program, there are always a great many individuals whose contributions should be recognized. The dedicated efforts of the entire Blowdown Heat Transfer program staff are reflected in this report. The authors express their appreciation to the following personnel:

M. C. Adair	G. S. Mailen	R. D. Stulting
J. L. Bartley	C. B. Mullins	H. E. Trammell
W. G. Craddick	D. G. Morris	B. J. Veazie
D. H. Cook	L. J. Ott	J. D. White
R. D. Dabbs	H. R. Payne	M. D. White
D. J. Fraysier	W. Ragan, Jr.	J. E. Wolfe
H. W. Hoffman	J. E. Robinson	G. L. Yoder

ORNL ROD BUNDLE HEAT TRANSFER TEST DATA

VOLUME 4. ORNL SMALL BREAK LOCA HEAT TRANSFER
TEST SERIES II: EXPERIMENTAL DATA REPORT

T. M. Anklam M. S. Thompson
D. F. Hunt A. G. Sutton
D. K. Felde S. S. Gould
 C. R. Hyman

ABSTRACT

This report presents experimental data and calculated steady-state and transient instrument uncertainties from the Oak Ridge National Laboratory Small Break LOCA Heat Transfer Test Series II. The subject test series was composed of six combined heat transfer and mixture level swell tests, six additional mixture level swell tests, five high-pressure reflood tests, and five high-pressure boiloff tests. Also, the data and uncertainties are reported from two supplemental mixture level swell tests that were not part of Test Series II. Calculated inlet and outlet mass flows and fuel rod simulator power levels are reported in the report appendices.

1. INTRODUCTION

Under sponsorship of the U.S. Nuclear Regulatory Commission, Oak Ridge National Laboratory (ORNL) has experimentally investigated rod bundle thermal hydraulics under conditions similar to those expected in a small break loss of coolant accident (LOCA). Two major test series have been run. The first test series, run in January 1980, consisted of six quasi-steady-state uncovered bundle heat transfer and mixture level swell tests and six high-pressure reflood tests.¹⁻⁴ After extensive test facility upgrading, the second test series was run in November 1980. The second series consisted of six uncovered bundle heat transfer tests, twelve high-pressure mixture level swell tests, five high-pressure reflood tests, and five high-pressure bundle boiloff tests. This report presents experimental data from the second test series (Tests 3.09.10I-X and 3.09.10AA-FF)^{5,6} and from two supplemental mixture level swell tests (3.09.10GG and HH). In addition to the experimental data, calculated mass flows and rod power levels are presented for each test in Appendices B and C, respectively.* It is expected that data will be of use primarily in the development of new heat transfer and void fraction correlations and in the validation of existing correlations and computer codes.

*Appendix C appears on microfiche.

All of the experimental testing was performed in the Thermal-Hydraulic Test Facility (THTF) at ORNL. The THTF is a high-pressure thermal-hydraulic loop containing an electrically heated 64-rod bundle. The THTF rod bundle power profile is uniform, both axially and radially, and rod diameter and pitch are typical of a 17 x 17 pressurized-water-reactor fuel assembly. Test matrices for the heat transfer, mixture swell, reflood, boiloff, and supplemental tests appear in Tables 1-5, respectively.

The matrices are self-explanatory with the exception of two points. First, it should be noted that Tests 3.09.10I-N were suitable for both heat transfer and mixture level swell analysis. Thus, the first six tests in Table 2 are identical to those in Table 1. The second point concerns the supplemental tests. These tests were mixture swell tests that were unsuitable for rigorous analysis. Test 3.09.10GG was unsuitable because the test section mass flow could not be computed. All inlet flow instrumentation was underranged, and fluid thermometry at the outlet indicated that liquid was probably being discharged from the test section outlet. Because the outlet flow may have been two phase, the outlet density was indeterminate, and thus the outlet mass flow could not be computed. Test 3.09.10HH was unsuitable because the two-phase mixture level was above the end of the heated length. As such, its position was indeterminate, and, thus, mixture level swell could not be computed. Despite these limitations, the data are of good quality and may be useful to future investigators. Therefore, data from Tests 3.09.10GG and 3.09.10HH have been included in this report.

Table 1. Uncovered bundle heat transfer test matrix^a

Test	System pressure [MPa (psia)]	Linear power/rod [kW/m (kW/ft)]	Mass flux [kg/m ² s (lb _m /h ft ²) x 10 ⁻⁴]	Mixture level [m (ft)]
3.09.10I	4.5 (650)	2.22 (0.68)	29.7 (2.19)	2.62 ± 0.04 (8.60 ± 0.13)
3.09.10J	4.2 (610)	1.07 (0.33)	12.7 (0.94)	2.47 ± 0.04 (8.10 ± 0.14)
3.09.10K	4.0 (580)	0.32 (0.10)	3.1 (0.23)	2.13 ± 0.30 (6.98 ± 0.98)
3.09.10L	7.5 (1090)	2.17 (0.66)	29.1 (2.15)	2.75 ± 0.09 (9.02 ± 0.29)
3.09.10M	7.0 (1010)	1.02 (0.31)	12.6 (0.93)	2.62 ± 0.04 (8.60 ± 0.13)
3.09.10N	7.1 (1030)	0.47 (0.14)	4.6 (0.34)	2.13 ± 0.03 (6.98 ± 0.98)

^aNumbers in this table have been rounded off, and thus unit conversions may not appear to be exact.

Table 2. Mixture level swell test matrix^a

Test	System pressure [MPa (psia)]	Linear power/rod [kW/m (kW/ft)]	Vapor ^b superficial velocity at mixture level [m/s (ft/s)]	Mixture level [m (ft)]	Collapsed ^c liquid level [m (ft)]
3.09.10I	4.50 (650)	2.22 (0.68)	1.30 ± 0.04 (4.25 ± 0.13)	2.62 ± 0.04 (8.60 ± 0.13)	1.34 ± 0.03 (4.39 ± 0.1)
3.09.10J	4.20 (610)	1.07 (0.33)	0.61 ± 0.02 (1.99 ± 0.07)	2.47 ± 0.04 (8.10 ± 0.14)	1.62 ± 0.03 (5.31 ± 0.1)
3.09.10K	4.01 (580)	0.32 (0.10)	0.15 ± 0.02 (0.50 ± 0.05)	2.13 ± 0.30 (6.98 ± 0.98)	1.62 ± 0.03 (5.31 ± 0.1)
3.09.10L	7.52 (1090)	2.17 (0.66)	0.73 ± 0.02 (2.39 ± 0.06)	2.75 ± 0.09 (9.02 ± 0.29)	1.76 ± 0.03 (5.77 ± 0.1)
3.09.10M	6.96 (1010)	1.02 (0.31)	0.37 ± 0.01 (1.20 ± 0.03)	2.62 ± 0.04 (8.60 ± 0.13)	1.89 ± 0.03 (6.20 ± 0.1)
3.09.10N	7.08 (1030)	0.47 (0.14)	0.12 ± 0.01 (0.40 ± 0.04)	2.13 ± 0.03 (6.98 ± 0.98)	1.86 ± 0.03 (6.10 ± 0.1)
3.09.10AA	4.04 (590)	1.27 (0.39)	1.04 ± 0.03 (3.40 ± 0.10)	3.42 ± 0.03 (11.23 ± 0.09)	2.00 ± 0.03 (6.56 ± 0.1)
3.09.10BB	3.86 (560)	0.64 (0.20)	0.48 ± 0.02 (1.59 ± 0.07)	3.31 ± 0.04 (10.85 ± 0.12)	2.32 ± 0.03 (7.61 ± 0.1)
3.09.10CC	3.59 (520)	0.33 (0.10)	0.40 ± 0.02 (1.31 ± 0.07)	3.60 ± 0.02 (11.80 ± 0.08)	2.88 ± 0.03 (9.45 ± 0.1)
3.09.10DD	8.09 (1170)	1.29 (0.39)	0.46 ± 0.01 (1.50 ± 0.03)	3.23 ± 0.04 (10.61 ± 0.13)	2.39 ± 0.03 (7.84 ± 0.1)
3.09.10EE	7.71 (1120)	0.64 (0.19)	0.27 ± 0.01 (0.88 ± 0.03)	3.47 ± 0.03 (11.40 ± 0.08)	2.85 ± 0.03 (9.35 ± 0.1)
3.09.10FF	7.53 (1090)	0.32 (0.98)	0.12 ± 0.01 (0.40 ± 0.03)	3.23 ± 0.04 (10.61 ± 0.13)	2.90 ± 0.03 (9.51 ± 0.1)

^aSome rounding off of numbers has been done. Accordingly, conversions between metric and English and the value of mixture level swell may not appear to be exact.

^bDefined as the total core volumetric vapor generation rate/unit flow area.

^cHydrostatic head of test section liquid inventory.

Table 3. Reflood test matrix

Test	Series	Initial pressure [MPa (psia)]	Flooding velocity [cm/s (in./s)]	Linear heat rate [kW/m (kW/ft)]
3.09.100	II	3.88 (563)	12.2 (4.8)	2.03 (0.62)
3.09.10P	II	4.28 (621)	9.2 (3.6)	0.997 (0.30)
3.09.10Q	II	3.95 (573)	5.9 (2.3)	1.02 (0.31)
3.09.10R	II	7.34 (1065)	11.7 (4.6)	2.16 (0.66)
3.09.10S	II	7.53 (1092)	10.2 (4.0)	1.38 (0.42)

Table 4. Bundle boiloff test matrix

Test	Duration (s)	Linear heat rate [kW/m-rod (kW/ft-rod)]	Depressurization rate [kPa/s (psi/s)]	Pressure range [MPa (psia)]	Core height uncovered (%) (100% = 3.66 m)	Peak rod surface temp. [K (°F)]
3.09.10T	200	0.951 (0.29)	-11.58 (-1.68)	5.93-3.72 (860-540)	75	1088 (1500)
3.09.10U	65	1.94 (0.59)	-33.44 (-4.85)	8.14-5.86 (1180-850)	91	994 (1330)
3.09.10V	135	0.656 (0.20) ^a	-17.79 (-2.58)	7.79-5.52 (1130-800)	64	819 (1015)
3.09.10W	96	0.623 (0.19) ^b	-21.72 (-3.15)	7.86-5.86 (1140-850)	42	705 (810)
3.09.10X	470	0.623 (0.19)	-0.765 (-0.111)	8.56-8.21 (1242-1190)	75	1112 (1542)

^aThis test experienced a power reduction to 0.56 kW/m-rod (0.17 kW/ft-rod) at 47 s.

^bThis test experienced a power reduction to 0.33 kW/m-rod (0.10 kW/ft-rod) at 12 s.

Table 5. Test conditions for supplemental tests^a

Test	Pressure [MPa (psia)]	Linear power/rod [kW/m (kW/ft)]	Mass flux ^b [kg/m ² s (lb _m /h ft ²) x 10 ⁻⁴]	Mixture level [m (ft)]
3.09.10GG	4.04 (586)	1.89 (0.58)	32.5 (24.0)	3.54 ± 0.04 (11.61 ± 0.13)
3.09.10HH	8.05 (1167)	1.92 (0.59)	32.9 (24.2)	>3.66 (>12.00)

^aNumbers have been rounded off; thus, unit conversions may not appear exact.

^bMass flux based on outlet volumetric flow and saturated vapor density. Should be used with caution because two-phase conditions may have existed at outlet.

2. FACILITY DESCRIPTION

Experimental testing was performed at ORNL in the THTF. The THTF is a large, high-pressure, nonnuclear thermal-hydraulic loop. System configuration was designed to produce a thermal-hydraulic environment similar to that expected in a small break LOCA.

2.1 Flow Circuit Description

Figure 1 is an illustration of the THTF in small break test configuration, and Fig. 2 is a simplified instrument application diagram for the loop. Flow leaves the main coolant pump and passes through FE-3, a 2-in. turbine meter. Upon leaving FE-3, flow enters the inlet flow manifold; the flow manifold is divided into two parallel flow lines: a 1/2-in. line used to meter very low flow rates and a 3/4-in. flooding line used for the higher flows experienced during reflood. The entire inlet flow manifold was constructed of high-pressure stainless steel tubing. Volumetric flow rates in the low flow 1/2-in. inlet line were measured by FE-18A (a low-flow orifice meter), FE-250, and FE-260 (1/2-in. turbine meters). The two inlet lines converge at the injection manifold from which fluid passes directly into the lower plenum. Fluid does not pass through a downcomer. Flow proceeds upward through the heated bundle and exits through the bundle outlet spool piece. Spool piece measurements include pressure, temperature, density, volumetric flow, and momentum flux. At very low outlet flow rates, the volumetric flow was measured by a bank of low flow orifice meters downstream of the outlet spool piece. Upon leaving the orifice manifold, flow passed through a heat exchanger and returned to the pump inlet.

System pressure was controlled via the loop pressurizer. The pressurizer was partially filled with subcooled water, and nitrogen cover gas was used to control pressure. By filling or venting nitrogen, the system pressure could be controlled more easily than by the conventional flashing and condensation of saturated water and steam.

As noted, flow was injected directly into the lower plenum and did not pass through a downcomer. The shroud plenum annulus (Fig. 3) was used in earlier THTF testing as an internal downcomer but was isolated from the primary flow circuit in these tests. The shroud plenum annulus pressure was equalized with the system pressure. This was accomplished by connecting the bottom of the annulus region to the pressurizer surge line and the top of the annulus to the test section outlet. The line between the annulus and pressurizer was opened, and the line between the annulus and test section outlet was closed during the initial boiloff phase of steady-state testing. This allowed any vapor generated by boiling in the annulus to displace liquid in the pressurizer. Note that the displacement of liquid will cause the mixture levels in the downcomer and bundle to equalize. This is why it was advantageous to install a line between the pressurizer and downcomer. However, once mixture levels had equalized, it was no longer advantageous to leave this line open because the steam flow through the outlet causes a substantial pressure drop between the test section and pressurizer. If the annulus was in communication with the pressurizer,

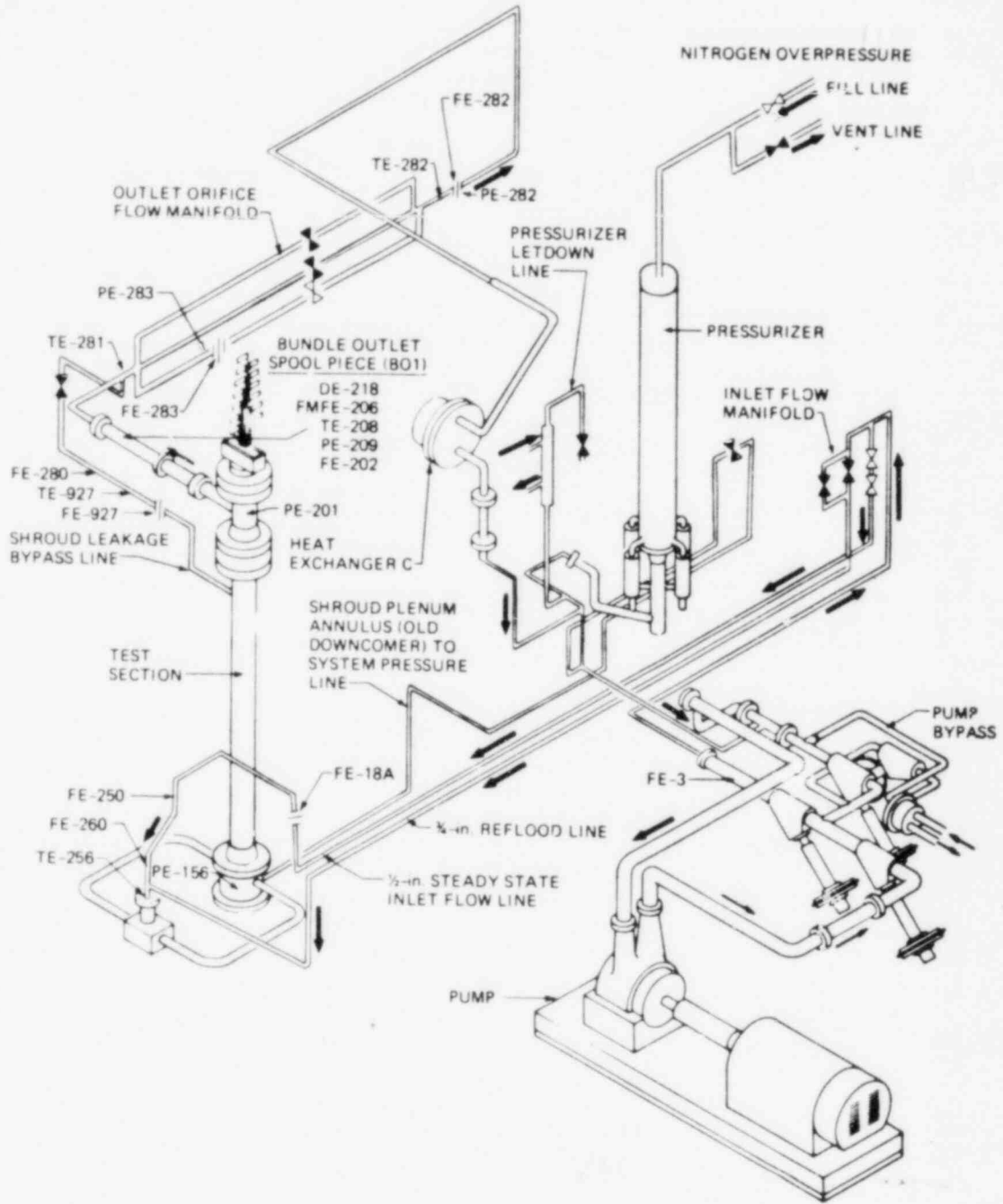


Fig. 1. THTF in small break test configuration.

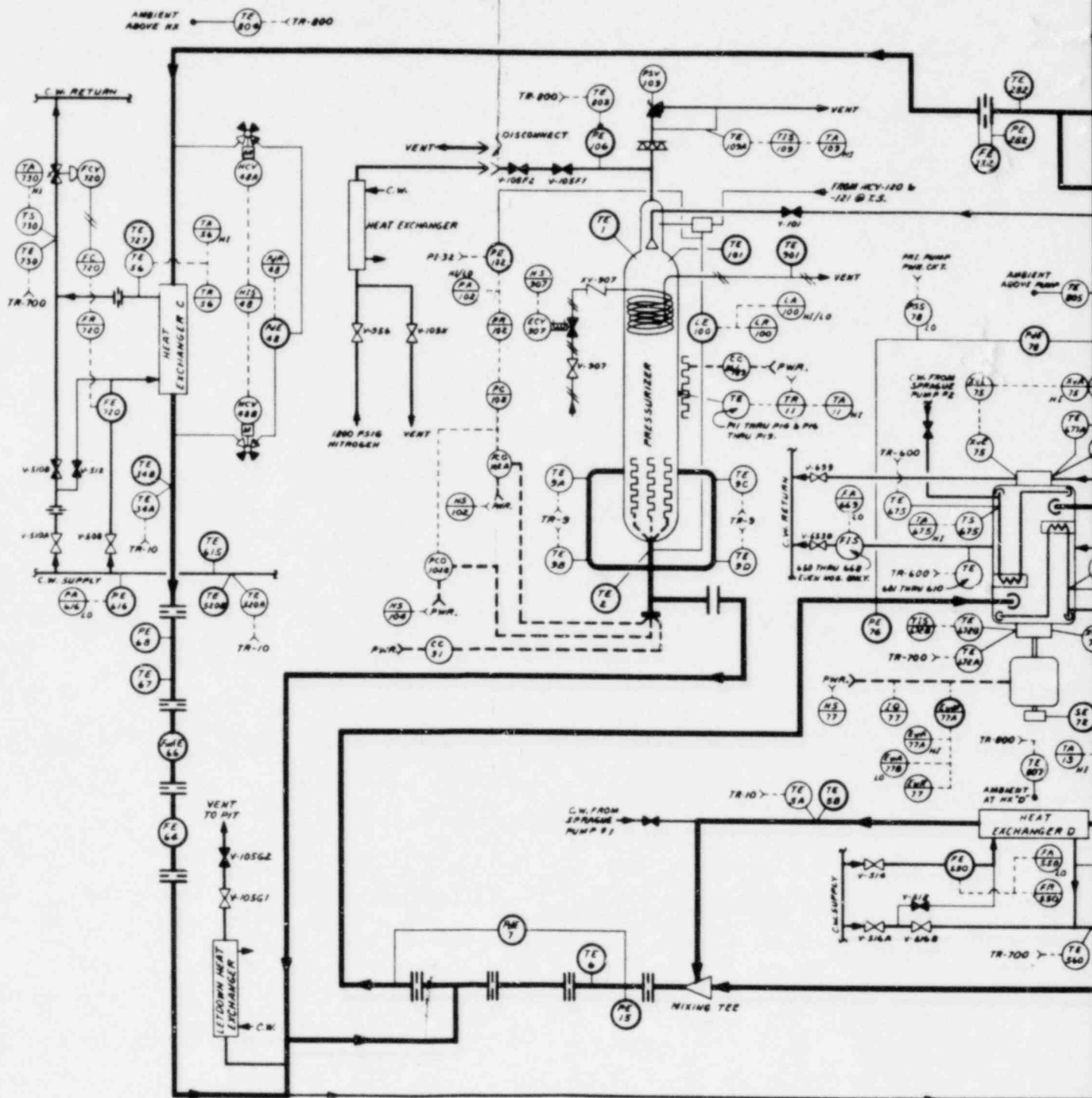


Fig. 2. Instrument application diagram for TNTF.

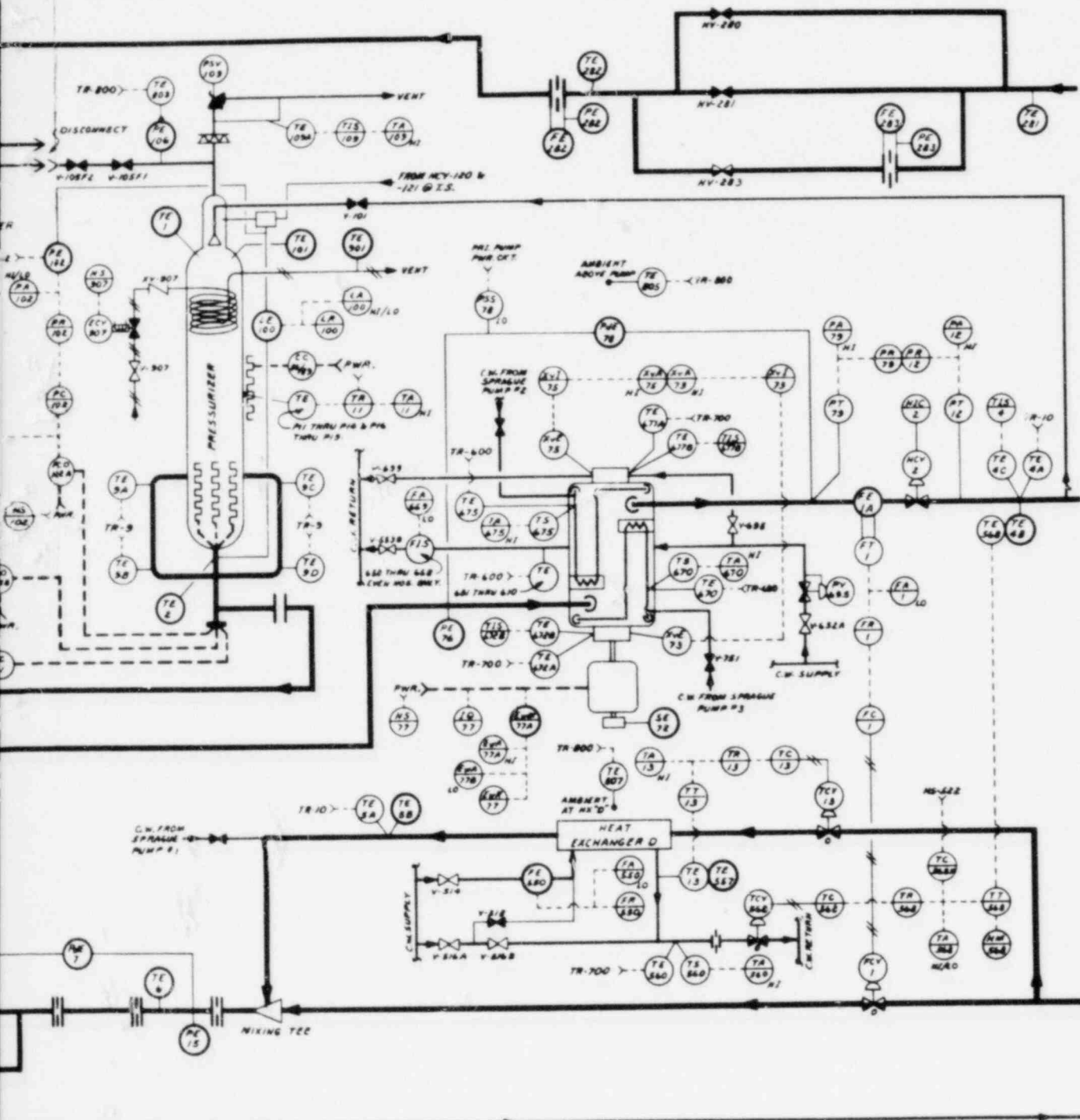


Fig. 2. Instrument application diagram for THTF.

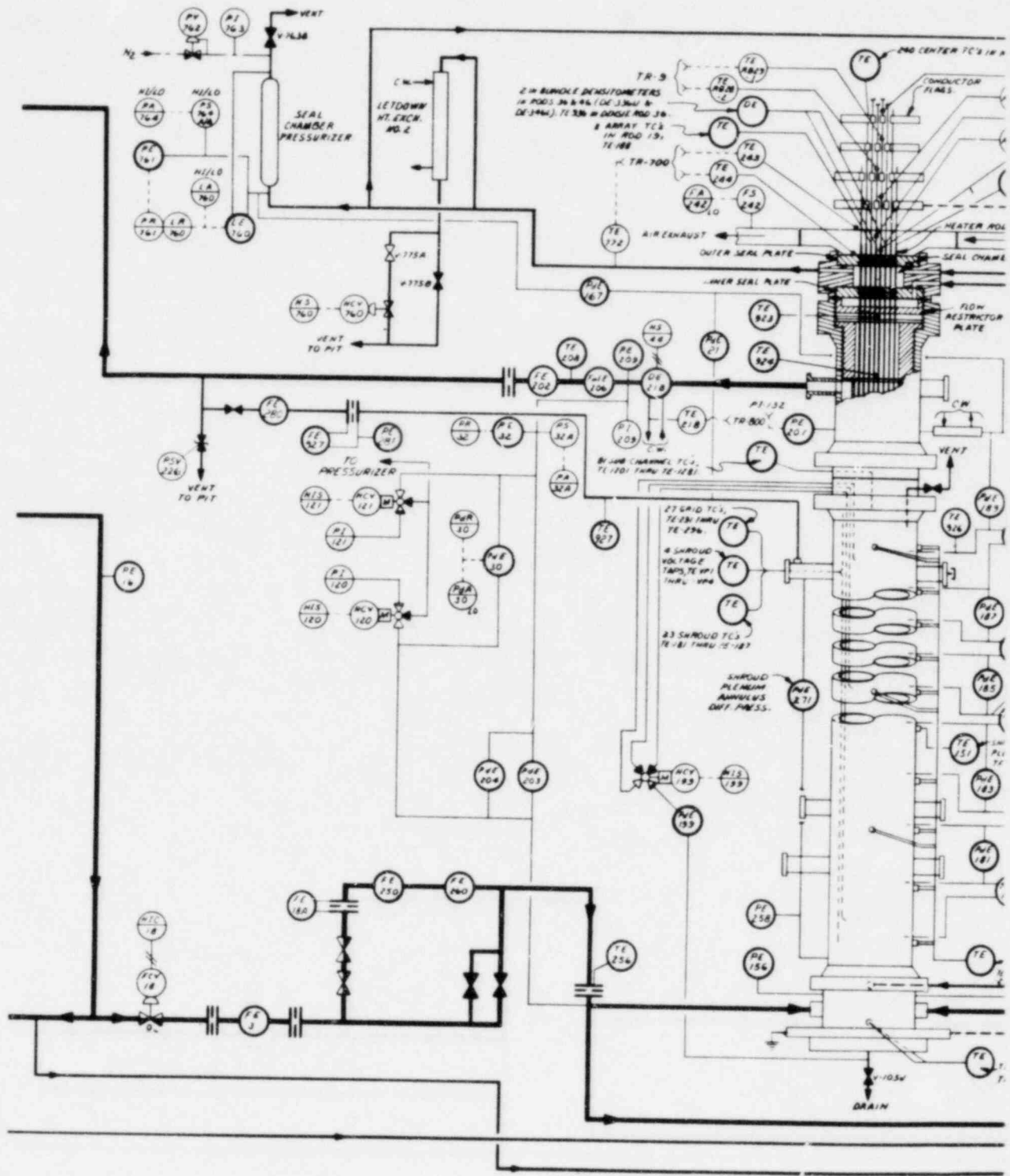
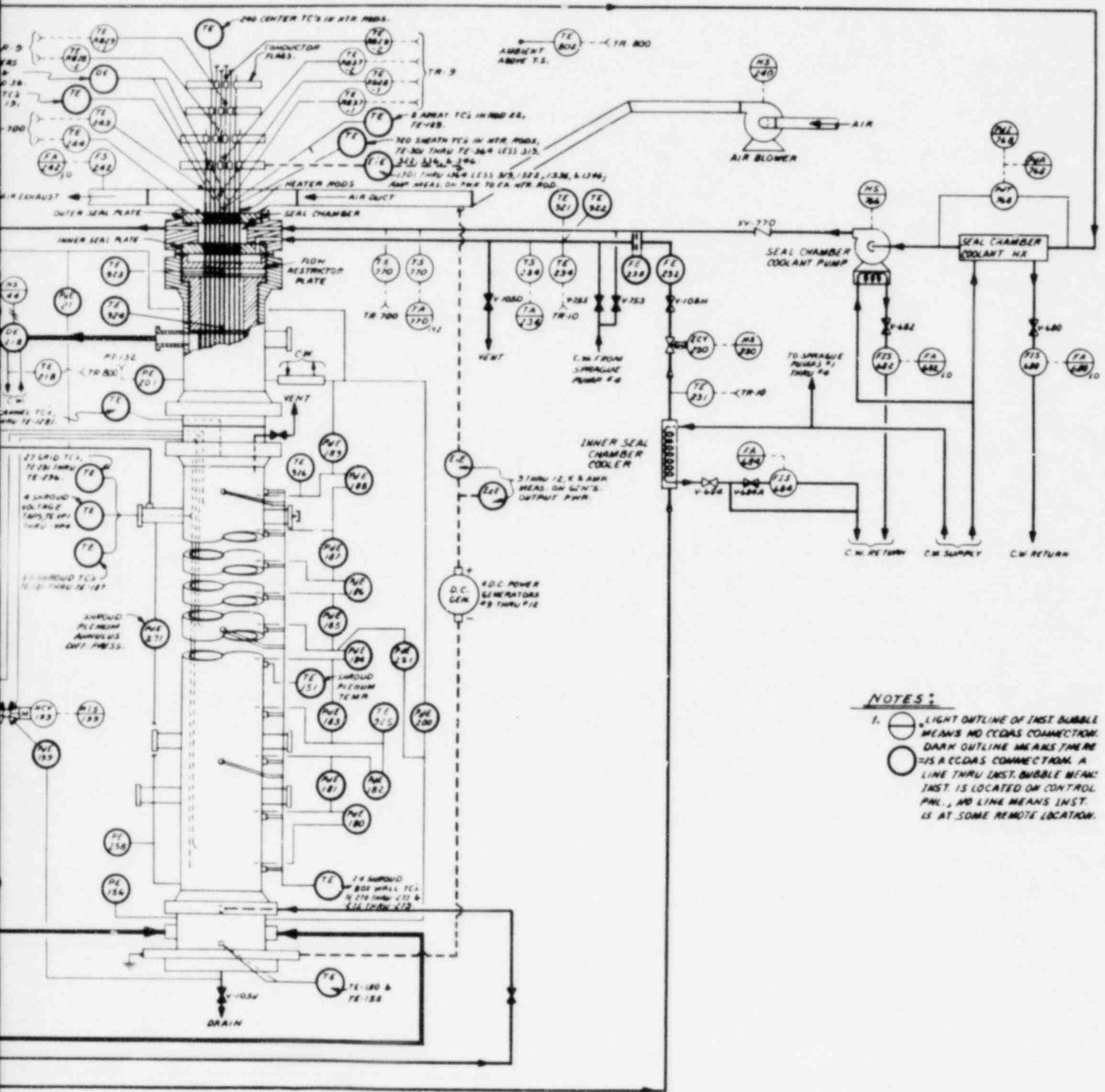


Fig. 2 (continued)



NOTES:


1.  LIGHT OUTLINE OF INST BUBBLE MEANS NO CCDA'S CONNECTION; DARK OUTLINE MEANS THERE IS A CCDA'S CONNECTION. A LINE THRU INST. BUBBLE MEAN: INST. IS LOCATED ON CONTROL PAN., AND LINE MEANS INST. IS AT SOME REMOTE LOCATION.

Fig. 2 (continued)

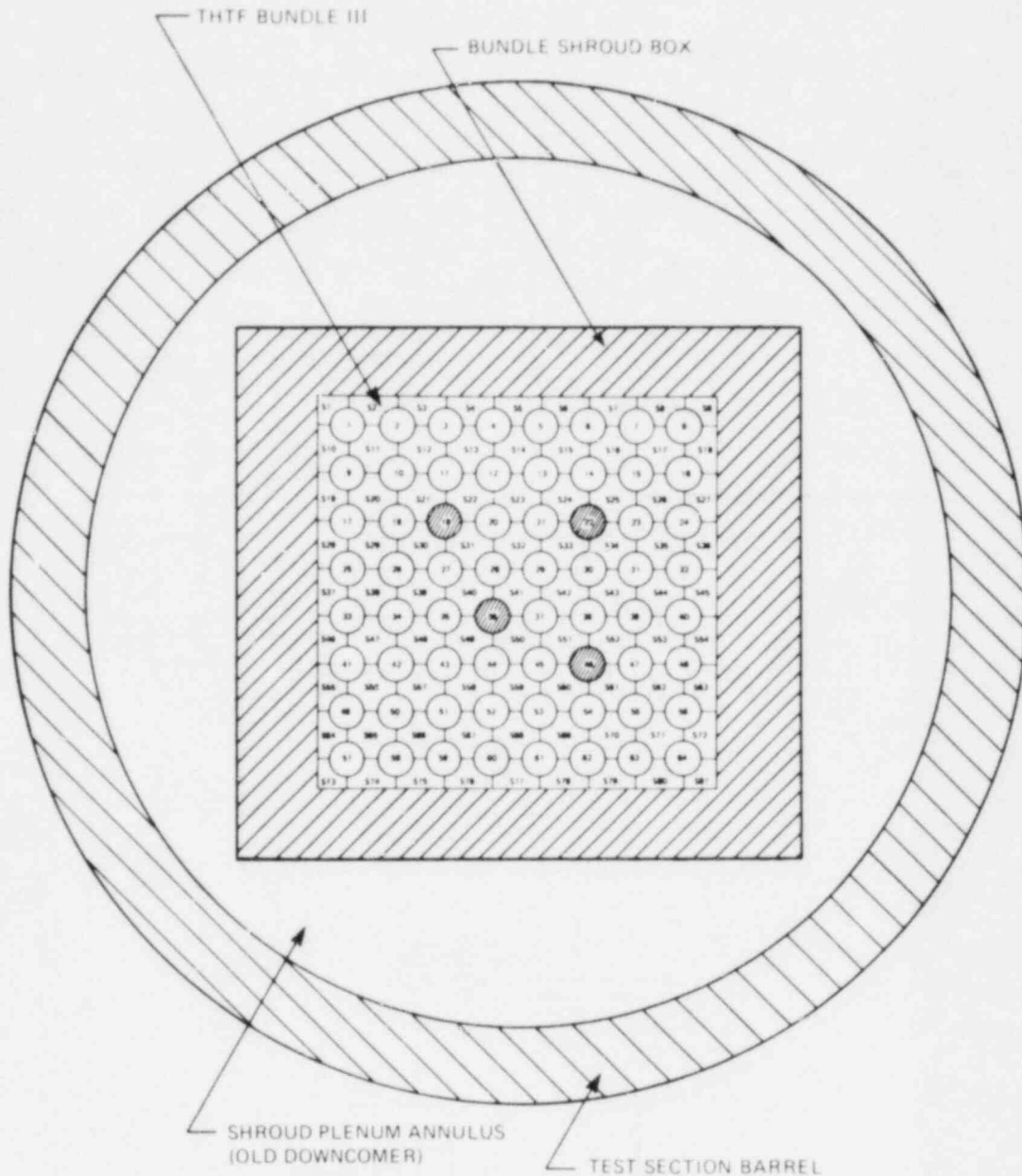


Fig. 3. Cross section of THTF test section.

then a large pressure difference between the test section bundle and downcomer would exist. This large pressure difference has been observed to cause substantial leakage from the bundle to the annulus. To minimize this leakage, the line between the pressurizer and annulus was closed after mixture level equalization had taken place. The shroud bypass line, which connects the top of the shroud annulus to the test section outlet, was opened to maintain pressure equalization (Fig. 1). The possibility of leakage from bundle to annulus was minimized by closing the shroud bypass

line shortly before data were taken. This completely isolated the annulus from the rest of the system, thus providing the least opportunity for undesired leakage.

2.2 Bundle Description

The THTF test section contains a 64-rod, electrically heated bundle. Figure 4 is a cross section of the bundle. The four unheated rods were designed to represent control rod guide tubes in a nuclear fuel assembly. Rod diameter and pitch are typical of a 17 x 17 fuel assembly.

Figure 5 is an axial profile of the THTF bundle illustrating the positions of spacer grids and fuel rod simulator (FRS) thermocouples. The

ORNL-DWG 77-5718D

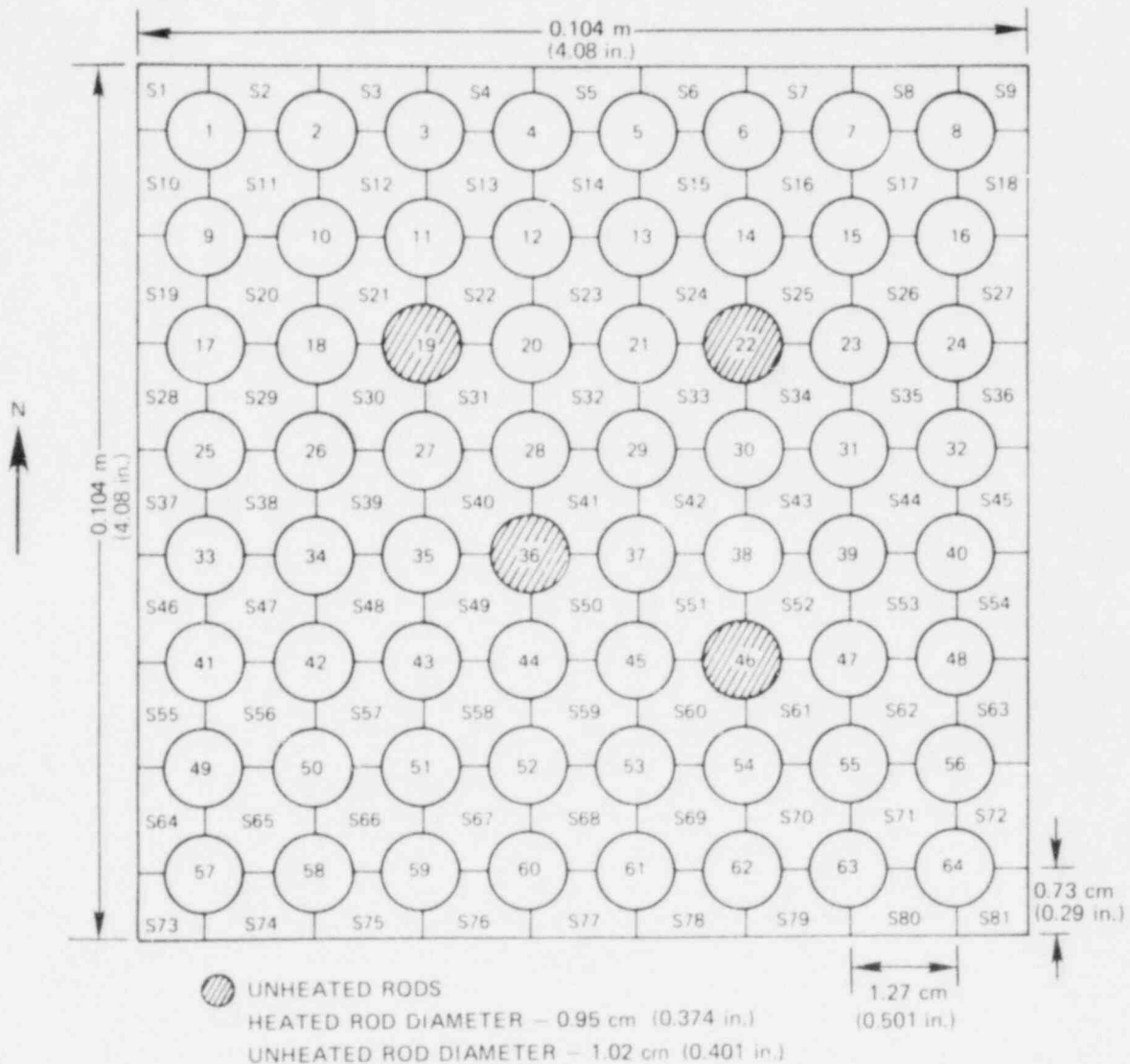


Fig. 4. Cross section of THTF Bundle 3.

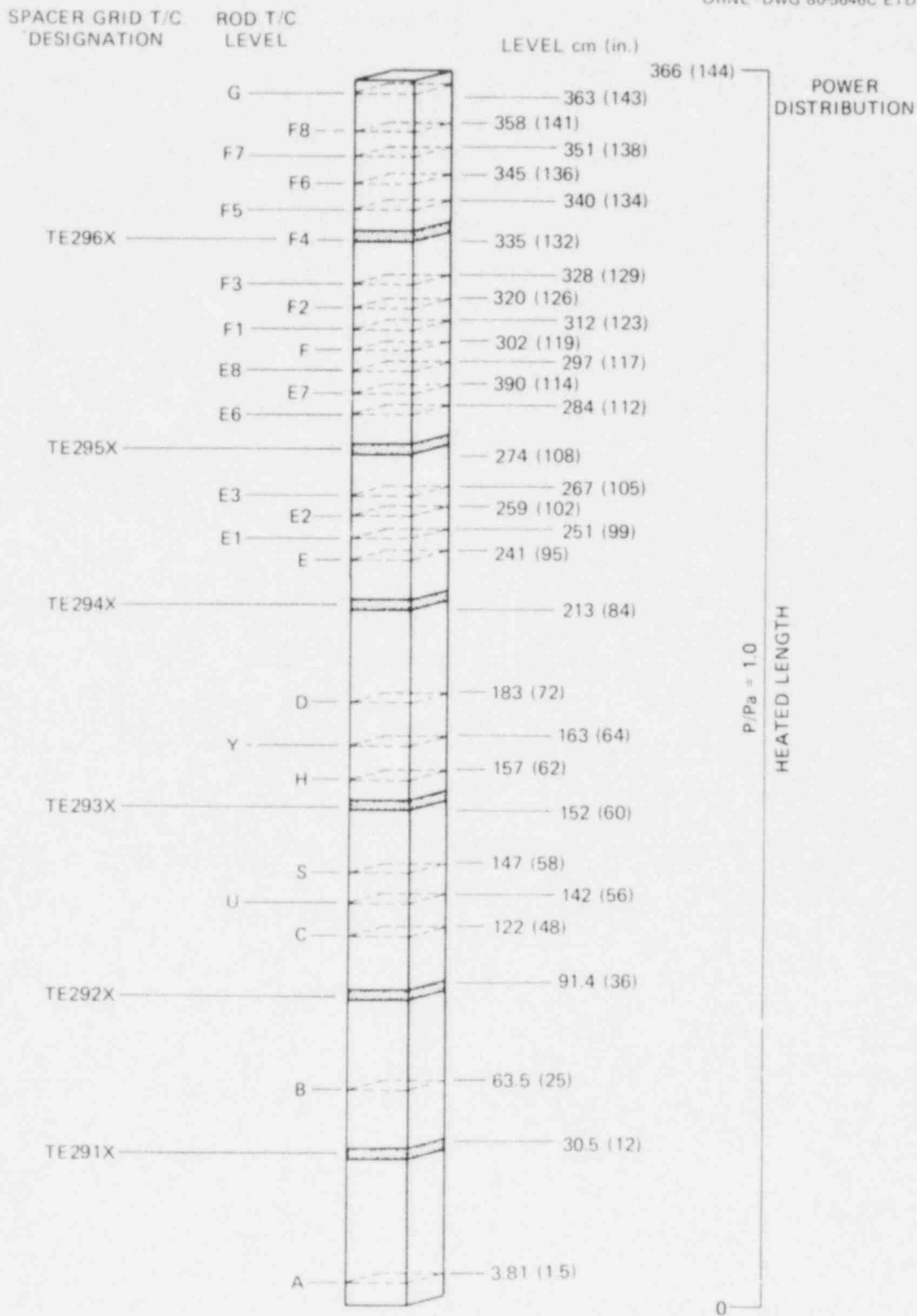


Fig. 5. Axial location of spacer grids in fuel rod simulator thermocouples.

heated length is 3.66 m (12 ft), and a total of 25 FRS thermocouple levels are distributed over that length. An FRS thermocouple level refers to an axial location where a selected number of FRSs are instrumented with sheath thermocouples. (FRS thermocouple levels A, B, C, D, E, F, and G contain most of the FRS sheath thermocouples and are referred to as primary thermocouple levels. All other FRS thermocouple levels are referred to as intermediate thermocouple levels.) Note that the upper third of the bundle is more heavily instrumented than the lower portion. For most tests the two-phase mixture level is in the top one-third of the heated length. The additional instrumentation in the top one-third of the bundle is used to better define the mixture level position. In addition, the increased instrumentation near the spacer grids can be used to ascertain to what extent spacer grids affect the heat transfer.

Figure 6 is a drawing of an FRS cross section. As can be seen, each FRS has 12 sheath and 4 center thermocouples. The thermocouples are either 0.05 or 0.04 cm (0.020 or 0.016 in.) in diameter. The thermocouples may have their junctions at any of the 25 axial levels mentioned previously. Each rod may have from none to three sheath thermocouple junctions at any particular axial level. When an FRS has three junctions at the same level, they are spaced evenly around the rod (i.e., 120° apart). Table 6 describes the convention for naming FRS sheath thermocouples.

In addition to the FRS thermometry, there are a number of locations where fluid temperature is measured. In-bundle fluid temperature measurement utilizes four different types of fluid thermocouples. The first type

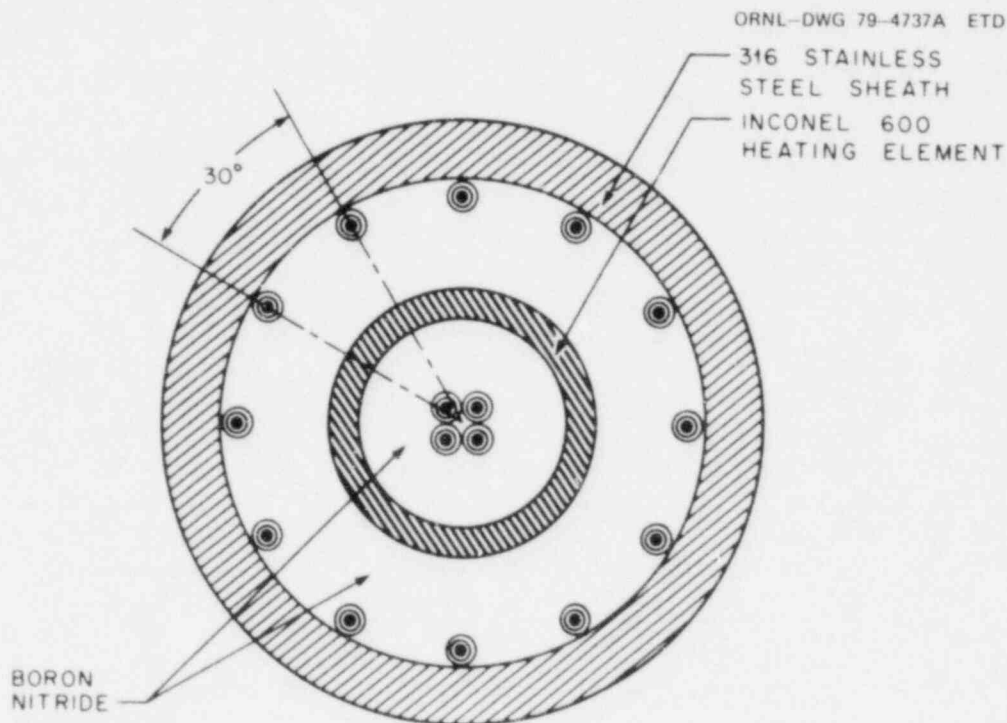


Fig. 6. Simplified cross section of a typical fuel rod simulator.

Table 6. Rod sheath thermocouple designations

Rod sheath thermocouples are designated according to one of the following two schemes:

1. TE - 3 17 A D

axial thermocouple level

azimuthal thermocouple location

rod number

The above designation refers to the sheath thermocouple in rod 17 at level D, azimuthal location A.

If the thermocouple designation ends with a number, then

2. TE - 3 54 F8

axial thermocouple level

rod number

The designation refers to the sheath thermocouple in rod 54 at level F8.

is a thermocouple array rod thermocouple. These are "exposed" fluid thermocouples that project from unheated rods. ("Exposed" in this context does not mean that the thermocouple junction actually contacts the fluid. The junction is encased in a stainless steel sheath but does not have a droplet shield.) Thermocouple array rod thermocouples are installed at 1.83, 2.41, 3.02, and 3.62 m (72, 95, 119, and 142.5 in.) above the beginning of the heated length (BOHL). The second type of fluid thermocouple is a shroud fluid thermocouple. These are "exposed" fluid thermocouples that project from the bundle shroud into subchannels adjacent to the shroud. Shroud box fluid thermocouples are installed at 0.38, 0.64, 1.22, 1.83, 2.41, 3.02, and 3.61 m (15, 25, 48, 72, 95, 119, and 142 in.) above BOHL. The third type of fluid thermocouple is a spacer grid fluid thermocouple. These thermocouples are "exposed" fluid thermocouples that project slightly upstream from each spacer grid. The fourth and final type of fluid thermocouple is a subchannel rake thermocouple. These thermocouples are attached to a rake located several centimeters above the end of the heated length. They are used to measure the cross-sectional temperature distribution.

As previously noted, the THTF bundle is surrounded by a shroud box (Fig. 3), whose walls have been instrumented with thermocouples in order

to estimate bundle heat losses. A typical instrumentation site consists of a pair of thermocouples embedded in the shroud box wall (Fig. 7). Since the thermocouples are separated, the radial temperature gradient can be calculated and the bundle heat losses estimated. Figure 8 shows the axial locations where the shroud box walls have been instrumented.

2.3 Differential Pressure Instrumentation

A primary objective of this test series was to obtain mixture level swell and void fraction distribution data under high-pressure, low heat flux conditions. These data were obtained through the use of "stacked" differential pressure cells. Figures 9 and 10 illustrate the differential pressure measurement sites. PdE-180 to 188 are ranged 0.0-0.63 m (0.0-25.0 in.) of standard water and PdE-189 is ranged 0.0-0.76 m (0.0-30.0 in.) of water. Spacing of the cells varies from 0.75-0.22 m (29.4-8.5 in.).

2.4 Summary

The THTF is a large and complex experimental facility. It would be impractical to discuss in detail the entire facility. However, what has been presented should allow the reader to interpret the results to be presented. Key aspects of the THTF design have been summarized in Table 7. A more detailed description of the THTF may be found in Ref. 7.

Table 7. THTF design summary

Design pressure, MPa (psia)	17.2 (2500)
Pump capacity, m ³ /s (gpm)	0.044 (700)
Heated length, m (ft)	3.66 (12.0)
Power profile	Flat
FRS diameter, cm (in.)	0.92 (0.374)
Lattice	Square
Pitch, cm (in.)	1.27 (0.501)
Number of heated rods	60
Number of unheated rods	4
Unheated rod diameter, cm (in.)	1.02 (0.40)
Bundle shroud configuration	Square
Bundle shroud thickness	
2 sides, cm (in.)	2.54 (1.0)
2 sides, cm (in.)	1.91 (0.75)
Number of grid spacers	7

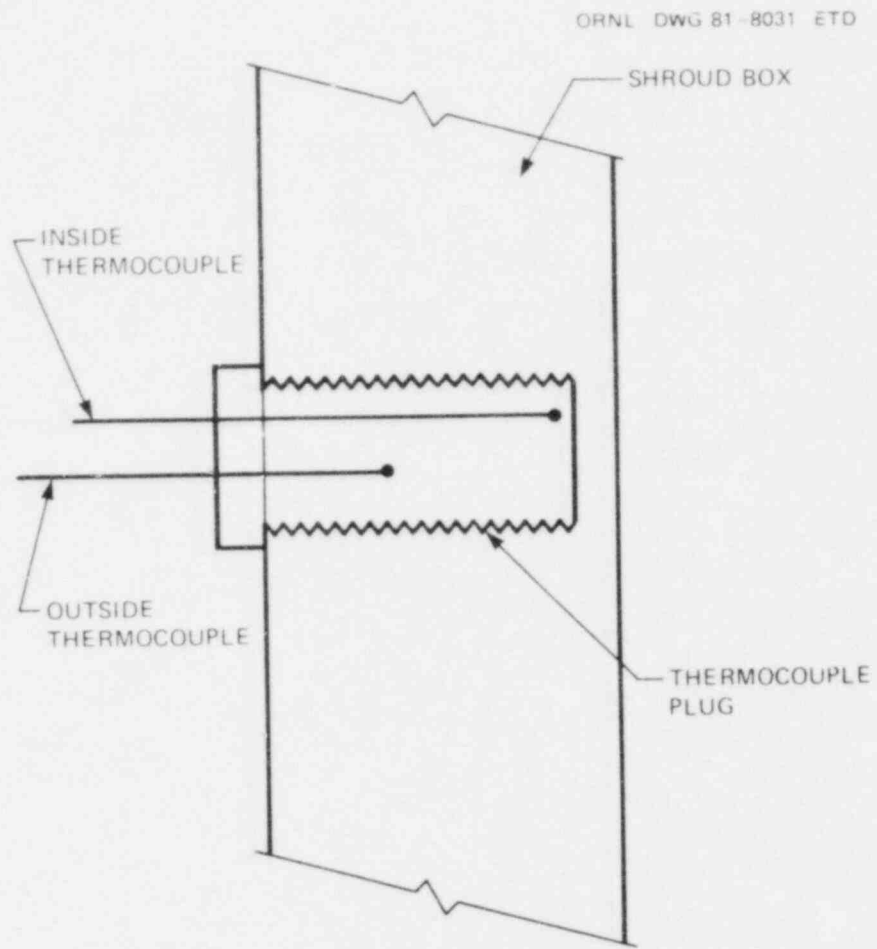


Fig. 7. Shroud wall thermocouple configuration.

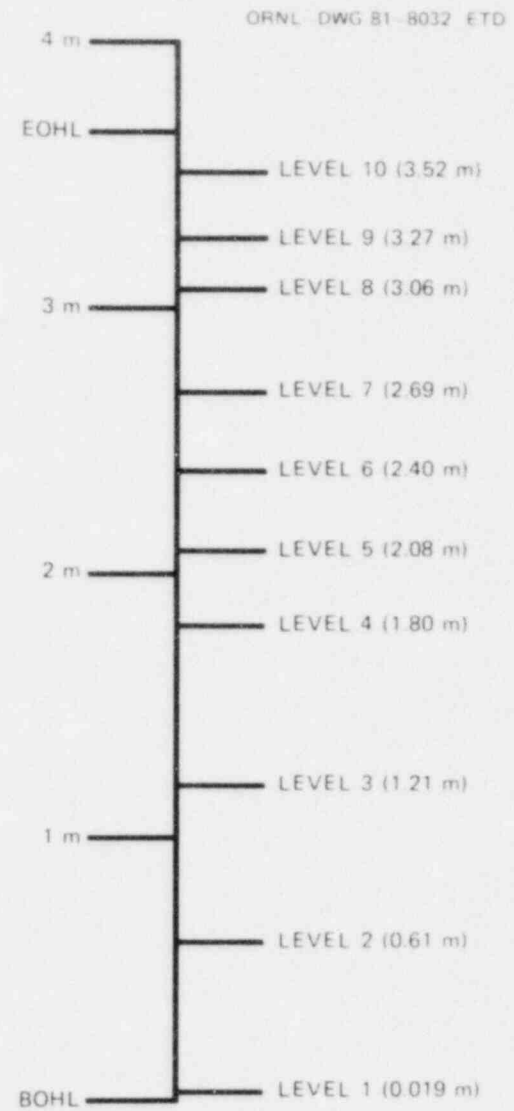


Fig. 8. Axial location of shroud wall thermometry.

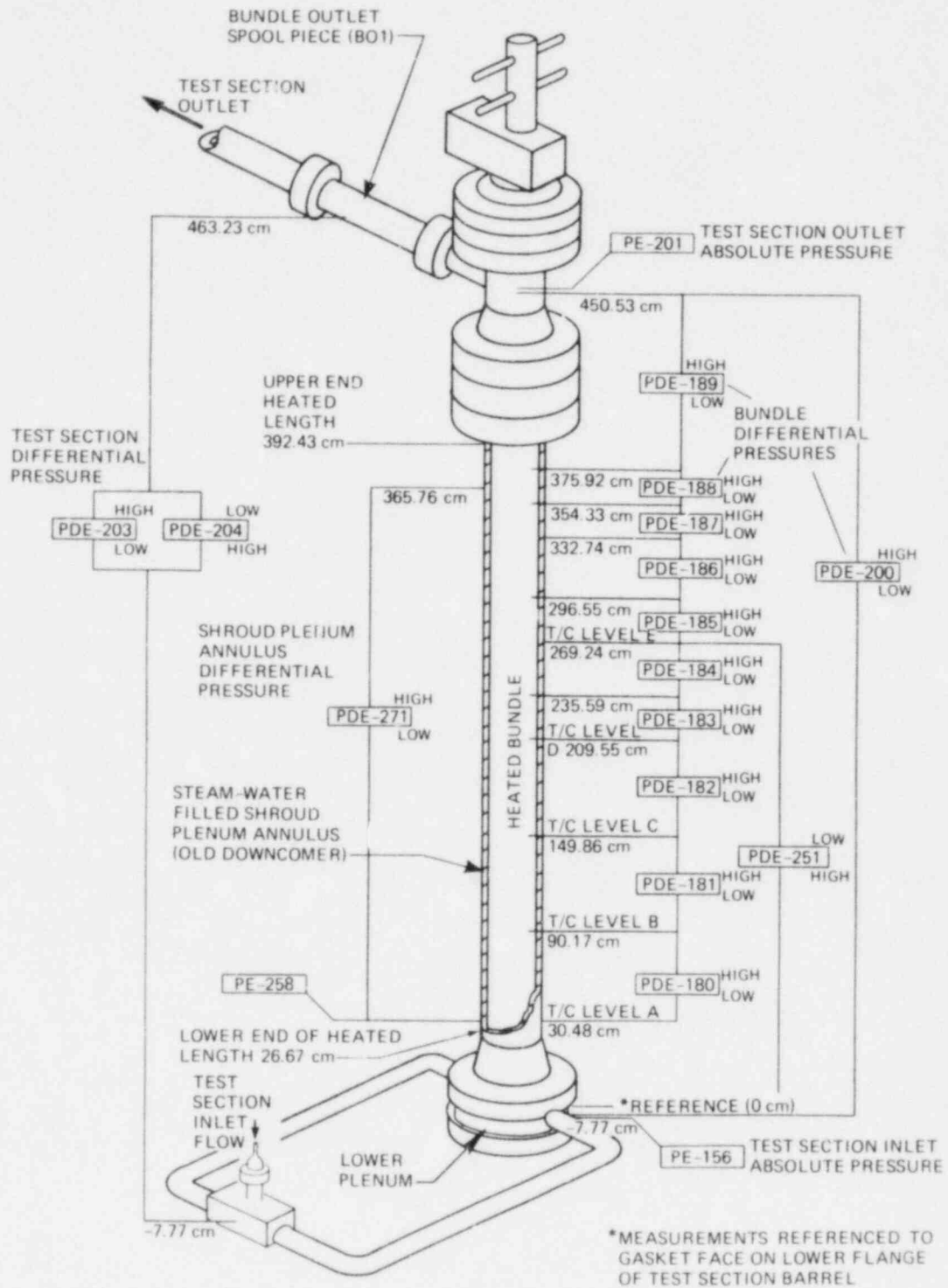


Fig. 9. THTF in-bundle pressure instrumentation (metric units).

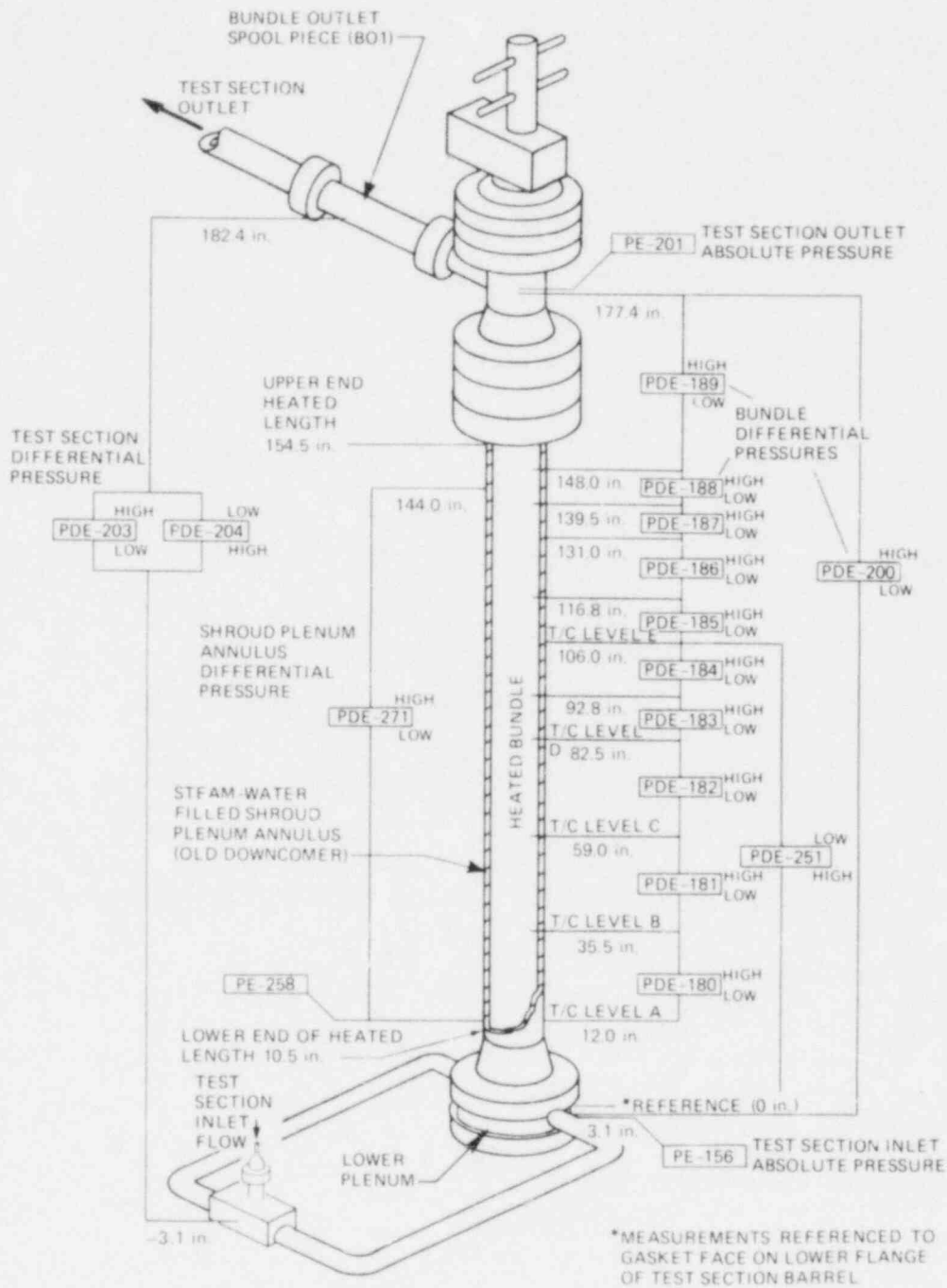


Fig. 10. THTF in-bundle pressure instrumentation (English units).

3. EXPERIMENTAL PROCEDURES

As noted in the introduction, this report is concerned with the second small break LOCA heat transfer test series conducted in November of 1980. All of these tests were run within a 24-h period. This enabled the use of a single instrumentation calibration and minimized the preheating time for the THTF. Preheating of the loop was accomplished by accumulating pump heat in the primary flow circuit and continued until a stable base loop temperature of 450-478 K (350-400°F) was obtained.

3.1 Quasi-Steady-State Heat Transfer and Mixture Level Swell Testing

Once the desired base loop temperature and pressure had been established, the test section flow was reduced to a predetermined level. This was accomplished by closing the 3/4-in. inlet flooding line and metering flow through the 1/2-in. flow line (Fig. 1). Excess pump capacity was diverted through the pump bypass loop.

When the loop was properly configured, bundle power was applied and boiloff began. Excess volume was accumulated in the pressurizer with nitrogen being vented from the pressurizer to maintain constant pressure. Eventually the THTF settled into a quasi-steady state with the rod bundle partially uncovered and inlet flow just sufficient to make up for the liquid being vaporized. During this boiloff process, the valves in the lines from the shroud annulus to the pressurizer and test section outlet were left open. This aided in the rapid equalization of bundle and downcomer mixture levels.

When the THTF reached steady state, the lines from the pressurizer to the shroud annulus and the line from the annulus to the test section outlet were closed. This isolated the shroud annulus fluid from the system fluid. After an additional period of stabilization, the bundle power was trimmed to produce peak FRS temperatures of about 1033 K (1400°F), the maximum temperature imposed by safety limits. This resulted in the maximum number of uncovered levels for the subject pressure and mass flow rate. Once again, the loop was allowed to stabilize, after which a 20-s data scan was taken. Data were recorded at a rate of 10 points per second per instrument. Once data had been acquired, the pressure, flow, and power were slowly changed to the next test point. In general, it was possible to do this without recovering the bundle.

3.2 High-Pressure Reflood Testing

Initial conditions for a reflood test were established in a manner identical to that used in the quasi-steady-state heat transfer tests. Reflood was initiated from a configuration in which the THTF bundle was partially uncovered and peak clad temperatures were on the order of 1033 K (1400°F).

To initiate reflood, the inlet flooding line was opened to a predetermined setting. This caused the test section inlet flow to increase, thus commencing bundle recovery. The equalization line between the shroud plenum annulus and the test section outlet remained open because the bundle underwent a pressure transient during reflood. Failure to allow the shroud annulus to equalize with the bundle would have resulted in large pressure differences across the shroud box. Data were taken approximately 15-20 s before opening of the flooding valve and until core recovery was complete. Scanning rate was 10 points per second per instrument, and time zero was defined as the approximate time at which the flooding valve was opened. Bundle power remained constant throughout reflood.

3.3 Bundle Boiloff Testing

Bundle boiloff data were acquired between dryout of the top of the heated length and the time when peak clad temperatures reached 1089 K (1500°F). Tests were initiated by complete closure of the inlet flow valves. As such, makeup flow was zero and the bundle began to boil. Nitrogen was vented as the excess vapor volume was accumulated in the pressurizer. The pressure equalization line between the shroud annulus and the test section outlet was open during the transient to minimize pressure differences across the shroud wall.

During the early boiloff period, a number of FRS thermocouples near the top of the heated length were monitored for indication of dryout. When dryout began to occur, a data scan began. At this time (defined as time 0.0), venting of nitrogen from the pressurizer was increased to produce the desired depressurization rate (if called for in the test matrix). Water in the pressurizer was maintained at a low enough temperature so that flashing did not occur. The test was continued until a peak clad temperature of 1089 K (1500°F) was reached. Power was then reduced in order to prevent bundle power trips due to high-temperature safety limits. This peak temperature of 1089 K (1500°F) could be tolerated in boiloff testing because the bundle would not remain at this temperature for extended periods. In quasi-steady-state testing, the bundle remained at elevated temperatures for long periods; a lower safety limit of 1033 K (1400°F) was used.

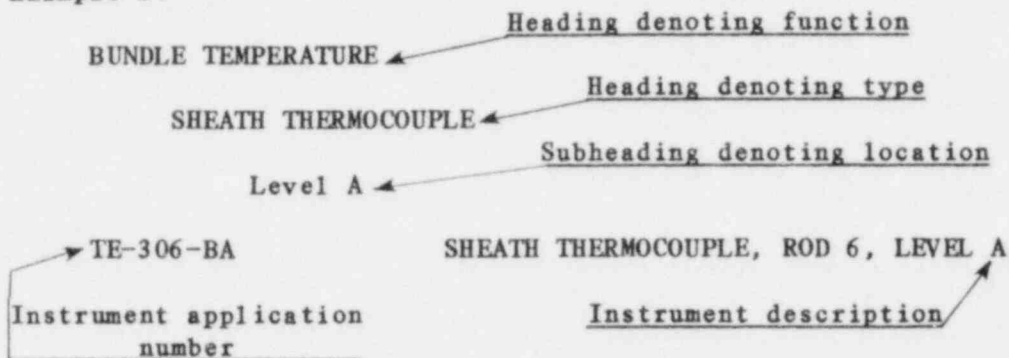
4. PRESENTATION OF DATA

This section of the report presents the quasi-steady-state and transient data obtained from the subject tests. In addition, the format of the data is explained.

4.1 Instrument Description and Status

Three types of tables are used to describe THTF instrumentation of relevance to small break testing. The first type (Table 8) lists headings and subheadings for instrumentation in terms of instrument function, type, and location; a brief description of each instrument; and an instrument application number (IAN).^{*} The IAN is a unique identifier (maximum length of eight characters) that is associated with each instrument. The following example illustrates the format used in Table 8:

Example 1:



The second type of table (Table 9) lists instruments in the order in which the transient instrument records are plotted. For example, entry 3 in Table 9 corresponds to the third transient data plot (Fig. 13). Contents of Table 9 include an IAN, instrument description, instrument range, instrument status, and the figure number of the corresponding transient plot.[†] Instrument status describes the state of an instrument during a particular test. In most cases these comments are self-explanatory. There are two exceptions: first, the comment "instrument failed" does not necessarily mean that an instrument has physically failed. Rather, it implies that there is clear evidence that a given instrument is not reliable and therefore should not be used. An example is PE-26, a pressure transducer that was disconnected from the data acquisition system for small break testing. The comment "instrument questionable" implies that, in the best judgment of the test engineer, a given instrument is unreliable and should not be used in the analysis. An example would be a fluid thermocouple that indicates steam superheat when redundant instrumentation indicates a saturated condition.

^{*}Table 8 appears in microfiche form at the back of this report.

[†]Table 9 appears in microfiche form at the back of this report.

The third type of table lists instruments alphabetically in terms of the IAN. Information contained in Tables 10 and 11 includes IAN, corresponding transient plot figure numbers, quasi-steady-state data table entry number, and instrument type code. Table 10 pertains to reflood testing and Table 11 to boiloff testing.* In each table there are five figure numbers corresponding to each instrument, one for each of the five reflood or boiloff tests. The entry number corresponds to the instrument location in the quasi-steady-state data tables (Tables 13-26 contained on microfiche at the back of this report). Instrument type code refers to the way in which raw data from an instrument are processed, and these methods are discussed in Appendix A. Tables 10 and 11 coordinate the information in Tables 8 and 9. One looks up an instrument by function using Table 8, and then the associated transient plot or entry number can be determined by using the IAN and Tables 10 and 11. Finally, Table 9 is employed to check the instrument status.

As noted, the IAN is a unique identifier for each instrument. Also, in the case of in-bundle thermometry, the IAN contains information pertaining to the type and location of thermocouples. Tables 6 and 12 explain the thermocouple nomenclature used in the IAN.

4.2 Quasi-Steady-State Data

Quasi-steady-state data for Tests 3.09.10I-N and 3.09.10AA-HH are presented in Tables 13-26.* The tables contain IAN, instrument description, average instrument reading, standard deviation of instrument reading, instrument status, and table entry number. The averages and standard deviations were computed from a 20-s data scan with a sampling rate of 10 Hz. Appendix D contains a set of tables identical to Tables 13-26 except that averages and standard deviations are expressed in English engineering units.

4.3 Transient Reflood and Boiloff Data

Reflood and boiloff test data are presented as a series of transient plots (microfiche Figs. 11 through 8611). Plots are arranged in the same order as the entries in Table 9.

4.4 Instrument Uncertainty

Table 27 lists critical instruments and associated measurement uncertainties. Uncertainty is divided into three categories. The first category is the steady-state uncertainty, of relevance to the quasi-steady-state data in Tables 13-26. The second and third categories pertain to uncertainties under transient conditions typical of reflood and boiloff. The nominal transient uncertainty refers to the uncertainty that is

*Tables appear in microfiche form at the back of this report.

Table 12. Thermocouple nomenclature

Spacer grid thermocouples: TE-29na

'n' - a number 1-6 designating the spacer grid level as follows:

<u>Number</u>	<u>Between T/C levels</u>
1	A and B
2	B and C
3	C and D
4	D and E
5	E and F
6	F and G

'a' - a letter 'A'-'F' designating the subchannel into which the thermocouple is projecting as follows:

<u>Letter</u>	<u>Subchannel</u>
A	32
B	43
C	57
D	70
E	17
F	38

The spacer grids numbered 1, 2, 5, and 6 above have four thermocouples in subchannels designated 'A'-'D.' The spacer grids numbered 3 and 4 above have six thermocouples in subchannels designated 'A'-'F.'

Shroud box fluid thermocouples: TE-18na

'n' - a number 1-7 designating the level of the thermocouple in the shroud box as follows:

<u>Number</u>	<u>T/C Level</u>
181	A
182	B
183	C
184	D
185	E
186	F
187	G

'a' - a letter designating the side of the box through which the thermocouple protrudes 'N,' 'E,' 'S,' 'W' (the compass direction most closely matching the direction the side faces).

Table 12 (continued)

Shroud box wall thermocouples: TE-27nab

'n' - a number 0-9 designating the level of the thermocouple in the shroud box as follows:

<u>'n'</u>	<u>T/C Level</u>
0	A
1	B
2	C
3	D
4	N/A
5	E
6	E3
7	F
8	F3
9	F7

'a' - a letter designating the thermocouple position depth

<u>'a'</u>	<u>Position</u>
A	At edge of inner shroud wall
B	At edge of outer shroud wall

'b' - a letter designating wall orientation

<u>'b'</u>	
E	East wall
S	South wall

Subchannel thermocouples: TE-12nn

'nn' - a number 01-81 equals the number of the subchannel in which it is located.

Thermocouple array rod thermocouples: TE-18na1

'n' - the number 8 or 9 designating in which bundle site the T/C array rod is located.

8 - grid position No. 19
9 - grid position No. 22

'a' - a letter 'A' or 'B' designating which of two subchannels associated with that rod the thermocouple protrudes into.

<u>Position</u>	<u>'A' subchannel No.</u>	<u>'B' subchannel No.</u>
19	22	30
22	24	34

'1' - the thermocouple level 'D'-'G' (same as FRS thermocouple level designations).

Table 27. Critical instrument uncertainties

IAN	Description	Steady-state uncertainty (2σ)	Transient uncertainty ^a (nominal)	Transient uncertainty ^a (worst case)
FE-18A	1.27-cm (0.5-in.) inlet flow orifice meter	4.2 E-6 m ³ /s (0.07 gpm)	8.3 E-6 m ³ /s (0.13 gpm)	8.3 E-6 m ³ /s (0.13 gpm)
FE-3	5.1-cm (2.0-in.) inlet flow turbine meter	4.1% of reading	Not significant	Not significant
FE-250	1.27-cm (0.5-in.) inlet flow turbine meter	4.1% of reading	Not significant	Not significant
FE-260	1.27-cm (0.5-in.) inlet flow turbine meter	4.1% of reading	Not significant	Not significant
FE-202	5.1-cm (2.0-in.) outlet flow turbine meter	4.1% of reading	Not significant	Not significant
FE-282 ^b	2.54-cm (1.0-in.) outlet flow orifice meter	6.2 E-5 m ³ /s (0.98 gpm)	1.4 E-5 m ³ /s (0.36 gpm)	2.9 E-5 m ³ /s (0.74 gpm)
FE-283 ^b	1.27-cm (0.5-in.) outlet flow orifice meter	8.3 E-6 m ³ /s (0.13 gpm)	1.4 E-5 m ³ /s (0.36 gpm)	2.9 E-5 m ³ /s (0.74 gpm)
TE-256	Inlet fluid thermocouple	10.3 K (18.5°F)	0.3 K (0.54°F)	1.3 K (2.3°F)
TE-208	Outlet fluid thermocouple	10.3 K (18.5°F)	0.3 K (0.54°F)	4.0 K (7.2°F)
TE-3nnal	FRS sheath thermocouple	10.3 K (18.5°F)	0.1 K (0.18°F)	3.8 K (6.8°F)
TE-18nal	Thermocouple array rod fluid thermocouple	10.3 K (18.5°F)	2.7 K (4.9°F)	40.6 K (73.1°F)
PE-156	Lower plenum pressure transducer	200 kPa (29 psia)	Not significant	Not significant
PE-201	Upper plenum pressure transducer	200 kPa (29 psia)	Not significant	Not significant
PdE-251	Bundle differential pressure cell	2 kPa (0.29 psia)	Not significant	Not significant

^aTotal uncertainties are defined as arithmetic sums of steady-state uncertainties and uncertainties due to transient effects.

^bUncertainty applies to flow at calibration density [1000 kg/m³ (62.4 lb_m/ft³)]. To find uncertainty at other densities, multiply by $\sqrt{\rho_{CAL}/\rho}$.

associated with the majority of the transient data. The worst-case transient uncertainty refers to the largest uncertainty that might be expected during testing. Generally, the worst-case uncertainty is applicable only over a small portion of a transient test. For example, the worst-case transient uncertainty for thermocouples occurs at the thermocouple quench. Total uncertainties are formulated as arithmetic sums of steady-state uncertainties, appearing in the first category, and uncertainties due to transient effects, appearing in the second and third categories. A description of how the uncertainties in Table 27 were determined and a detailed list of uncertainties for all instrumentation appear in Appendix A.

REFERENCES

1. T. M. Anklam, *ORNL Small Break LOCA Test Series I: Rod Bundle Heat Transfer Analysis*, ORNL/NUREG/TM-445 (August 1981).
2. T. M. Anklam, *ORNL Small Break LOCA Test Series I: High Pressure Reflood Analysis*, ORNL/NUREG/TM-446 (August 1981).
3. T. M. Anklam, *ORNL Small Break LOCA Test Series I: Two-Phase Mixture Level Swell Results*, ORNL/NUREG/TM-447 (August 1981).
4. T. M. Anklam, *ORNL Rod Bundle Heat Transfer Data*, NUREG/TM-407/V1 (April 1982).
5. C. R. Hyman et al., *Experimental Investigations of Bundle Boiloff and Reflood Under High Pressure Low Heat Flux Conditions*, ORNL-5846 (March 1982).
6. T. M. Anklam et al., *Experimental Investigations of Uncovered Bundle Heat Transfer and Two-Phase Mixture Level Swell Under High Pressure Low Heat Flux Conditions*, ORNL-5848 (March 1982).
7. D. K. Felde et al., *Facility Description - Thermal-Hydraulic Test Facility (THTF) MOD3 - ORNL PWR Blowdown Heat Transfer Separate-Effects Program*, ORNL/TM-7842 (to be published).

Appendix A

INSTRUMENT UNCERTAINTY ANALYSIS FOR THE THTF LOOP

Summary of Results

Two standard deviation uncertainty bands are described for critical instrumentation in the Thermal Hydraulic Test Facility (THTF). The analyzed instruments and their minimum, steady-state, 2σ error bands [root sum square (RSS), 95% confidence interval] include:

1. Turbine flowmeter	4.1% reading
2. Gamma densitometer	10.4% FS*
3. Strain gage pressure cell	1.0% FS*
4. Differential pressure cell	2.0% FS min to 9.9% FS max
5. Thermocouples	3.7°C min to 10.3°C max
6. Rod power instrumentation	1.1% reading
7. Strain gage drag disk	56% reading below 10% FS* 19% reading above 10% FS*

Summary of Theory

The measure of the value of a group of n data points (x_i) with statistical significance is the mean (\bar{x}) or expected value given by

$$\bar{x} = \sum \frac{x_i}{n}, \quad (\text{A.1})$$

where Σ is the usual sum from data point 1 to data point n . The standard measure of the dispersion of the data is the variance [σ^2 or $V(x)$] defined by

$$\sigma^2 = \sum \frac{(x_i - \bar{x})^2}{n}. \quad (\text{A.2})$$

However, $V(x)$ has dimensions of engineering units squared, which may be inconvenient. The square root of $V(x)$, the standard deviation (σ), is usually reported. Furthermore, in normally distributed data with mean \bar{x} and variance σ^2 (a good approximation for much variation in physical data), statistical inferences may be drawn in terms of probabilities based on the measured values of \bar{x} and σ as follows:

*Full-scale values are found in Tables A.5-A.8 under instrument range.

68% probability that $\bar{x} - \sigma < x_t < \bar{x} + \sigma$,

95% probability that $\bar{x} - 2\sigma < x_t < \bar{x} + 2\sigma$,

99.7% probability that $\bar{x} - 3\sigma < x_t < \bar{x} + 3\sigma$,

where x_t is the true value of the variable.

Brownlee has shown¹ that the variance of a linear function

$$Z = A_0 + A_1 X_1 + A_2 X_2 + \dots + A_n X_n$$

is a linear function of the variance of the variables as long as the correlation coefficients are zero, i.e., as long as they are physically unrelated. (Linearly independent variables have zero correlation coefficients, but linear independence is not a requirement.) That is,

$$V(Z) = A_1^2 V(X_1) + A_2^2 V(X_2) + \dots + A_n^2 V(X_n), \quad (\text{A.3})$$

where the A_i 's are constants and the X_i 's are independent variables.

Similarly, Scarborough has shown² that an analogous relation holds for a system where the independent variables are not linear:

$$Z = F(Y_1, Y_2, \dots, Y_n).$$

The variance of Z is given by

$$V(Z) = \left(\frac{\partial Z}{\partial Y_1}\right)^2 V(Y_1) + \left(\frac{\partial Z}{\partial Y_2}\right)^2 V(Y_2) + \dots + \left(\frac{\partial Z}{\partial Y_n}\right)^2 V(Y_n), \quad (\text{A.4})$$

where the correlation coefficients of the Y_i 's are zero and the value of $V(Y)$ is small compared to $(\partial Z/\partial Y_i)^2$. Notice that in situations where the standard deviation can be expressed legitimately as a percentage of the value of $\partial Z/\partial Y_i$, Eq. (A.4) can be rewritten as

$$\sigma\%(Z) = \sqrt{(\sigma\%Y_1)^2 + (\sigma\%Y_2)^2 + \dots + (\sigma\%Y_n)^2}. \quad (\text{A.5})$$

The above equations can best be understood through the use of an illustrative example. Consider the amplifier of Fig. A.1. The uncertainty in the input voltage can be derived from the function $V_{in} = F(V_{out})$,

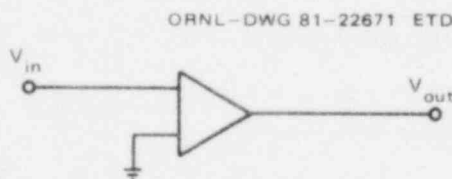


Fig. A.1. Amplifier.

V_{offset} , GAIN) given the measured values for V_{out} , $V(V_{\text{out}})$, V_{offset} , $V(V_{\text{offset}})$, and GAIN, $V(\text{GAIN})$, where V_{in} is the input voltage, GAIN is the amplifier gain, and V_{offset} is the offset voltage.

Assuming the following data, the value of V_{in} is given by

$$V_{\text{in}} = \frac{V_{\text{out}} - V_{\text{offset}}}{\text{GAIN}},$$

and the variance in the input voltage can be found by applying Eq. (A.4) or (A.5).

$$V(V_{\text{in}}) = \frac{V(V_{\text{out}})}{\text{GAIN}^2} + \frac{V(V_{\text{offset}})}{\text{GAIN}^2} + \frac{V(\text{GAIN}) (V_{\text{offset}} - V_{\text{out}})^2}{\text{GAIN}^4}, \quad (\text{A.6})$$

where

$$V_{\text{out max}} = 20.0 \text{ volts},$$

$$V_{\text{out}} = 10.0 \text{ volts},$$

$$V(V_{\text{out}}) = (0.2 \text{ volts})^2 = (2\%)^2 \text{ reading},$$

$$V_{\text{offset}} = 0.5 \text{ volts},$$

$$V(V_{\text{offset}}) = (0.05 \text{ V})^2 = (0.5\%)^2 \text{ reading},$$

$$\text{GAIN} = 200 \text{ volts/volt},$$

$$V(\text{GAIN}) = (1 \text{ volt/volt})^2 = (0.5\%)^2 \text{ reading},$$

$$V_{\text{in}} = \frac{(10.0 \text{ volts} - 0.5 \text{ volt})}{200} = 0.0475 \text{ volts},$$

$$V(V_{\text{in}}) = \frac{(0.2)^2}{(200)^2} + \frac{(0.05)^2}{(200)^2} + 1^2 \frac{(-9.5)^2}{(200)^4},$$

$$\sigma(V_{\text{in}}) = 10^{-3} \text{ volts or } 2.1\% \text{ reading}.$$

Because V_{in} is a function of V_{out} , V_{offset} , and GAIN in the form given above, it is reasonable to assume that stating the variances as percentages of the readings is equivalent to stating the variances as percentages of the respective partial differentials. In fact, this will always be reasonable as long as the variables are of the first order. The arithmetic for computing $\sigma(V_{\text{in}})$ becomes simply

$$\sigma(V_{\text{in}}) = \sqrt{(2\%)^2 + (0.5\%)^2 + (0.5\%)^2} = 2.1\% \text{ reading}.$$

Equation (A.4) or (A.5) applied to each major component of a complex information loop is often the only method available to arrive at an uncertainty value. However, in the case of the gamma densitometer and the

strain gage pressure cell, in situ standards are available that allow direct measurement of the uncertainty. Heise gages are used as in situ standards for strain gage pressure cells. Pressure and temperature measurements in subcooled water can be used to determine density with steam tables for comparison with the gamma densitometers. Such a comparison is made using a linear regression analysis based on the method of Gauss.

The equation of a line in slope-intercept form is given by

$$y = Ax + B ,$$

where A is the slope ($\Delta y/\Delta x$) and B is the value of the y intercept.

The best-fit values of A and B can be found by minimizing the sum of the distances between the experimentally determined points and the best-fit line.

The pertinent equations are

$$A = \frac{\sum x_i y_i - n \sum (x_i y_i)}{(\sum x_i)^2 - n \sum (x_i)^2} \quad (A.7)$$

and

$$B = \frac{\sum (x_i y_i) \sum x_i - \sum y_i \sum (x_i)^2}{(\sum x_i)^2 - n \sum (x_i)^2} , \quad (A.8)$$

where the x_i 's are the values determined by the instrument under discussion and y_i 's are the corresponding values determined by the in situ standard. The uncertainty of the instrument values can then be defined analogously to Eq. (A.2):

$$\sigma = \sqrt{\frac{\sum (Y_i - y_i)^2}{n}} , \quad (A.9)$$

where the Y_i 's are computed from the best-fit equation and the instrument values are y_i . A perfectly calibrated and properly operating instrument will have $A = 1.0$, $B = 0$, and $\sigma \ll \text{reading}$.

Although the slope-intercept form of an equation is one of the easiest to interpret, it does have a disadvantage: A and B are not linearly independent variables, so drawing statistical inferences about A and B in terms of their variances is hindered. A solution to this problem is to solve for the best-fit line equation in the form:

$$Y = \alpha(x - \bar{x}) + \beta . \quad (A.10)$$

The variances of α and β are then known to be

$$V(\alpha) = \frac{\sigma^2}{n} \quad (A.11)$$

and

$$V(\beta) = \frac{\sigma^2}{\sum (x_i - \bar{x})^2}, \quad (\text{A.12})$$

as shown by Brownlee,³ where σ is defined as in Eq. (A.9). We can still arrive at an estimate of $V(A)$ and $V(B)$ by modifying Eq. (A.10) to show

$$Y = ax - a\bar{x} + \beta,$$

which implies $a = A$ and $B = (-a\bar{x} + \beta)$. Applying Eq. (A.4) yields

$$V(A) = \frac{\sigma^2}{n} \quad (\text{A.13})$$

and

$$V(B) = \frac{\sigma^2}{n} \bar{x}^2 + \frac{\sigma^2}{\sum (x_i - \bar{x})^2} = \sigma^2 \left[\frac{\bar{x}^2}{n} + \frac{1}{\sum (x_i - \bar{x})^2} \right]. \quad (\text{A.14})$$

Equations (A.2)–(A.5) and (A.9) should be applied with caution for several reasons.

Definitions for variance assume perfect knowledge. However, actual sampling procedures are limited to finite sample sizes, and formulas impose limits on the degrees of freedom by imposing constraints. To adjust for the limits to the number of degrees of freedom, Eq. (A.2) is modified to provide an estimator for the standard deviation denoted S such that

$$S = \sqrt{\frac{\sum (x_i - \bar{x})^2}{(n-1)}}. \quad (\text{A.15})$$

Equation (A.9) becomes

$$S = \sqrt{\frac{\sum (Y_i - y_i)^2}{(n-2)}}. \quad (\text{A.16})$$

Equations (A.15) and (A.16) are the proper equations to use in all sampling situations where the standard deviation is to be used as the measure of the uncertainty. Furthermore, the value for S should be substituted for the value of σ and S^2 for $V(X)$ or $V(Y)$ in each of the other equations where σ appears. Because of the common association between the standard deviation defined by Eqs. (A.15) and (A.16) with the symbol σ , the symbol σ will be used for S in the balance of this paper. In a practical sense, where the standard deviation is reported as two significant figures, there is essentially no difference between σ and S [Eqs. (A.4) and (A.9) versus Eqs. (A.15) and (A.16)] as long as the number of data points is large.

A class of practical problems that arises in the actual error analysis is centered around the interpretation placed on uncertainties supplied by manufacturers. These uncertainties are often supplied as percentages in such a manner that it is difficult to determine whether it is reasonable to apply Eq. (A.5). Either it is difficult to determine how the stated error relates to the standard deviation, or it is difficult to determine whether the error can be applied as a percentage of the partial differentials required by Eq. (A.5). Furthermore, it is seldom stated whether the given uncertainties meet the required criterion of zero correlation coefficient. It is common for manufacturers to quote error bands as 2σ (95% confidence) or 3σ (99% confidence) though sometimes without assigning confidence limits. In this report it is conservatively assumed that the error reported by instrument manufacturers is 2σ . Unless otherwise stated, it is also assumed that a statement of error as a percent with respect to the partial differentials of Eq. (A.5) is reasonable and that the correlation coefficient is zero for all variables.

The second class of problems relating to the uncertainty analysis dealt with multiple estimates of σ for a class of instruments where σ varied widely from instrument-to-instrument and from trial-to-trial. The method of choice was to use a value of σ large enough to include about 95% of the measured values. This was accomplished by using

$$\sigma \approx \bar{\sigma} + \sigma(\sigma) .$$

That is, the value of the standard deviation used was the average value for all instruments and files read plus one standard deviation of σ . This is different from the probability statements above because σ is a span that includes zero to σ . Such a distribution cannot be normal in the sense that the probability statements require.

A generalized procedure for data analysis follows:

A common form for a large system is generalized in Fig. A.2. This system consists of a number of transducers (T_i), their associated signal conditioning equipment (S_i), and the data acquisition system (DAS). The DAS is understood to include both the hardware and the software. The standard deviations of the output signals are measured by reading the information from the magnetic tape written by the DAS and applying Eq. (A.2) or (A.14) over an arbitrary length of time where the process is defined as being in a steady state. The measured value of the DAS output can then be incorporated with other measures of uncertainty using Eq. (A.5). If an in situ standard is going to be used to develop the total uncertainty directly, the data for the secondary standard need to be accessed and correlated in time and space with the instruments under consideration.

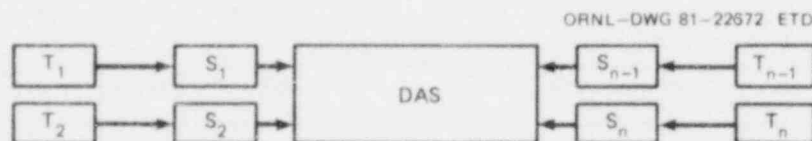


Fig. A.2. Generalized form for a large system.

The development of software to perform the above estimates may be the most time-consuming part of the analysis. The software has to be able to perform the following functions for a magnetic-tape-based system:

1. Confirm that the tape is at the beginning.
2. Confirm that the tape density and number of tracks are system compatible.
3. Locate the instrument data base (IDB) and transfer the IDB to disk or core in a rapid access format.
4. Extract certain system constants from the IDB (record length, etc.).
5. Locate the scan table.
6. Use the scan table and instrument identifier code to determine the location of the desired instrument data in data records.
7. Locate the first data file of the type desired.
8. Read a fixed number of records from the data file.
9. Store data in arrays or keep running totals for averaging.
10. Compute averages and standard deviations for steady-state data in the file.
11. Write the desired combinations of data, averages, and standard deviations to arrays.
12. Locate the next data file of the type desired and repeat steps 8-12 until end-of-tape is detected.
13. At end-of-tape, write the arrays to disk for later analysis.
14. At each tape operation, check for proper positioning.
15. Analyze data written to disk as required.

The following sections provide a detailed analysis of the critical instrumentation in the THTF loop. As stated above, the exact nature of the uncertainties is not always known. The RSS value of the uncertainty is the statistically defined one if variables are unrelated (correlation coefficient = 0) and the percentage uncertainty is given as a percent of partials required for Eq. (A.5). However, to the extent that the uncertainties stated do not comply with the assumptions, the more conservative strict sum of errors may need to be applied. Both the RSS value and the strict sum value are given in the text. The RSS values are reported in tabular form at the end of this Appendix. The superscript (*) is used to denote manufacturer derived data.

A.1 Turbine Flowmeter

The turbine flowmeter channel consists of a turbine flowmeter with integral magnetic pickup, an electronics package that conditions the signal to provide an output voltage proportional to flow rate, and the DAS, which converts the analog signal in volts to digital information and writes it to magnetic tape. In operation, the turbine blade generates an electrical pulse as it passes the magnetic pickup. The ORNL electronics package senses this pulse and within 250 μ s resets the count registers and begins accumulating the count until the next pulse disables the count. During the disabled period the count is passed to the digital-to-analog converter where it is converted to millivolt reading. The voltage divider

then inverts the millivolt signal and outputs a voltage proportional to the angular velocity of the turbine blade, with 10-V full scale (FS) corresponding to 1200-Hz input signal from the flowmeter pickup. The DAS then converts the output of the ORNL electronics to a digital value and writes it to magnetic tape.

The identified sources of error in the turbine flowmeter are:

Channel noise (blade angle tolerance)	3.2%
Calibration uncertainty	2.4%
Inherent turbine linearity*	0.5%
ORNL electronics package	0.4%
A/D conversion at DAS*	0.3%
Effect of bearing change each run*	0.3%
Strict sum, 2σ error band	7.1%
RSS, 2σ error band	4.1%

The following items need to be considered when applying the above error bands to THTF data:

1. The above uncertainties are all reasonably expressed as a percent of reading. However, the value of turbine linearity quoted applies only over the range 10% rated FS through 100% rated FS. Below 10% rated FS, error bands increase rapidly (see Fig. A.3) as frictional drag becomes more significant, with a cutoff of useful information occurring near 6% of rate FS flow due to signal-to-noise problems in the electronics.

2. Random noise was measured for 30 records of data taken during Reactor Simulation Test 3.05.5B. When the standard deviation was computed for each of the 10 flowmeters without excessive channel noise, the average value (1.53% of reading) was found to agree very well with the predicted

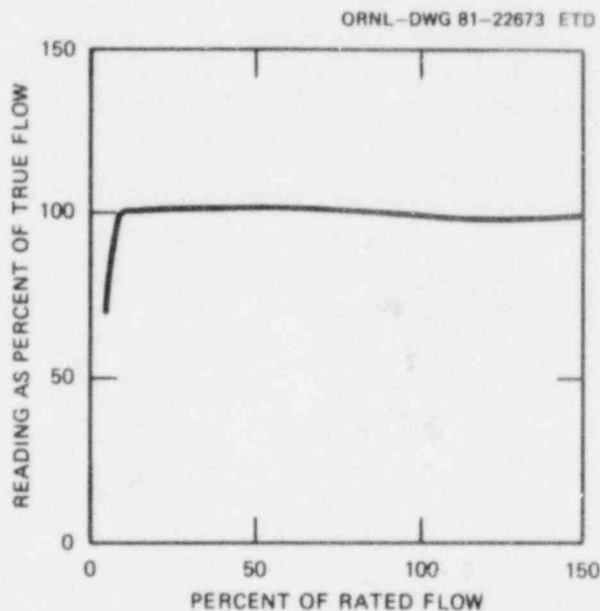


Fig. A.3. Error due to turbine linearity: characteristic curve.

channel noise because of blade manufacturing tolerances ($72^\circ \pm 1.56\%$). It would be optimistic, however, to conclude that this is the only source of random error. Data taken over a much wider range of flows would be needed to confirm this conclusion.

3. The calibration uncertainty was estimated from two different calibration laboratories (Flow Technology, Inc., and Measurements, Inc.) independently calibrating the same turbine flowmeters. The results of those calibrations indicated approximately 1.2% (as 1σ) differences from laboratory-to-laboratory.

4. The most troublesome problems of interpreting flowmeter error are those that occur during two-phase flow. In a 1977 report⁴ MPA Associates, Inc., investigated the possible errors due to slug flow, annular flow regimes, steam-water ratios, and differential two-phase velocities. This investigation was strictly theoretical, based on momentum exchange between the blade and the fluid. These analyses were based on steady-state flow, balancing the transverse momentum of one phase against that of the second. Assuming no net momentum exchange with the rotor, the turbine response was interpreted in light of the point effective radius (established as the calibration constant) in the presence of two phases with different flow regimes and different velocity profiles. The conclusion reached was that errors up to $\pm 2.5\%$ might be expected.

By assuming equal probabilities for the parameters investigated, it was determined that a 1σ error band of 10% might reasonably be expected. However, until experimental verification of both model and results can be obtained, it would only be prudent to use the above figures in a qualitative manner.

A.2 Gamma Densitometer

The gamma densitometers consist of a nearly monoenergetic ^{137}Cs gamma source, an ionization chamber to detect the gamma rays, an instrument amplifier, and the DAS. In use, the gamma rays pass through the steel pipe, through the water (in whatever phase) in the pipe, and into the ionization chamber. In the ionization chamber the gamma rays are converted into an electric current such that the current is proportional to the intensity of the impinging gamma rays. The instrument amplifier takes this current and converts it into a voltage that is proportional to the input current. At the DAS the voltage is converted to a digital value and stored on magnetic tape.

Given that the source approximates a point source, the density of the water (ρ_w) in the pipe should be given by

$$\rho_w = \text{KFACTOR} \ln \left(\frac{V_p - V_o}{V - V_o} \right),$$

where KFACTOR is an experimentally determined constant that includes the effect of pipe diameter and the mass absorption coefficient of the water (including any dissolved salts), V_p is the output voltage when the pipe is

empty, V_o is the output voltage with the source shielded (dark voltage or zero offset), and V is the output voltage when there is water in the pipe.

Due to the strong theoretical dependence of density error as a function of density, the 1σ error band was investigated as a statistical function of the density reading compared to an in situ standard based on the physical properties of the water in the pipe under known conditions of temperature and pressure and a steady-state, one-phase flow. Ten gamma densitometers in service during Test 3.05.5B were used as a basis of the study. The output voltage of each instrument was sampled 150 times in each of ten 3-s files. The output voltage was then used to compute the water density using values of KFACTOR, V_p , and V_o measured in a recent calibration run. Those densities were then compared to the expected densities based on water properties derived from the temperature and pressure instruments located adjacent to each gamma densitometer.

The measured uncertainty expressed as 1σ in kg/m^3 (and lb/ft^3) is shown in Table A.1. It was discovered, however, that at least part of the large variation in the uncertainties resulted from a systematic error that varied from instrument to instrument (see Fig. A.4, where the densitometer density is plotted against the water property density for DE-204B). Furthermore, the expected strong dependence of error on total density is not obvious over the range of data compared. Not all densitometers showed positive deviations from the standard as did DE-204B.

Table A.1. Absolute error analysis

Densitometer	σ (kg/m^3)	σ (lb/ft^3)
DE-20	18.9	1.18
DE-36	199.0	12.42
DE-168	3.6	0.22
DE-218	87.5	5.46
DE-204A	4.4	0.27
DE-204B	57.7	3.60
DE-204C	33.6	2.10
DE-262A ^a		
DE-262B	22.9	1.43
DE-262C	37.5	2.34
Average	52.0	3.20

^aProbable equipment failure during test.

The data for each densitometer were fit to a straight line, densitometer calculated density to water property density, using linear regression analysis. The random error, expressed as 1σ , was then calculated for each gamma densitometer using the formula above, but Y_i is the best average value from the linear regression equation. The value of uncertainty was much more uniform from densitometer to densitometer (see Table A.2). A

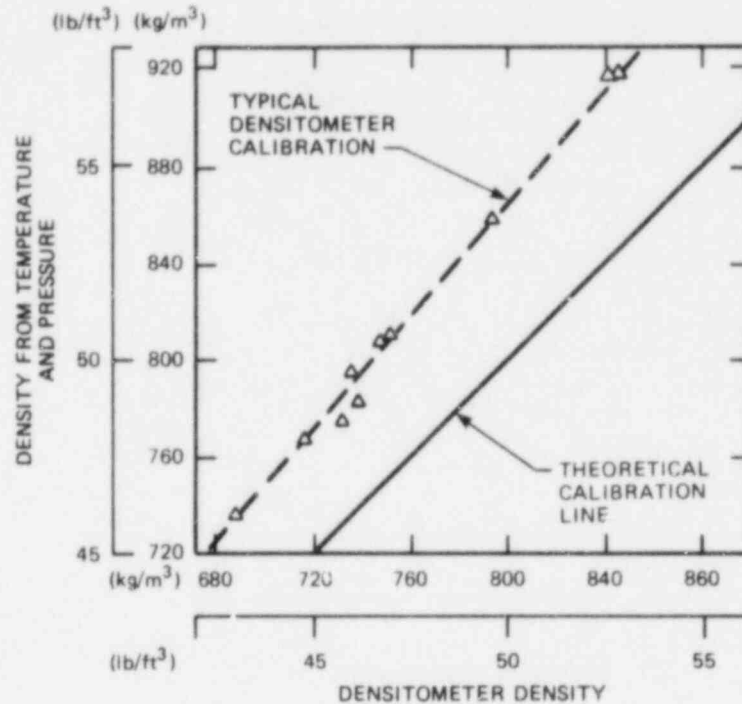


Fig. A.4. Typical densitometer calibration.

Table A.2. Least-squares best-fit line
 $RHO = A * DERHO + B$

Densitometer	A	B	σ (kg/m ³)	σ (lb/ft ³)
DE-20	0.945	64.9	8.6	0.54
DE-36	0.131	745.0	9.7	0.61
DE-168	1.00	-0.4	0.9	0.06
DE-218	0.711	176.0	2.5	0.16
DE-204A	0.981	14.0	4.4	0.27
DE-204B	1.19	-85.9	6.0	0.37
DE-204C	1.01	24.8	12.4	0.77
DE-262A ^a				
DE-262B	0.740	246.0	5.3	0.33
DE-262C	1.16	-100.0	4.5	0.28
Average			5.8	0.36

^a Probable equipment failure during test.

preliminary analysis of the calibration procedure indicates that it may be possible to recalibrate the densitometers analytically to remove the systematic error. Since the analysis performed on the experimental data does not use the densitometer responses, it was not deemed worthwhile to expend the effort required to perform this recalibration.

Since the density of water at room temperature is approximately 1000 kg/m³ (62.4 lb/ft³), the above results can be summarized as follows:

2 σ error band under current operating procedures (10.4% FS)

The following items need to be considered when applying the above error bands to THIF data analysis:

1. An analysis of data scatter indicates an average σ of 31 kg/m³ or 3.1% FS over 150-point data files. Therefore, individual points within a file have much higher uncertainties than those stated for files as a whole.

2. No other factor has been identified which would degrade the error bands beyond the steady-state, one-phase flow values listed above. However, it should be understood that the densities computed from densitometer voltages during transients and two-phase flow are time-and-path averaged values. Furthermore, direct application of the above data to transient, two-phase flow is done at the risk of the data user until experimental verification can be obtained.

A.3 Strain Gage Pressure Cells

The pressure channel investigated consists of a strain gage pressure cell, an instrument amplifier, and the DAS. In operation, pressure on the diaphragm of the pressure cell causes a change of resistance in the foil strain gages attached to the diaphragm. The change in resistance in the gages causes a voltage output from the cell that is proportional to the applied pressure. This output is amplified by the instrument amplifier. The DAS converts the amplifier output to digital format and writes it onto magnetic tape.

The following errors were identified as contributing to the pressure cell uncertainty:

Nonlinearity (P-sensor)*	0.3% FS
Repeatability (P-sensor)*	0.1% FS
Hysteresis (P-sensor)*	0.1% FS
Tempco, gage factor (P-sensor)*	0.5% Reading
Tempco, zero offset (P-sensor)*	0.5% FS
Gain instability (instrument amplifier)* ...	0.1% Reading
Output offset (instrument amplifier)*	0.1% FS
DAS calibration*	0.3% Reading
Channel noise	0.1% FS
Location of calibration standards	0.4% FS
Strict sum 2 σ error band	2.5% FS
RSS 2 σ error band	1.0% FS

The following items need to be considered when applying the above error bands to THTF data:

It is fairly obvious that the results of the in situ calibration run (see item 2 below) agree respectably with the 2σ error band determined above. The probable reasons that in situ calibration errors are smaller than the theoretically determined value can be attributed primarily to smaller than estimated temperature changes in actual operation for both gages and amplifiers. In the absence of contradictory experimental evidence, the 2σ error band for the strain gage pressure cells should be set at 1.0% FS or 200 kPa (29 psi).

1. The temperature effects were assumed to be operable over a range of only 56°C (100°F) in actual use. This seems like a reasonable assumption since the sensors themselves are installed at the end of a connecting tube ensuring cooling by ambient air flow and the instrument amplifier is mounted where ambient air flow should keep the temperature change within the 56°C (100°F) range. Channel noise was measured during Test 3.05.5B using Y_i [see Eq. (A.16)] as the average within a data file. Five instruments were sampled with 30 points per data file, 10 data files each. The 1σ value measured in this manner was quite variable, so that it was deemed expedient to select a value of σ large enough to include about 95% of the data.

2. The strain gage pressure cell does have a useable in situ standard for comparison. With data from a recent pressure cell calibration run, the standard deviation for system pressure was determined for six strain gage pressure instruments by comparing P-cell output converted to pressure using the measured calibration constants with the average reading of two Heise bourdon tube gages accurate to 20 kPa (3 psi). The results of that comparison are:

Instrument	σ (kPa)	σ (psi)	σ (% FS)
PE-26	37.2	5.4	0.18
PE-42	66.2	9.6	0.32
PE-44	18.6	2.7	0.09
PE-76	43.4	6.3	0.21
PE-106	47.6	6.9	0.23
PE-156	91.0	13.2	0.44
Average	51.0	7.4	0.24
Plus location of calibration standard	40.0	5.8	0.18
Total 2σ value	130	18.9	0.6

3. The in situ calibration uses the average reading of two Heise gages as system pressure. These gages may be separated by 8.53 m (26 ft) vertically. The result of the difference in static water pressure can produce an offset of ~40 kPa (5.8 psi) (1σ) depending on the location of the specific instrument.

4. The DAS seems to be the limiting factor in instrument response time, including the response time of the transducer itself since pressure waves should reach the diaphragm much faster than the normal sample rate. No other source of error has been identified to degrade the error band established for steady-state, one-phase flow. However, the application of the above error bands to transient or two-phase flow without corroborating data might be overly optimistic, and any such use is the responsibility of the data user.

A.4 Differential Pressure (dp) Cells

The strain gage dp cell (A, B, C) instruments are very similar to the strain gage pressure cells above, except that they have lower full-scale capability.

- A. The identified sources of error in the BLH strain gage (1380 and 6870 kPa or 200 and 1000 psi, respectively) dp cell are

Bench calibration (note 1)	2.4% FS
Tempco, gage factor (P-sensor)*	0.1% FS
Tempco, zero offset (P-sensor)*	0.1% FS
Gain instability (instrument amplifier)* ...	0.1% FS
Output offset (instrument amplifier)*	0.1% FS
A/D inaccuracy (DAS)*	0.3% FS
Random noise (note 2)	2.0% FS
Strict sum 2σ error band	5.1% FS
RMS 2σ error band	3.1% FS

- B. The identified sources of error in the BLH strain gage (1380 kPa or 200 psi) (pit) dp cell are

Bench calibration (note 1)	2.4% FS
Tempco, gage factor (P-sensor)*	0.5% Reading
Tempco, zero offset (P-sensor)*	0.5% FS
Gain instability (instrument amplifier)* ...	0.1% Reading
Output offset (instrument amplifier)*	0.1% FS
A/D inaccuracy (DAS)*	0.3% Reading
Random noise (note 2)	9.6% FS
Strict sum 2σ error band	13.5% FS
RMS 2σ error band	9.9% FS

- C. The identified sources of error in the GENISCO (41 kPa or 6 psi) strain gage dp cell are

Static pressure offset	2.6% FS
Zero balance*	2.0% FS
Linearity, hysteresis*	0.4% FS
Tempco sensitivity*	0.3% FS
Tempco zero offset*	0.3% FS

Noise (note 1)	2.0% FS
A/D conversion DAS*	0.3% FS
Strict sum 2 σ error band	7.9% FS
RSS 2 σ error band	3.9% FS

D. The identified sources of error in the ITT Barton (25 kPa or 100 in.) dp cell are

Transduction accuracy*	0.25% FS
Static pressure effect*	0.4% FS
Tempco zero offset*	0.2% FS
Tempco sensitivity*	0.2% FS
Noise	2.0% FS
DAS*	0.3% FS
Strict sum 2 σ error band	3.4% FS
RSS 2 σ error band	2.1% FS

E. The identified sources of error in the Rosemount Capacitance dp cell are (see note 4)

	6.2 and 7.4 kPa (25 and 30 in.)	37 and 50 kPa (150 and 200 in.)
Transduction accuracy	0.25% FS	0.25% FS
Tempco combined*	0.95% FS	0.14% FS
Static pressure offset	1.0% FS	1.0% FS
Stability*	0.25% FS	0.25% FS
Noise	0.2% FS	0.2% FS
DAS*	0.3% FS	0.3% FS
Strict sum 2 σ error band ...	3.0% FS	2.1% FS
RSS 2 σ error band	1.5% FS	1.1% FS

F. The identified sources of error in the FOXBORO Force Balance dp cell are

Transduction accuracy*	0.25% FS
Noise	2.0% FS
DAS	0.3% FS
Strict sum 2 σ error band	2.6% FS
RSS 2 σ error band	2.0% FS

The following notes need to be considered in evaluating the above 2 σ error bands:

1. Bench calibration data were substituted for the values of nonlinearity, repeatability, and hysteresis since bench data were available and indicated significantly larger error bands for strain gage. The dp sensors in use show a dependence on system pressure for both gain and offset (see Figs. A.5 and A.6). The approach has been to use a calibration equation based on a linear regression calibration of both gain and zero offset in the form:

$$P_{dp} = (P^*A_g + B_g)[V - (P^*A_z + B_z)] ,$$

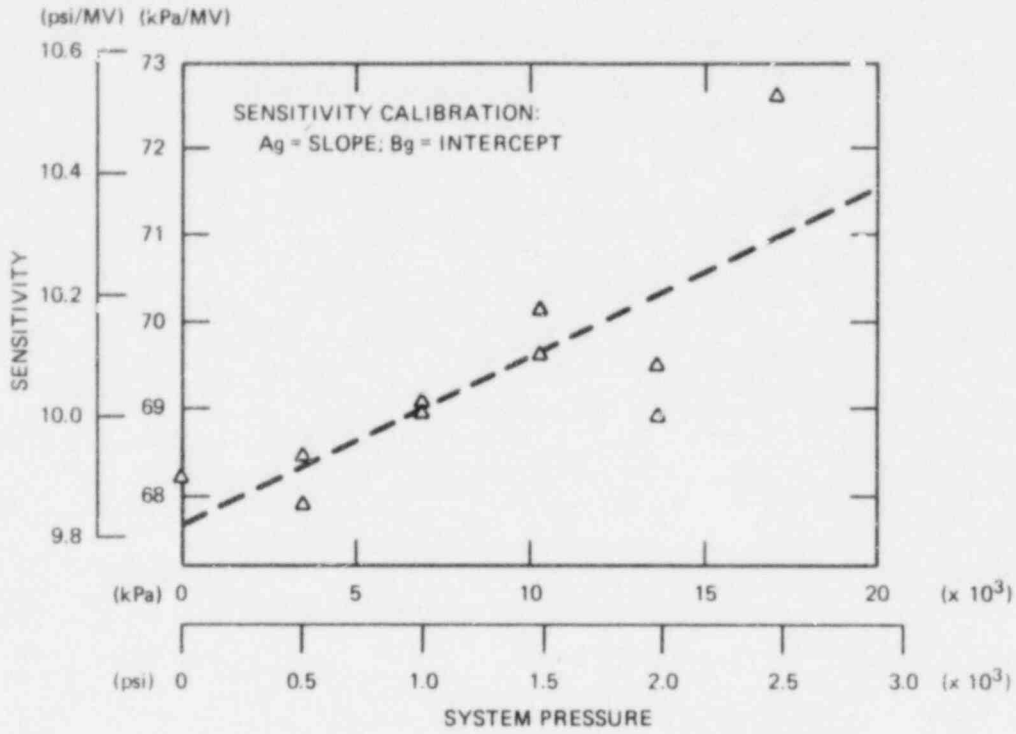


Fig. A.5. Sensitivity calibration.

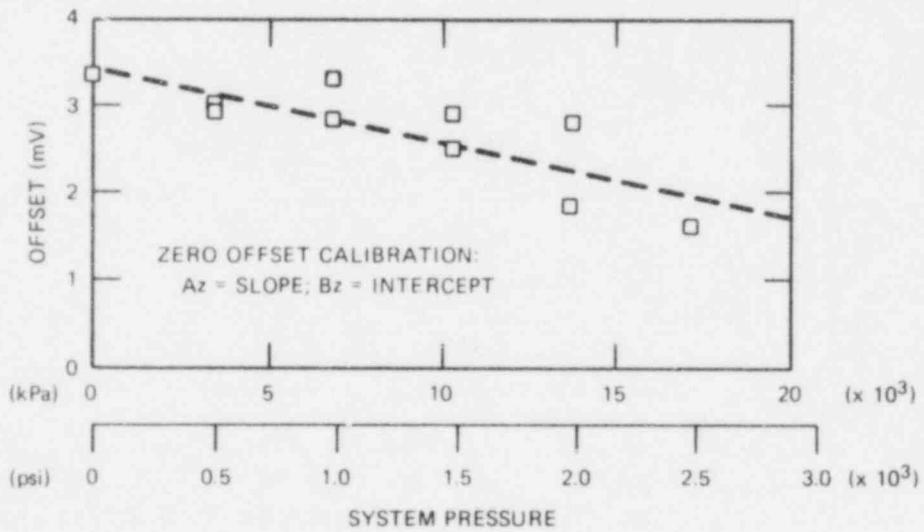


Fig. A.6. Zero offset calibration.

where P_{dp} is the differential pressure measured by the dp cell; A_z , B_z , A_g , B_g are the calibration coefficients; V is the sensor output voltage; and P is the system pressure. However, the linear correlation of system pressure and the constants A_z , B_z , A_g , and B_g are not high enough to make the correlation better than 1.2% (3σ) overall.

2. When the error band was checked using digital data from Reactor Simulation Test 3.05.5B, an average value of σ equivalent to 1.0% FS was measured using 13 PDE's in service prior to blowdown. The average output was used as the standard.

3. When the strain gage dp cells are used as pit dp cells, they are connected to different parts of the system by long lines of small diameter tubing. Analysis of Test 101 showed that resonant ringing could account for an increase in the noise level (as 1σ) to 4.8% FS just prior to blowdown and up to 65% FS after blowdown when the 28-Hz (the measured resonant frequency) notch filter is used as a standard (see Fig. A.7).

4. An in situ calibration was made during steady-state scans for Small Break LOCA II tests of October and November 1980. The uncertainty estimate used water properties as a basis of known differential pressure. The results indicated an average 1σ uncertainty of ± 0.05 kPa (0.2 in.) (0.8% FS).

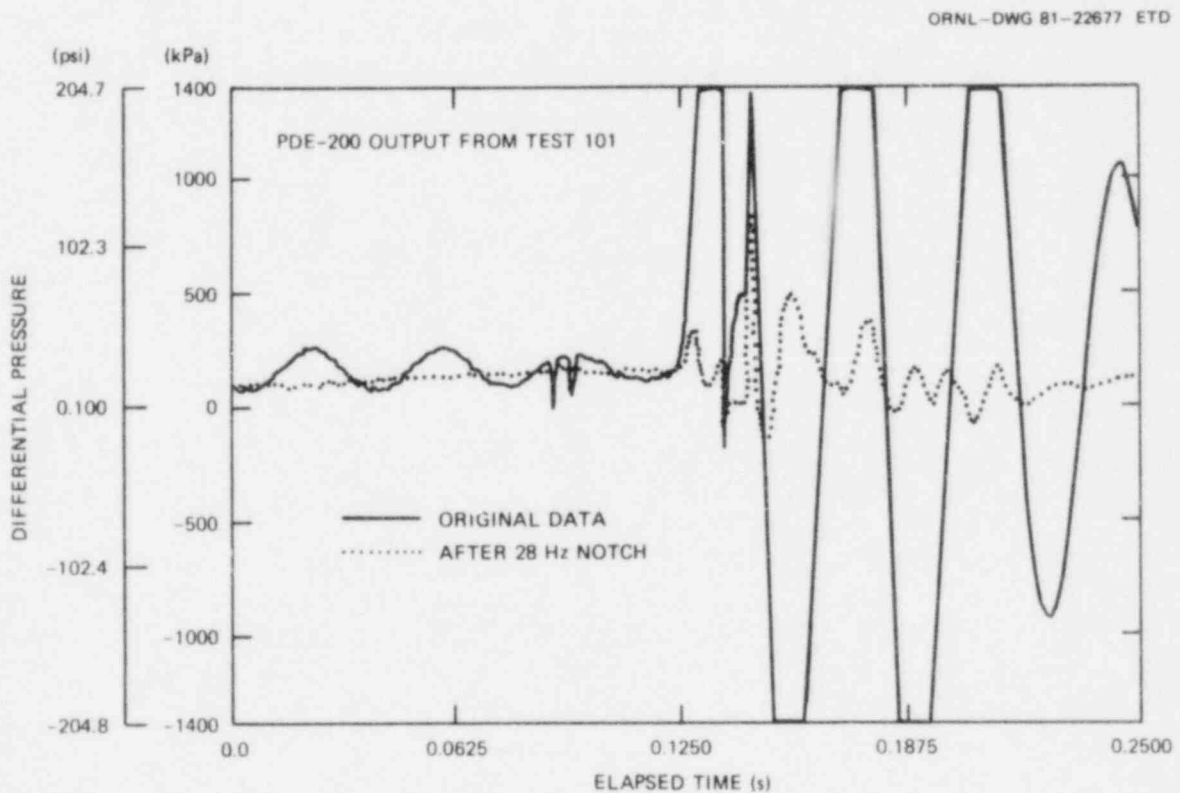


Fig. A.7. PDE-200 output from Test 101.

5. Temperature coefficients were applied over a range of 15°C (27°F).

6. No parameter was identified that would degrade error bands beyond those listed above during two-phase flow. However, extension of the stated error bands to two-phase flow or transient conditions without supporting experimental evidence is done at the data user's risk.

A.5 Thermocouple Temperature Instruments

The thermocouple instruments consist of Chromel-Alumel thermocouples, a "cold-junction" reference box, and the DAS.

The following error sources were identified for thermocouple instruments:

	Minimum value		Above 350°C (660°F)
	(°C)	(°F)	
Thermocouple material*	2.2	4.0	0.76%
Random noise	0.5	1.0	0.2%
DAS calibration	1.8	3.2	0.46%
Reference junction calibration	2.2	4.0	2.2°C (4.0°F)
Reference junction controller	0.16	0.3	0.16°C (0.3°F)
Strict sum 2σ error band	6.9	12.4	(See below)
RSS 2σ error band	3.7	6.7	(See below)

Conversion of the above percentage values to °C results in the following:

Temperature		2σ Error band		2σ Error band strict sum	
(°C)	(°F)	(°C)	(°F)	(°C)	(°F)
350	662	3.7	6.7	7.4	13.3
400	752	4.2	7.6	8.3	14.9
450	842	4.7	8.5	9.1	16.4
500	932	5.1	9.2	10.0	18.0
550	1022	5.6	10.1	10.8	19.4
600	1112	6.1	11.0	11.7	21.1
650	1202	6.6	11.9	12.5	22.5
700	1292	7.1	12.8	13.4	24.1
750	1382	7.6	13.7	14.2	25.6
800	1472	8.0	14.4	15.1	27.8
850	1562	8.5	15.3	15.9	28.6
900	1652	9.0	16.2	16.8	30.2

The following items need to be considered when applying the above error band estimates to THTF data:

1. The reference junction box calibration error was determined by analyzing long-term calibration data from February 4, 1976 to February 10, 1981, and includes any offset from the mean set-point value of 2.666 mV. Reference junction box anomalies were discovered during a 7-day steady-state period. Controller errors up to 0.08°C (0.14°F) were observed for periods of approximately 1 h duration. Operating four units continuously over 7 days, the average error was determined to be less than 0.006°C (0.01°F).

2. Random noise was determined by analyzing the data from Reactor Simulation Test 3.05.5B for five Type Code = 6 and nine Type Code = 1 thermocouples in operation during that test for steady-state, one-phase flow conditions. Because of considerable scatter from instrument-to-instrument and file-to-file, a value of σ large enough to include approximately 95% of all data was chosen. In an effort to provide a conservative estimate, it was assumed that the noise at higher temperatures would be proportional to the millivolt signal above 350°C (660°F).

3. Data Acquisition System calibration was checked after a test calibration with the voltage output compared with a 32.0-mV input signal.

4. A thermocouple that had been in service at the THTF facility was analyzed by R. L. Anderson^s of the I&C standards lab to determine the effect of nickel crystal reordering. The results indicate that errors from 1.2°C (2.2°F) [near 150°C (300°F)] to 16.3°C (29.3°F) [near 900°C (1650°F)] may be expected in addition to the above values. However, the recent history of a specific thermocouple coupled with its end-to-end temperature gradient makes it difficult to extrapolate to all THTF thermocouples. The effect of crystal reordering would be to produce readings higher than actually experienced at the junction.

5. An isothermal scan taken during Test 3.06.6B was used to compare the output of 615 thermocouples believed to be operational. The measured standard (2σ) deviation of 4.0°C (7.2°F) agrees closely with the RSS estimated value of 3.7°C (6.7°F) (2σ).

A.6 Rod Power Instrumentation

The rod power instrumentation consists of two operational amplifiers, a calibrated low resistance shunt, and the DAS (see Fig. A.8). Amplifier 1 reads the voltage across the rod itself. V_1 is the output from the voltage divider. Amplifier 2 reads the voltage across the shunt. The current in the rod is then inferred using Ohm's law such that

$$I = V_2 / R_s ,$$

where I is the current in amps, V_2 is the potential across the shunt in volts, and R_s is the resistance of the shunt in ohms.

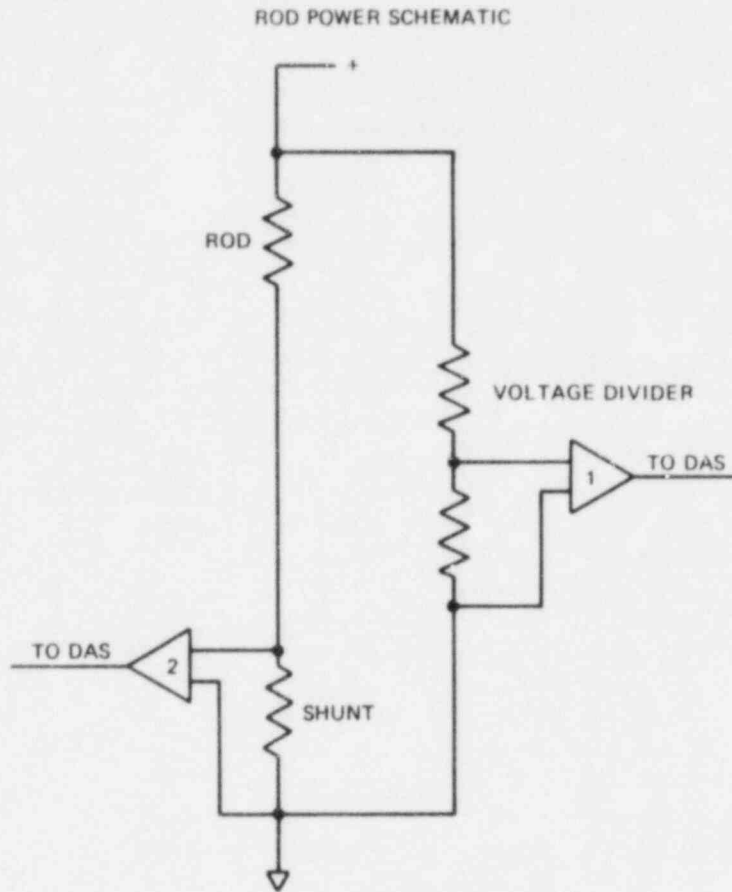


Fig. A.8. Rod power schematic.

The following items were identified as probable sources of error when determining rod power:

R_s	Calibration inaccuracy*	0.26% Reading
R_s	Temperature coefficient	0.2% Reading
V_2	Nonlinearity*	0.01% Reading
V_2	Channel noise	0.72% Reading
V_2	Gain tempco*	0.02% Reading
V_2	Offset tempco*	0.03% FS
V_2	DAS calibration inaccuracy*	0.30% Reading
V_1	Nonlinearity*	0.01% Reading
V_1	Channel noise	0.7% Reading

V_1 Gain tempco*	0.02% Reading
V_1 Offset tempco*	0.03% Reading
V_1 DAS calibration inaccuracy*	0.30% Reading
Strict sum 2σ error band	2.6% Reading
RSS sum 2σ error band	1.1% Reading

The following items need to be considered when applying the above error bands to THTF rod power data:

1. Temperature changes at the amplifiers were assumed to be less than or equal to 20°C (36°F). The temperature changes at the shunt were assumed to be less than or equal to 40°C (72°F). The temperature changes chosen may be excessively large resulting in larger than necessary error bands.
2. No error source was identified which would degrade the steady-state, 2σ error band beyond those listed above.
3. Because of matched voltage divider temperature coefficients and the current calibration procedures, the error contributed by the voltage dividers is considered negligible. However, channel noise was measured at low power, so that the values used might be unnecessarily conservative. Furthermore, the resistance of the shunt is very much less than the rod, so that the voltage drop across the rod is essentially unaffected by the shunt.

A.7 Strain Gage Drag Disks

An analysis of steady-state, single-phase drag disk uncertainties based on subcooled flow calibrations from four THTF tests is presented. The data are from pretest drag disk calibrations performed on the same day of the test during heatup to blowdown conditions for Tests 3.04.7, 3.05.5B, 3.06.6B, and 3.08.6C.

The drag disks are calibrated using the turbine flow meters (velocity, V) and pressure- and temperature-deduced density (ρ) to obtain an in situ standard momentum flux $[(\rho V^2)_{std}]$. A calibration equation is generated from a least-squares fit to the drag disk signal corresponding to the momentum flux over a range of momentum fluxes. The measured momentum flux $[(\rho V^2)_{meas}]$ is obtained by applying the calibration equation to the instrument signal. The calibration equation takes the form:

$$(\rho V^2)_{meas} = A(IS - Z)^E,$$

where IS is the instrument signal in millivolts and A, Z, and E are calibration parameters determined by the least-squares fit. The value of E is generally near 1.0.

An estimate of the uncertainty in the drag disk instrument is made by comparing the in situ standard to the instrument-measured momentum flux.

The errors are formulated in terms of percent of actual momentum flux, which is approximately equivalent to percent of reading. For each data point, the percent error is calculated from

$$\% \text{ error} = \frac{(\rho V^2)_{\text{std}} - (\rho V^2)_{\text{meas}}}{(\rho V^2)_{\text{std}}}$$

Two different drag disk instrument ranges and two different geometries (2-in. and 4-in. spool piece configurations) resulted in three different instrument measurement ranges. It was observed that values of σ for the three different types of drag disks (target and geometry) agree well with each other. It would appear reasonable to combine the data for all three types and report average uncertainties. However, separate uncertainty estimates are made for instrument signals below 10% of maximum range due to a pronounced temperature effect that is especially noticeable at the lower readings. This effect is caused by the strain gage elements being in intimate contact with the fluid. The value of Z is the average of values taken at two different temperatures. The attempted temperature compensation is not very accurate at low signal values.

The resulting uncertainty bands for strain gage drag disks are:

2σ error band below 10% FS	56% reading
2σ error band above 10% FS	19% reading

The following items need to be considered when applying the above error bands to THTF data:

1. Percentage error estimates for the drag disks were compared with the subcooled data immediately preceding blowdown for the tests from which the calibration data were obtained. Average error values of 9.2% of readings (1σ) above 10% FS and 30% of readings (1σ) below 10% FS tend to support the uncertainty bands derived from calibration runs.

2. The strain gage transducer elements are exposed to the temperature environment of the loop. Temperatures significantly outside of the temperature range used during calibration will degrade the accuracy of the instrument further, especially below 10% FS.

A.8 Transient Response and Transient Errors

It is generally understood that no instrument responds infinitely fast to changes in the physical parameters being measured. That is, if the environment were to change suddenly from 200 arbitrary units to 400 arbitrary units, an instrument would initially read some value near 200 units and would approach a reading of 400 units asymptotically. A good approximation for many instruments is first-order lag (see Fig. A.9) defined by

$$V_r = V_o + (1 - e^{-T/\tau})(V_f - V_o)$$

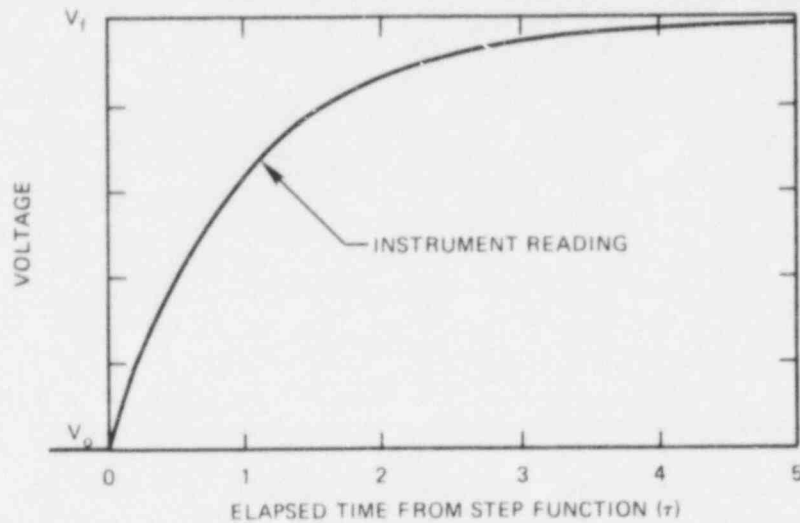


Fig. A.9. Instrument reading as a function of response time assuming first-order lag.

That is, the value indicated by the instrument (V_i) is equal to the original value (V_o) plus the value of the step function ($V_f - V_o$) multiplied by an exponential delay factor. T is the elapsed time and τ is the 63.2% instrument response time. V_f is the final value of the step function. Instrument error as a function of time would be represented by the area between V_f and the instrument reading line.

An additional problem in the THTF uncertainty analysis is introduced because the signal is sampled over discrete time intervals instead of continuously. It may be difficult to identify the exact starting point of a step function. If the step change in physical parameter occurs very near in time to the DAS sample (relative to the instrument response time), the instrument reading at that point will be in error by the total value of the change. If the DAS samples five or more response times after the step function, less than a one percent error (expressed as percent of the step function) will result.

Some arbitrariness is required, therefore, to provide a consistent definition of transient error. The method chosen was to assume that the step function occurred midway between two DAS sampling intervals (n and $n + 1$ in Fig. A.10). The error is measured at each sample point as the distance in engineering units between the modeled instrument reading and the assumed final value of the physical parameter V_f (vertical dashed lines in Fig. A.10). The uncertainty is expressed as the average of all the errors observed during an averaging interval (typically, 150 or 500 ms). The size of the step function and the length of the averaging interval were chosen with test conditions in mind.

As an example, let us consider the errors in the reading of a gamma densitometer (Sect. A.2) as a function of time. The response time on the ionization chamber is estimated at 16 ms. Assuming that the observed density decreases instantly from 750 kg/m (46.8 lb/ft) to 0 (a worst-case,

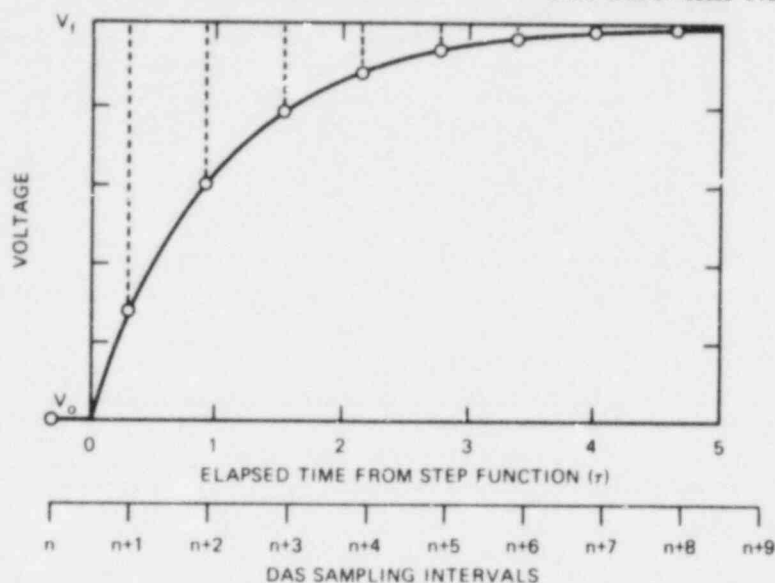


Fig. A.10. Instrument error as a function of DAS sampling assuming first-order lag.

Table A.3

DAS interval ($1n = 0.010$ s)	Error	
	kg/m ³	lb/ft ³
1	549	34.2
2	249	18.3
3	157	9.8
4	84	5.3
5	45	2.8
6	24	1.5
7	13	0.8
8	7	0.4
9	4	0.2
10	2	0.1
Average	118	7.4

blowdown situation), the errors observed at the DAS and the average error for a 100-ms averaging interval reported are shown in Table A.3.

The following items need to be considered when applying transient uncertainty values in the appendices to THTF data:

1. Although first-order lag modeling is appropriate for most instruments, it is at best a close approximation to the true instrument response.

2. The instrument response times are estimates. When these estimates are known from averages, the standard deviation is large, indicating wide variation from instrument-to-instrument. As a result, a particularly

slow instrument of a given type might show errors a factor of 2 or more worse than the average would indicate.

3. The average uncertainty values noted in the tables are extremely sensitive to the averaging interval chosen. Average errors that appear insignificant over a 500-ms averaging interval may well become significant over a 150-ms interval. A careful analysis of Table A.3 is illustrative in this light.

4. Step functions were chosen that were thought to be either representative or worst-case possibilities on a test-by-test basis. It is possible, however, that steps more severe than those chosen may have occurred.

A.9 General Comments

1. All of the above error bands were derived assuming that the specified instrument was in nominal working condition and had been recently calibrated using normal THTF calibration techniques. The error bands will not apply to defective instruments.

2. The error bands stated apply only to those items covered in the above discussion. Although every attempt has been made for the examination to be exhaustive and the results to be conservatively stated, there is always the possibility that excessive instrument noise or out-of-spec components will cause actual readings to be outside of the given error limits (stated as 2σ).

3. The error bands given herein represent the experimenter's best judgment of the applicable uncertainties. Two points should be noted, however. First, the estimation of transient contributions to the uncertainty involves a number of assumptions and judgments. These have been documented in Sect. A.8, and the steady-state and transient contributions to the uncertainty have been listed separately in the tables to facilitate the reader who wishes to use his own estimate of the transient contribution to uncertainty if he chooses. Second, most of the data available on specific sources of instrument errors were obtained in single-phase flow. Thus, the experimenters had to rely primarily on engineering judgment to combine and extrapolate this data to two-phase flow. In most cases there is no experimental, two-phase flow data that can be used to verify the resulting uncertainty estimates.

A.10 Steady-State and Transient Instrument Uncertainties

The following tables summarize the steady-state and transient uncertainty bands for all THTF instruments.

Table A.4 provides a cross reference for instrument application numbers (IAN) and type codes. The first column provides the type code as an integer between 1 and 113. The second column lists the form of the IAN, and the "Remarks" column provides additional information to properly correlate type code to IAN for all instruments.

Tables A.5-A.8 provide a summary listing of steady-state and transient error bands by test. Tables A.5 and A.6 have values stated in SI

Table A.4. Type code - IAN No. table

Type code	IAN	Remarks
1	TE-3nnal	Special FRS sheath thermocouples [0.38 mm (0.015 in.)] nn = 01, 14, 17, 21, 34, 37, 38, 50, 54, or 60 a = A, E, or F l = 1, 2, 3, 4, 5, 6, 7, 8; or E, F, or G
1	TE-3nnal	Regular FRS sheath thermocouples [0.51 mm (0.020 in.)] nn = 01-64 (except 19, 22, 36, 46) and (excluding 01, 14, 17, 21, 34, 37, 38, 50, 54, 60 for Tests 3.06.6B, 3.08.6C, 3.07.9, 3.09.10I-X, and 3.10.11A-H a = A, B, or C l = A, B, C, D, E, F, G, H, U, or Y
2	TE-3nnMl	Special FRS middle thermocouples [0.38 mm (0.015 in.)] nn = 01, 14, 17, 21, 34, 37, 38, 50, 54, or 60 M = M l = 1, 2, 3, 4, 5, 6, 7, 8; or E, F, or G
2	TE-3nnMl	Regular FRS middle thermocouples [0.51 mm (0.020 in.)] nn = 01-64 (except 19, 22, 36, 46) and (excluding 01, 14, 17, 21, 34, 37, 38, 50, 54, 60 for tests 3.06.6B, 3.08.6C, 3.07.9, 3.09.10I-X, and 3.10.11A-H M = M l = A, B, C, D, E, F, or G
3	TE-12nn	Subchannel thermocouples nn = 01-81
4	TE-18na	Shroud wall thermocouples n = 1, 2, 3, 4, 5, 6, or 7 a = N, E, S, or W
5	TE-xxx	Miscellaneous and process thermocouples xxx = 5B, 408B, 520B, 521, 901, 920, 921, 922, 923, 924, 925, 926, 927, or 936
6	TE-xxx	Loop and process thermocouples xxx = 1, 2, 6, 24, 29, 40, 45, 57, 62, 67, 116, 150, 151, 152, 153, 172, 208, 212, 222, 228, 256, 266, 281, 282, 284
7	TE-29na	Spacer grid thermocouples n = 1, 2, 3, 4, 5, or 6 a = A, B, C, D, E, or F
8	TE-18nal	Array rod thermocouples n = 8 or 9 a = A or B l = A, B, C, D, E, F, or G
9	TE-361aj	O-ring area thermocouples a = A, B, or C J = J

Table A.4 (continued)

Type code	IAN	Remarks
10	TE-nab	Shroud box thermocouples n = 0, 1, 2, 3, 4, 5, 6, 7, 8, or 9 a = A or B b = E or S
23	PE-xxx	Strain gage pressure cells [20700 kPa (3000 psi)] xxx = 15, 16, 26, 27, 42, 43, 44, 58, 63, 68, 76, 88, 106, 118, 156, 174, 201, 209, 224, 258, 268, 276, 281, 282, 283, 286, 425, 427, 454, 474
24	PE-32	Force balance pressure cell (both ranges)
25	PE-102	Strain gage pressure cell [1380 kPa (200 psi)]
26	PDE-xxx	Strain gage dp cell [± 1380 kPa (± 200 psi)] xxx = 35, 46, 167, 217 21 except for Tests 3.09.10I-X, 3.09.10AA-HH, and 3.10.11A-H 60 except for Test 3.05.5B
27	PDE-78	Strain gage dp cell [± 6900 kPa (1000 psi)]
28	PDE-xxx	Strain gage dp cell [± 345 kPa (± 50 psi)] xxx = 7, 53, 65, 111, 203 21 only for Tests 3.09.10I-X, 3.09.10AA-HH, and 3.10.11A-H 60 only for Test 3.05.5B 200 except for 3.02.10C-H and 3.10.11A-H 251 except for 3.02.10C-H, 3.09.10I-X, and 3.09.10AA-HH
29	PE-nnn	Strain gage pressure cell [2400 kPa (350 psi)] nnn = 526 or 616
31	EIE-13nn	FRS heater rod currents nn = 01-64 (excluding 19, 22, 36, 46)
32	EIE-xx	Generator currents xx = 9, 10, 11, 12
33	EEE-xx	Generator voltage xx = 9, 10, 11, 12
34	EWE-77A	Primary pump power
35	FMFE-xxx	Momentum flux flow (drag disk) [9-cm (3.5-in.) spool piece] xxx = 22, 38, 170, 220 206 except for 3.09.10I-X and 3.09.10AA-HH 254, 264 only for 3.05.5B
36	SE-72	Primary pump speed
37	XE-430a	Break wire detector a = A or B

Table A.4 (continued)

Type code	IAN	Remarks
40	FMFE-xxx	Momentum flux flow (drag disk) [5-cm (2-in.) spool piece] xxx = 14, 55, 61, 66, 114, 154, 155 206 only for 3.09.10I-X and 3.09.10AA-HH 254, 264 except for 3.04.5B
41	PDE-200	Strain gage dp cell [± 25 kPa (± 100 in.) water] only for Tests 3.02.10C-H
42	PDE-204	Strain gage dp cell [± 125 kPa (± 500 in.) water] only for Test 3.05.5B
	PDE-261	except for 3.08.6C, 3.07.9, 3.09.10I-X, 3.09.10AA-HH, and 3.10.11A-H
43	PDE-nnn	Strain gage dp cell [± 41 kPa (± 6 psi)] nnn = 199, 271 204 except for 3.05.5B 251 only for 3.02.10C-H 261 only for 3.08.6C, 3.07.9, 3.09.10I-X, 3.09.10AA-HH, and 3.10.11A H
50	LE-14nn	Experimental INEL level probe nn = 01-19
71	TE-28B	Linearized resistance thermometer device
75	PDE-nnn	Capacitive dp cell nnn = 180-189 [0-37.5 kPa (0-150 in.) only for Test 3.05.5B] 180-188 [0-6.25 kPa (0-25 in.) except for Test 3.05.5B] 189 [0-7.5 kPa (0-30 in.) except for Test 3.05.5B] 200 [0-25 kPa (0-100 in.) only for Test 3.10.11A-H] 251 [0-50 kPa (0-200 in.) only for Test 3.10.11A-H]
76	ZE-336U ZE-346L	In-bundle gamma densitometer position indicator only for 3.09.10I-X, 3.09.10AA-HH, and 3.10.11A-H
77	ZE-346L	In-bundle gamma densitometer position indicator only for 3.09.10I-X, 3.09.10AA-HH, and 3.10.11A-H
80	PDE-189	Capacitance dp cell [7.5 kPa (30 in.)] only for 3.09.10I-X, 3.09.10AA-HH, and 3.10.11A-H
95	FE-nnn	Turbine flowmeter - heat exchanger secondary flow nnn = 522, 620, 720
96	FE-550	Turbine flowmeter - heat exchanger secondary flow

Table A.4 (continued)

Type code	IAN	Remarks
97	PDE-48	Force balance dp cell [166 kPa (24 psi)]
98	PDE-30	Force balance dp cell [345 kPa (50 psi)]
99	TDE-28	Differential temperature
105	PDE-761 LE-100	Force balance dp cell
106	DE-xxx	Single-beam gamma densitometer xxx = 20, 36, 168, 218 Triple-beam gamma densitometer xxx = 204A, 204B, 204C, 252A, 252B, 252C, 262A, 262B, 262C
107	FE-xxx	Orifice plate/force balance flowmeter xxx = 1A [0-5.0E-2 m ³ /s (0-800 gpm)] 238 [0-1.0E-4 m ³ /s (0-1.6 gpm)] only 3.09.10I-X Orifice plate/capacitance flowmeter xxx = 282 [0-2.5E-3 m ³ /s (0-39.3 gpm)] 283 [0-3.3E-4 m ³ /s (0-5.2 gpm)] 927 [0-1.4E-4 m ³ /s (0-2.1 gpm)]
108	FE-18A FE-18A FE-238	Orifice plate/force balance flowmeter [4.4E-2 m ³ /s (700 gpm)] except for 3.01.10C-H, 3.09.10I-X, 3.09.10AA-HH, and 3.10.11A-H [1.7E-4 m ³ /s (2.7 gpm)] only for 3.01.10C-H, 3.09.10I-X, 3.09.10AA-HH, and 3.10.11A-H except for 3.09.10I-X
109	FE-xxx	Instrument spool piece turbine flowmeter [3E-4 m ³ /s (5 gpm)] xxx = 250, 260 only for Tests 3.01.10C-H, 3.09.10I-X, 3.09.10AA-HH, and 3.10.11A-H [6E-4 m ³ /s (10 gpm)] xxx = 232, 280 [1.4E-2 m ³ /s (225 gpm)] xxx = 3, 51, 59, 64, 110 [1.4E-2 m ³ /s (225 gpm)] xxx = 250, 260 except for 3.01.10C-H, 3.05.5B, 3.09.10I-X, 3.09.10AA-HH, and 3.10.11A-H [1.4E-2 m ³ /s (225 gpm)] xxx = 202 only for Tests 3.01.10C-H, 3.09.10I-X, and 3.09.10AA-HH [6E-2 m ³ /s (1000 gpm)] xxx = 19, 34, 166, 216, 440, 460 [6E-2 m ³ /s (1000 gpm)] xxx = 250, 260 for 3.05.5B [6E-2 m ³ /s (1000 gpm)] xxx = 202 except for Tests 3.01.10C-H, 3.09.10I-X, and 3.09.10AA-HH
110	TE-xxx	Resistance thermometer device xxx = 4B, 101, 210A, 525, 557, 615, 627, 727
111	DE-xxx	In-bundle gamma densitometer xxx = 336U, 346L

Table A.5. Nominal case instrument uncertainties

THTF instrument error bands						
Instrument description	Type code	Instrument range	Steady-state error	Transient error	Estimated response time	Assumed value of step Fn.
Rod sheath thermocouple 9.370mm OD	1	273 K 1309 K	3.7 K < 623 K 10.3 K	N.S. ^{a,j}	7 ms	5 K
Rod sheath thermocouple 0.51-mm OD	1	273 K 1309 K	3.7 K < 623 K 10.3 K	0.1 K ^a	12 ms	5 K
Rod middle thermocouple 0.38-mm OD	2	273 K 1309 K	3.7 K < 623 K 10.3 K	N.S. ^a	7 ms	5 K
Rod middle thermocouple 0.51-mm OD	2	273 K 1309 K	3.7 K < 623 K 10.3 K	0.1 K ^a	12 ms	5 K
Bundle sub-channel thermocouple 1.02-mm OD	3	273 K 1309 K	3.7 K < 623 K 10.3	2.7 K	140 ms	10 K
Shroud box thermocouple 1.57-mm OD	4	273 K 1309 K	3.7 K < 623 K 10.3 K	5.3 K	350 ms	10 K
System thermocouple 3.2-mm OD	5	273 K 1309 K	3.7 K < 623 K 10.3 K	7.6 K	870 ms	10 K
System (Namac) thermocouple 6.4-mm OD	6	273 K 1309 K	3.7 K < 623 K 10.3 K	0.3 K	18 ms	10 K
Spacer grid thermocouple 1.02-mm OD	7	273 K 1309 K	3.7 K < 623 K 10.3 K	2.7 K	140 ms	10 K
Array rod thermocouple 1.02-mm OD	8	273 K 1309 K	3.7 K < 623 K 10.3 K	2.7 K	140 ms	10 K
Rod sheath thermocouple 0.51-mm OD	9	273 K 1309 K	3.7 K < 623 K 10.3 K	0.1 K ^a	12 ms	5 K

Table A.5 (continued)

THIF instrument error bands						
Instrument description	Type code	Instrument range	Steady-state error	Transient error	Estimated response time	Assumed value of step Fn.
Shroud box thermocouple 1.57-mm OD	10	273 K 1309 K	3.7 K < 623 K 10.3 K	5.3 K	350 ms	10 K
Strain gage pressure cell	23	20700 kPa	200 kPa	N.S.	0.16 ms	20 kPa
Force balance pressure cell	24	3400 kPa 17000 kPa	100 kPa	10 kPa	300 ms	20 kPa
Force balance pressure cell	24	3400 kPa 27000 kPa	160 kPa	10 kPa	300 ms	20 kPa
Strain gage pressure cell	25	1380 kPa	17 kPa	N.S.	0.32 ms	20 kPa
Strain gage dp cell	26	±1380 kPa	43 kPa	N.S.	0.32 ms	20 kPa
Strain gage dp cell	27	±6900 kPa	210 kPa	N.S.	0.32 ms	20 kPa
Strain gage ^g dp cell	28	±345 kPa	11 kPa	N.S.	0.32 ms	20 kPa
Strain gage pressure cell	29	2400 kPa	24 kPa	N.S.	0.16 ms	20 kPa
Rod heater current	31	800 A	0.85% Reading	N.A. ^k	50 ms	N.A.
Generator current	32	1000 A	0.85% Reading	N.A.	50 ms	N.A.
Generator voltage	33	300 V	0.76% Reading	N.A.	50 ms	N.A.
Primary pump power	34	750 kW	greater of 0.5 kW or 0.3% Reading	2.9 kW	150 ms	10 kW
Strain gage drag disk	35	±0.1E5 kg/ms ² ±1.0E5 kg/ms ²	56% Reading 19% Reading	31 kg/ms ²	16 ms	1E3 kg/ms ²
Primary pump speed	36	100 rpm 5400 rpm	20 rpm	6 rpm	150 ms	20 rpm
Breakwire detector	37	5 V	30 ms	N.A.	20 ms	N.A.
Strain gage drag disk	40	±0.2E5 kg/ms ² ±2.1E5 kg/ms ²	56% Reading 19% Reading	31 kg/ms ²	16 ms	1E3 kg/ms ²

Table A.5 (continued)

THTP instrument error bands						
Instrument description	Type code	Instrument range	Steady-state error	Transient error	Estimated response time	Assumed value of step Fn.
Strain gage dp cell	41	± 25 kPa	0.8 kPa	N.S.	0.32 ms	20 kPa
Strain gage dp cell	42	± 125 kPa	4 kPa	N.S.	0.32 ms	20 kPa
Strain gage dp cell	43	± 41 kPa	2 kPa	N.S.	0.32 ms	20 kPa
Level ⁱ indicator	50	± 10 V	***	***	***	***
RTD	71	273 K 700 K	1.1 K 2.7 K	9.7 K	10 s	10 K
Capacitive dp cell	75	6.2 kPa	0.1 kPa	N.S.	131 ms	0.01 kPa
Capacitive dp cell	75	37.5 kPa	0.4 kPa	N.S.	74 ms	0.01 kPa
Position indicator	76	3.92 m	0.5% Reading	N.A.	N.A.	N.A.
Position indicator	77	3.33 m	0.5% Reading	N.A.	N.A.	N.A.
Capacitive dp cell	80	7.5 kPa	0.1 kPa	N.S.	125 ms	0.01 kPa
Turbine ^f flowmeter	95	0.9E-3 m ³ /s 9.5E-3 m ³ /s	4.1% Reading	N.S.	11 ms 1.2 ms	6E-5 m ³ /s 12E-5 m ³ /s
Turbine ^f flowmeter	96	0.3E-3 m ³ /s 3.2E-3 m ³ /s	4.1% Reading	N.S.	8 ms 1 ms	6E-5 m ³ /s 12E-5 m ³ /s
Force balance dp cell	97	166 kPa	1 kPa	10 kPa	300 ms	20 kPa
Capacitive dp cell	98	345 kPa	18 kPa	1.5 kPa	38 ms	20 kPa
Differential temperature	99	228 K 283 K	3.8 K	9.8 K	10 s	10 K
Liquid level	105	3.81 m	0.023 m	0.10 m	300 ms	0.2 m
Liquid level	105	1408 m	8.5 m	0.10 m	300 ms	0.2 m
Gamma densitometer	106	1000 kg/m ³	104 kg/m ³	N.A.	16 ms	N.A.
Orifice ^c flowmeter	107	1.0E-4 m ³ /s	2.5E-6 m ³ /s	4.9E-6 m ³ /s	300 ms	1E-5 m ³ /s

Table A.5 (continued)

THIF instrument error bands						
Instrument description	Type code	Instrument range	Steady-state error	Transient error	Estimated response time	Assumed value of step Fn.
Orifice ^c flowmeter	107	1.35E-4 m ³ /s	3.4E-6 m ³ /s	6.6E-6 m ³ /s	300 ms	1.4E-5 m ³ /s
Orifice ^c flowmeter	107	3.32E-4 m ³ /s	8.3E-6 m ³ /s	1.4E-5 m ³ /s	300 ms	2.9E-5 m ³ /s
Orifice ^c flowmeter	107	2.48E-3 m ³ /s	6.2E-5 m ³ /s	1.4E-5 m ³ /s	300 ms	2.9E-5 m ³ /s
Orifice ^c flowmeter	107	5.0E-2 m ³ /s	1.3E-3 m ³ /s	2.4E-3 m ³ /s	300 ms	5E-3 m ³ /s
Orifice ^d flowmeter	108	1.7E-4 m ³ /s	4.2E-6 m ³ /s	8.3E-6 m ³ /s	300 ms	1.7E-5 m ³ /s
Orifice ^e flowmeter	108	4.4E-2 m ³ /s	1.1E-3 m ³ /s	2.1E-3 m ³ /s	300 ms	4.4E-3 m ³ /s
Turbine ^{f_sh} flowmeter	109	±0.3E-4 m ³ /s ±3.0E-4 m ³ /s	4.1% Reading	N.S.	8 ms 1 ms	6E-5 m ³ /s 1.2E-4 m ³ /s
Turbine ^{f_sh_sb} flowmeter	109	±0.6E-4 m ³ /s ±6.1E-4 m ³ /s	2.5% Reading	N.A.	8 ms 1 ms	N.A.
Turbine ^{f_sh_sl} flowmeter	109	±1.3E-3 m ³ /s ±1.4E-2 m ³ /s	4.1% Reading	N.S.	13 ms 2 ms	6E-5 m ³ /s 1.2E-4 m ³ /s
Turbine ^{f_sh_sl} flowmeter	109	±0.6E-2 m ³ /s ±6.1E-2 m ³ /s	4.1% Reading	N.S.	18 ms 2 ms	6E-5 m ³ /s 1.2E-4 m ³ /s
RTD	110	273 K 700 K	1.1 K 2.7 K	9.8 K	10 s	10 K
In-bundle gamma densitometer	111	1000 kg/m ³	104 kg/m ³	N.A.	16 ms	N.A.
Steady-state error bands:	Two standard deviations compared to in situ standard or twice the root-sum-square of uncertainties, whichever is applicable.					
Transient error bands:	Assuming first-order lag function, response times (TAU), and step function ($V_f = V_o$) indicated - the average error seen by the DAS assuming the step function occurred midway between DAS samples. The averaging interval is 500 ms for thermocouples and 500 ms for all other instruments.					
Total error:	The total error due to steady-state error and transient error is the sum of the steady-state and transient error bands.					

Table A.5 (continued)

^aError bands apply to the environment as sensed at the surface of the thermocouple sheath. Larger errors may occur when data are modeled to provide temperatures at other points. Transient response is estimated by using the response time (25 ms or less) prior to swaging the sheath (0.028 in. swaged to 0.020-in. OD) and then scaling using the rule that response time is inversely proportional to the outside diameter squared (OD² scaling). An additional 7% improvement in response time was allowed for packing of the boron nitride during swaging. The smaller thermocouples (0.020 in. swaged to 0.015 in.) were estimated from the values of the larger thermocouples by first scaling the 25-ms response time to the unswaged 0.020-in. diameter using OD² scaling and then applying OD² scaling and the 7% improvement for packing to the swaged 0.015-in. OD.

^bThis instrument is fitted with Flow Technology electronics that time 10-blade passings. Averaging improves the steady-state error bands but degrades transient response.

^cRange applies specifically to instruments calibrated in subcooled liquid at a density of 62.4 lb/ft³.

^dRange applies specifically to instruments calibrated in subcooled liquid at a density of 53.7 lb/ft³.

^eRange applies specifically to instruments calibrated in subcooled liquid at a density of 46.8 lb/ft³.

^fError bands apply specifically to instruments calibrated in subcooled liquid. Extended range electronics provide readings out to 3600 gpm for the 3.5-in.-diam models and 445 gpm for the 2-in.-diam models, but the error bands apply only to 150% of nominal maximum range.

^gStrain gage dp cells used as pit cells are connected to different segments of the test section by long lines. These long lines induce resonant oscillations in the instrument that increase the steady-state error bands to 5 psi and the transient error bands to 60 psi in the interval immediately following blowdown.

^hThe turbine flowmeters (type code 109) have a flow range such that

-5.0 < Flow < -0.5	or	0.5 < Flow < 5.0,
-10.0 < Flow < -1.0	or	1.0 < Flow < 10.0,
-225 < Flow < -22	or	22 < Flow < 225,
-1000 < Flow < -100	or	100 < Flow < 1000.

ⁱThe INEL level probe is an experimental device and as such does not have well-documented error bands.

^jNo significant error over the averaging interval.

^kN.A. implies not applicable.

^lFlow Technology supplies calibration constants over the ranges 10-300 gpm and 80-1000 gpm, respectively. The uncertainty bands for these instruments should approach the quoted values for these ranges, but special care may be required. (See the section on turbine flowmeters in the critical instruments section.)

Table A.5 (continued)

Basis for steady-state and transient error bands by type code		
Type Code	Steady state	Transient
1	Critical instrument	Manufacturer's specification, OD ² scaling
2	Critical instrument	Manufacturer's specification, OD ² scaling
3	Critical instrument	Work of Carroll and Sheppard
4	Critical instrument	Work of Carroll and Sheppard
5	Critical instrument	Work of Carroll and Sheppard
6	Critical instrument	Manufacturer's specification
7	Critical instrument	Work of Carroll and Sheppard
8	Critical instrument	Work of Carroll and Sheppard
9	Critical instrument	Manufacturer's specification, OD ² scaling
10	Critical instrument	Work of Carroll and Sheppard
23	Critical instrument	Table B.2
24	Manufacturer's specification	Table B.2
25	Bench calibration + DAS	Table B.2 (inferred)
26	Critical instrument	Table B.2
27	Critical instrument	Table B.2
28	Critical instrument	Table B.2
29	Critical instrument	Table B.2 (inferred)
31	Critical instrument	Table B.2 (inferred)
32	Inferred (type code 31)	Table B.2 (inferred)
33	Critical instrument	Table B.2 (inferred)
34	Manufacturer's specification	Manufacturer's specification
35	Critical instrument	Table B.2
36	Bench calibration + DAS	Inferred (type code 34)
37	From Test 3.03.6AR	From Test 3.03.6AR
40	Critical instrument	Table B.2
43	Critical instrument	Table B.2 (inferred)
50	*****	*****
71	Bench calibration and specifications	Table B.2
75	Critical instrument	Manufacturer's specification
76	Engineering judgment	N.A.
77	Engineering judgment	N.A.
78	Critical instrument	Inferred (type code 75)
79	Inferred (type code 75)	Inferred (type code 75)
80	Inferred (type code 75)	Inferred (type code 75)
95	Inferred (type code 109)	Work of N. Chen
96	Inferred (type code 109)	work of N. Chen
97	Critical instrument	Table B.2

Table A.5 (continued)

Basis for steady-state and transient error bands by type code		
Type Code	Steady state	Transient
98	Critical instrument	Inferred (type code 75)
99	Inferred (type code 71)	Inferred (type code 71)
105	Manufacturer's specification	Table B.2 (inferred)
106	Critical instrument	Work of R. Shipp (manufacturer's specification)
107	In situ calibration	Table B.2 (inferred)
108	Inferred (type code 107)	Table B.2 (inferred)
109	Critical instrument	Work of N. Chen
110	Bench calibration and specifications	Table B.2
111	Inferred (type code 106)	Inferred (type code 109)

Table A.6. Worst-case instrument uncertainties

THIF instrument error bands						
Instrument description	Type code	Instrument range	Steady-state error	Transient error	Estimated response time	Assumed value of step Fn.
Rod sheath thermocouple 0.38-mm OD	1	273 K 1309 K	3.7 K < 623 K 10.3 K	0.8 K ^a	7 ms	300 K
Rod sheath thermocouple 0.51-mm OD	1	273 K 1309 K	3.7 K < 623 K 10.3 K	3.8 K ^a	12 ms	300 K
Rod middle thermocouple 0.38-mm OD	2	273 K 1309 K	3.7 K < 623 K 10.3 K	0.8 K ^a	7 ms	300 K
Rod middle thermocouple 0.51-mm OD	2	273 K 1309 K	3.7 K < 623 K 10.3 K	3.8 K ^a	12 ms	300 K
Bundle sub-channel thermocouple 1.02-mm OD	3	273 K 1309 K	3.7 K < 623 K 10.3 K	40.6 K	140 ms	150 K
Shroud box thermocouple 1.57-mm OD	4	273 K 1309 K	3.7 K < 623 K 10.3 K	79.8 K	350 ms	150 K
System thermocouple 3.2-mm OD	5	273 K 1309 K	3.7 K < 623 K 10.3 K	114.1 K	870 ms	150 K
System (Namac) thermocouple 6.4-mm OD	6	273 K 1309 K	3.7 K < 623 K 10.3 K	4.0 K 1.3 K	18 ms	150 K 50 K
Spacer grid thermocouple 1.02-mm OD	7	273 K 1309 K	3.7 K < 623 K 10.3 K	40.6 K	140 ms	150 K
Array rod thermocouple 1.02-mm OD	8	273 K 1309 K	3.7 K < 623 K 10.3 K	40.6 K	140 ms	150 K
Rod sheath thermocouple 0.51-mm OD	9	273 K 1309 K	3.7 K < 623 K 10.3 K	3.8 K ^a	12 ms	300 K

Table A.6 (continued)

THTF instrument error bands						
Instrument description	Type code	Instrument range	Steady-state error	Transient error	Estimated response time	Assumed value of step Fn.
Shroud box thermocouple 1.57-mm OD	10	273 K 1309 K	3.7 K < 623 K 10.3 K	79.8 K	350 ms	150 K
Strain gage pressure cell	23	20700 kPa	200 kPa	N.S. ^j	0.16 ms	20 kPa
Force balance pressure cell	24	3400 kPa 17000 kPa	100 kPa	117 kPa	300 ms	240 kPa
Force balance pressure cell	24	3400 kPa 27000 kPa	160 kPa	117 kPa	300 ms	240 kPa
Strain gage pressure cell	25	1380 kPa	17 kPa	N.S.	0.32 ms	20 kPa
Strain gage dp cell	26	±1380 kPa	43 kPa	N.S.	0.32 ms	20 kPa
Strain gage dp cell	27	±6900 kPa	210 kPa	N.S.	0.32 ms	20 kPa
Strain gage ^g dp cell	28	±345 kPa	11 kPa	N.S.	0.32 ms	20 kPa
Strain gage pressure cell	29	2400 kPa	24 kPa	N.S.	0.16 ms	20 kPa
Rod heater current	31	800 A	0.85% Reading	N.A. ^k	50 ms	N.A.
Generator current	32	1000 A	0.85% Reading	N.A.	50 ms	N.A.
Generator voltage	33	300 V	0.76% Reading	N.A.	50 ms	N.A.
Primary pump power	34	750 kW	Greater of 0.5 kW or 0.3% Reading	2.9 kW	150 ms	10 kW
Strain gage drag disk	35	±0.1E5 kg/ms ² ±1.0E5 kg/ms ²	56% Reading 19% Reading	31 kg/ms ²	16 ms	1E3 kg/ms ²
Primary pump speed	36	100 rpm 5400 rpm	20 rpm	6 rpm	150 ms	20 rpm
Breakwire detector	37	5 V	30 ms	N.A.	20 ms	N.A.
Strain gage drag disk	40	±0.2E5 kg/ms ² ±2.1E5 kg/ms ²	56% Reading 19% Reading	31 kg/ms ²	16 ms	1E3 kg/ms ²

Table A.6 (continued)

THTF instrument error bands						
Instrument description	Type code	Instrument range	Steady-state error	Transient error	Estimated response time	Assumed value of step Fn.
Strain gage dp cell	41	± 25 kPa	0.8 kPa	N.S.	0.32 ms	20 kPa
Strain gage dp cell	42	± 125 kPa	4 kPa	N.S.	0.32 ms	20 kPa
Strain gage dp cell	43	± 41 kPa	2 kPa	N.S.	0.32 ms	20 kPa
Level ⁱ indicator	50	± 10 V	***	***	***	***
RTD	71	273 K 700 K	1.1 K 2.7 K	9.7 K	10 s	10 K
Capacitive dp cell	75	6.2 kPa	0.1 kPa	0.03 kPa	131 ms	0.1 kPa
Capacitive dp cell	75	37.5 kPa	0.4 kPa	0.01 kPa	74 ms	0.1 kPa
Position indicator	76	3.92 m	0.5% Reading	N.A.	N.A.	N.A.
Position indicator	77	3.33 m	0.5% Reading	N.A.	N.A.	N.A.
Capacitive dp cell	80	7.5 kPa	0.1 kPa	0.02 kPa	125 ms	0.1 kPa
Turbine ^f flowmeter	95	$0.9E-3$ m ³ /s $9.5E-3$ m ³ /s	4.1% Reading	$8.1E-6$ m ³ /s	11 ms 1.2 ms	$1.3E-3$ m ³ /s
Turbine ^f flowmeter	96	$0.3E-3$ m ³ /s $3.2E-3$ m ³ /s	4.1% Reading	$8.1E-6$ m ³ /s	8 ms 1 ms	$1.3E-3$ m ³ /s
Force balance dp cell	97	166 kPa	1 kPa	10 kPa	300 ms	20 kPa
Capacitive dp cell	98	345 kPa	18 kPa	1.5 kPa	38 ms	20 kPa
Differential temperature	99	228 K 283 K	3.8 K	9.8 K	10 s	10 K
Liquid level	105	3.81 m	0.023 m	0.10 m	300 ms	0.2 m
Liquid level	105	1408 m	8.5 m	0.10 m	300 ms	0.2 m
Gamma densitometer	106	1000 kg/m ³	104 kg/m ³	N.A.	16 ms	N.A.
Orifice ^c flowmeter	107	$1.0E-4$ m ³ /s	$2.5E-6$ m ³ /s	$4.9E-6$ m ³ /s	300 ms	$1E-5$ m ³ /s

Table A.6 (continued)

THIF instrument error bands						
Instrument description	Type code	Instrument range	Steady-state error	Transient error	Estimated response time	Assumed value of step Fn.
Orifice ^c flowmeter	107	1.35E-4 m ³ /s	3.4E-6 m ³ /s	6.6E-6 m ³ /s	300 ms	1.4E-5 m ³ /s
Orifice ^c flowmeter	107	3.32E-4 m ³ /s	8.3E-6 m ³ /s	2.9E-5 m ³ /s	300 ms	6.0E-5 m ³ /s
Orifice ^c flowmeter	107	2.48E-3 m ³ /s	6.2E-5 m ³ /s	2.9E-5 m ³ /s	300 ms	6.0E-5 m ³ /s
Orifice ^c flowmeter	107	5.0E-2 m ³ /s	1.3E-3 m ³ /s	2.4E-3 m ³ /s	300 ms	5E-3 m ³ /s
Orifice ^d flowmeter	108	1.7E-4 m ³ /s	4.2E-6 m ³ /s	8.3E-6 m ³ /s	300 ms	1.7E-5 m ³ /s
Orifice ^e flowmeter	108	4.4E-2 m ³ /s	1.1E-3 m ³ /s	2.1E-3 m ³ /s	300 ms	4.4E-3 m ³ /s
Turbine ^{f_sh} flowmeter	109	±0.3E-4 m ³ /s ±3.0E-4 m ³ /s	4.1% Reading	N.S.	8 ms 1 ms	1.5E-4 m ³ /s
Turbine ^{f_sh₃b} flowmeter	109	±0.6E-4 m ³ /s ±6.1E-4 m ³ /s	2.5% Reading	N.A.	8 ms 1 ms	N.A.
Turbine ^{f_sh₃l} flowmeter	109	±1.3E-3 m ³ /s ±1.4E-2 m ³ /s	4.1% Reading	N.S.	13 ms 2 ms	1.3E-3 m ³ /s
Turbine ^{f_sh₃l} flowmeter	109	±0.6E-2 m ³ /s ±6.1E-2 m ³ /s	4.1% Reading	N.S.	18 ms 2 ms	1.3E-3 m ³ /s
RTD	110	273 K 700 K	1.1 K 2.7 K	9.8 K	10 s	10 K
In-bundle gamma densitometer	111	1000 kg/m ³	104 kg/m ³	N.A.	16 ms	N.A.

Steady-state error bands: Two standard deviations compared to in situ standard or twice the root-sum-square of uncertainties, whichever is applicable.

Transient error bands: Assuming first-order lag function, response times (TAU), and step function ($V_f - V_0$) indicated - the average error seen by the DAS assuming the step function occurred midway between DAS samples. The averaging interval is 500 ms for thermocouples and 500 ms for all other instruments.

Total error: The total error due to steady-state error and transient error is the sum of the steady-state and transient error bands.

Table A.6 (continued)

^aError bands apply to the environment as sensed at the surface of the thermocouple sheath. Larger errors may occur when data are modeled to provide temperatures at other points. Transient response is estimated by using the response time (25 ms or less) prior to swaging the sheath (0.71 mm swaged to 0.51-mm OD) and then scaling using the following rule: the response time is inversely proportional to the outside diameter squared (OD² scaling). An additional 7% improvement in response time was allowed for packing of the boron nitride during swaging. The smaller thermocouples (0.51 mm swaged to 0.38-mm OD) were estimated from the values of the larger thermocouples by scaling the 25-ms response time to the unswaged 0.51-mm diameter using OD² scaling and then applying OD² scaling and the 7% improvement for packing to the swaged 0.38-mm OD.

^bThis instrument is fitted with Flow Technology electronics that time 10-blade passings. Averaging improves the steady-state error bands but degrades transient response.

^cRange applies specifically to instruments calibrated in subcooled liquid at a density of 1000 kg/m³.

^dRange applies specifically to instruments calibrated in subcooled liquid at a density of 860 kg/m³.

^eRange applies specifically to instruments calibrated in subcooled liquid at a density of 750 kg/m³.

^fError bands apply specifically to instruments calibrated in subcooled liquid. Extended range electronics provide readings out to 0.227 m³/s for the 8.89E-2-m-diam models and 0.028 m³/s for the 5.08E-2-m-diam models, but the error bands apply only to 150% of nominal maximum range.

^gStrain gage dp cells used as pit cells are connected to different segments of the test section by long lines. These long lines induce resonant oscillations in the instrument that increase the steady-state error bands to 35 kPa and the transient error bands to 400 kPa.

^hThe turbine flowmeters (type code 109) have a flow range such that

$$\begin{array}{ll} -3.0\text{E-}4 < \text{Flow} < -0.3\text{E-}4 & \text{or} & 0.3\text{E-}4 < \text{Flow} < 3.0\text{E-}4, \\ -6.1\text{E-}4 < \text{Flow} < -0.6\text{E-}4 & \text{or} & 0.6\text{E-}4 < \text{Flow} < 6.1\text{E-}4, \\ -1.4\text{E-}3 < \text{Flow} < -0.1\text{E-}3 & \text{or} & 0.1\text{E-}3 < \text{Flow} < 1.4\text{E-}3, \\ -6.1\text{E-}2 < \text{Flow} < -0.6\text{E-}2 & \text{or} & 0.6\text{E-}2 < \text{Flow} < 6.1\text{E-}2. \end{array}$$

ⁱThe INEL level probe is an experimental device and as such does not have well-documented error bands.

^jNo significant error over a 500-ms averaging interval.

^kN.A. implies not applicable.

^lFlow Technology supplies calibration constants over the ranges 6.3E-4 to 1.9E-2 m³/s and 5.0E-3 to 6.3E-2 m³/s, respectively. The uncertainty bands for these instruments should approach the quoted values for these ranges, but special care may be required. (See the section on turbine flowmeters in the critical instruments section.)

Table A.6 (continued)

Basis for steady-state and transient error bands by type code		
Type Code	Steady state	Transient
1	Critical instrument	Manufacturer's specification, OD ² scaling
2	Critical instrument	Manufacturer's specification, OD ² scaling
3	Critical instrument	Work of Carroll and Sheppard
4	Critical instrument	Work of Carroll and Sheppard
5	Critical instrument	Work of Carroll and Sheppard
6	Critical instrument	Manufacturer's specification
7	Critical instrument	Work of Carroll and Sheppard
8	Critical instrument	Work of Carroll and Sheppard
9	Critical instrument	Manufacturer's specification, OD ² scaling
10	Critical instrument	Work of Carroll and Sheppard
23	Critical instrument	Table B.2
24	Manufacturer's specification	Table B.2
25	Bench calibration + DAS	Table B.2 (inferred)
26	Critical instrument	Table B.2
27	Critical instrument	Table B.2
28	Critical instrument	Table B.2
29	Critical instrument	Table B.2 (inferred)
31	Critical instrument	Table B.2 (inferred)
32	Inferred (type code 31)	Table B.2 (inferred)
33	Critical instrument	Table B.2 (inferred)
34	Manufacturer's specification	Manufacturer's specification
35	Critical instrument	Table B.2
36	Bench calibration + DAS	Inferred (type code 34)
37	From Test 3.03.6AR	From Test 3.03.6AR
40	Critical instrument	Table B.2
43	Critical instrument	Table B.2 (inferred)
50	*****	*****
71	Bench calibration and specifications	Table B.2
75	Critical instrument	Manufacturer's specification
76	Engineering judgment	N.A.
77	Engineering judgment	N.A.
80	Inferred (type code 75)	Inferred (type code 75)
95	Inferred (type code 109)	Work of N. Chen
96	Inferred (type code 109)	Work of N. Chen
97	Critical instrument	Table B.2
98	Critical instrument	Inferred (type code 75)
99	Inferred (type code 71)	Inferred (type code 71)

Table A.6 (continued)

Basis for steady-state and transient error bands by type code		
Type Code	Steady state	Transient
105	Manufacturer's specification	Table B.2 (inferred)
106	Critical instrument	Work of R. Shipp (manufacturer's specification)
107	In situ calibration	Table B.2 (inferred)
108	Inferred (type code 107)	Table B.2 (inferred)
109	Critical instrument	Work of N. Chen
110	Bench calibration and specifications	Table E.2
111	Inferred (type code 106)	Inferred (type code 109)

Table A.7. Nominal case instrument uncertainties

THIF instrument error bands						
Instrument description	Type code	Instrument range	Steady-state error	Transient error	Estimated response time	Assumed value of step Fn.
Rod sheath thermocouple 0.015-in. OD	1	32 F 1900 F	6.7 F < 662 F 18.5 F	N.S. ^{a,j}	7 ms	9 F
Rod sheath thermocouple 0.020-in. OD	1	32 F 1900 F	6.7 F < 662 F 18.5 F	0.2 F ^a	12 ms	9 F
Rod middle thermocouple 0.015-in. OD	2	32 F 1900 F	6.7 F < 662 F 18.5 F	N.S. ^a	7 ms	9 F
Rod middle thermocouple 0.020-in. OD	2	32 F 1900 F	6.7 F < 662 F 18.5 F	0.2 F ^a	12 ms	9 F
Bundle sub-channel thermocouple 0.040-in. OD	3	32 F 1900 F	6.7 F < 662 F 18.5 F	4.9 F	140 ms	18 F
Shroud box thermocouple 0.062-in. OD	4	32 F 1900 F	6.7 F < 662 F 18.5 F	9.5 F	350 ms	18 F
System thermocouple 0.125-in. OD	5	32 F 1900 F	6.7 F < 662 F 18.5 F	13.7 F	870 ms	18 F
System (Nanmac) thermocouple 0.25-in. OD	6	32 F 1900 F	6.7 F < 662 F 18.5 F	0.5 F	18 ms	18 F
Spacer grid thermocouple 0.040-in. OD	7	32 F 1900 F	6.7 F < 662 F 18.5 F	4.9 F	140 ms	18 F
Array rod thermocouple 0.040-in. OD	8	32 F 1900 F	6.7 F < 662 F 18.5 F	4.9 F	140 ms	18 F
Rod sheath thermocouple 0.020-in. OD	9	32 F 1900 F	6.7 F < 662 F 18.5 F	0.2 F ^a	12 ms	9 F

Table A.7 (continued)

IHIF instrument error bands						
Instrument description	Type code	Instrument range	Steady-state error	Transient error	Estimated response time	Assumed value of step Fn.
Shroud box thermocouple 0.062-in. OD	10	32 F 1900 F	6.7 F < 662 F 18.5 F	9.5 F	350 ms	18 F
Strain gage pressure cell	23	3000 psi	29 psi	N.S.	0.16 ms	2.9 psi
Force balance pressure cell	24	500 psi 2500 psi	15 psi	1.5 psi	300 ms	2.9 psi
Force balance pressure cell	24	500 psi 3900 psi	23 psi	1.5 psi	300 ms	2.9 psi
Strain gage pressure cell	25	200 psi	2.5 psi	N.S.	0.32 ms	2.9 psi
Strain gage dp cell	26	±200 psi	6.2 psi	N.S.	0.32 ms	2.9 psi
Strain gage dp cell	27	±1000 psi	30 psi	N.S.	0.32 ms	2.9 psi
Strain gage ^g dp cell	28	±50 psi	1.6 psi	N.S.	0.32 ms	2.9 psi
Strain gage pressure cell	29	350 psi	3.5 psi	N.S.	0.16 ms	2.9 psi
Rod heater current	31	800 A	0.85% Reading	N.A. ^k	50 ms	N.A.
Generator current	32	1000 A	0.85% Reading	N.A.	50 ms	N.A.
Generator voltage	33	500 V	0.76% Reading	N.A.	50 ms	N.A.
Primary pump power	34	750 kW	Greater of 0.5 kW or 0.3% Reading	2.9 kW	150 ms	10 kW
Strain gage drag disk	35	±0.7E4 lb/ ft·s ² ±7.0E4 lb/ ft·s ²	56% Reading 19% Reading	21 lb/ft·s ²	16 ms	670 lb/ ft·s ²
Primary pump speed	36	100 rpm 5400 rpm	20 rpm	6 rpm	150 ms	20 rpm
Breakwire detector	37	5 V	30 ms	N.A.	20 ms	N.A.

Table A.7 (continued)

IHTF instrument error bands						
Instrument description	Type code	Instrument range	Steady-state error	Transient error	Estimated response time	Assumed value of step Fn.
Strain gage drag disk	40	$\pm 1.4E4$ lb/ft \cdot s 2 $\pm 1.4E5$ lb/ft \cdot s 2	56% Reading 19% Reading	21 lb/ft \cdot s 2	16 ms	670 lb/ft \cdot s 2
Strain gage dp cell	41	± 100 in.	3.2 in.	N.S.	0.32 ms	12 in.
Strain gage dp cell	42	± 500 in.	16 in.	N.S.	0.32 ms	12 in.
Strain gage dp cell	43	± 6 psi	0.3 psi	N.S.	0.32 ms	2.9 psi
Level ⁱ indicator	50	± 10 V	***	***	***	***
RTD	71	32 F 800 F	2.0 F 4.9 F	17.8 F	10 s	18 F
Capacitive dp cell	75	25 in.	0.4 in.	N.S.	131 ms	0.04 in.
Capacitive dp cell	75	150 in.	1.6 in.	N.S.	74 ms	0.04 in.
Position indicator	76	155 in.	0.5% Reading	N.A.	N.A.	N.A.
Position indicator	77	131 in.	0.5% Reading	N.A.	N.A.	N.A.
Capacitive dp cell	80	30 in.	0.4 in.	N.S.	125 ms	0.04 in.
Turbine ^f flowmeter	95	15 gpm 150 gpm	4.1% Reading	N.S.	11 ms 1.2 ms#	1 gpm 2 gpm
Turbine ^f flowmeter	96	5 gpm 50 gpm	4.1% Reading	N.S.	8 ms 1 ms	1 gpm 2 gpm
Force balance dp cell	97	24 psi	0.15 psi	1.5 psi	300 ms	2.9 psi
Capacitive dp cell	98	50 psi	2.6 psi	0.2 psi	38 ms	2.9 psi
Differential temperature	99	± 50 F	6.8 F	17.8 F	10 s	18 F
Liquid level	105	150 in.	0.9 in.	6.2 in.	300 ms	7.9 in.
Liquid level	105	$5.5E4$ in.	336 in.	6.2 in.	300 ms	7.9 in.

Table A.7 (continued)

IHTF instrument error bands						
Instrument description	Type code	Instrument range	Steady-state error	Transient error	Estimated response time	Assumed value of step Fn.
Gamma densitometer	106	62.4 lb/ft ³	6.5 lb/ft ³	N.A.	16 ms	N.A.
Orifice ^c flowmeter	107	1.6 gpm	4E-2 gpm	0.13 gpm	300 ms	0.16 gpm
Orifice ^c flowmeter	107	2.1 gpm	0.054 gpm	0.17 gpm	300 ms	0.22 gpm
Orifice ^c flowmeter	107	5.3 gpm	0.13 gpm	0.36 gpm	300 ms	0.45 gpm
Orifice ^c flowmeter	107	39.3 gpm	0.98 gpm	0.36 gpm	300 ms	0.45 gpm
Orifice ^c flowmeter	107	800 gpm	21 gpm	62 gpm	300 ms	80 gpm
Orifice ^d flowmeter	108	2.7 gpm	0.067 gpm	0.21 gpm	300 ms	0.27 gpm
Orifice ^e flowmeter	108	700 gpm	17.4 gpm	0.55 gpm	300 ms	70 gpm
Turbine ^{f,h} flowmeter	109	±0.5 gpm ±5.0 gpm	4.1% Reading	N.S.	8 ms 1 ms	1 gpm 2 gpm
Turbine ^{f,h,b} flowmeter	109	±1.0 gpm ±10 gpm	2.5% Reading	N.A.	8 ms 1 ms	N.A.
Turbine ^{f,h,l} flowmeter	109	±22 gpm ±225 gpm	4.1% Reading	N.S.	13 ms 2 s	1 gpm 2 gpm
Turbine ^{f,h,l} flowmeter	109	±100 gpm ±1000 gpm	4.1% Reading	N.S.	18 ms 2 ms	1 gpm 2 gpm
RTD	110	32 F 800 F	2.0 F 4.9 F	17.8 F	10 s	18 F
In-bundle gamma densitometer	111	62.4 lb/ft ³	6.5 lb/ft ³	N.A.	16 ms	N.A.
Steady-state error bands:	Two standard deviations compared to in situ standard or twice the root-sum-square of uncertainties, whichever is applicable.					
Transient error bands:	Assuming first-order lag function, response times (TAU), and step function ($V_f - V_o$) indicated - the average error seen by the DAS assuming the step function occurred midway between DAS samples. The averaging interval is 500 ms for thermocouples and 500 ms for all other instruments.					
Total error:	The total error due to steady-state error and transient error is the sum of the steady-state and transient error bands.					

Table A.7 (continued)

^aError bands apply to the environment as sensed at the surface of the thermocouple sheath. Larger errors may occur when data are modeled to provide temperatures at other points. Transient response is estimated by using the response time (25 ms or less) prior to swaging the sheath (0.71 mm swaged to 0.51-mm OD) and then scaling by using the following rule: the response time is inversely proportional to the outside diameter squared (OD² scaling). An additional 7% improvement in response time was allowed for packing of the boron nitride during swaging. The smaller thermocouples (0.51 mm swaged to 0.38-mm OD) were estimated from the values of the larger thermocouples by first scaling the 25-ms response time to the unswaged 0.51-mm diameter using OD² scaling and then applying OD² scaling and the 7% improvement for packing to the swaged 0.38-mm OD.

^bThis instrument is fitted with Flow Technology electronics that time 10-blade passings. Averaging improves the steady-state error bands but degrades transient response.

^cRange applies specifically to instruments calibrated in subcooled liquid at a density of 1000 kg/m³.

^dRange applies specifically to instruments calibrated in subcooled liquid at a density of 860 kg/m³.

^eRange applies specifically to instruments calibrated in subcooled liquid at a density of 750 kg/m³.

^fError bands apply specifically to instruments calibrated in subcooled liquid. Extended range electronics provide readings out to 0.227 m³/s for the 8.89E-2-m-diam models and 0.28 m³/s for the 5.08E-2-m-diam models, but the error bands apply only to 150% of nominal maximum range.

^gStrain gage dp cells used as pit cells are connected to different segments of the test section by long lines. These long lines induce resonant oscillations in the instrument that increase the steady-state error bands to 35 kPa and the transient error bands to 400 kPa.

^hThe turbine flowmeters (type 109) have a flow range such that

-3.0E-4 < Flow < -0.3E-4	or	0.3E-4 < Flow < 3.0E-4,
-6.1E-4 < Flow < -0.6E-4	or	0.6E-4 < Flow < 6.1E-4,
-1.4E-3 < Flow < -0.1E-3	or	0.1E-3 < Flow < 1.4E-3,
-6.1E-2 < Flow < -0.6E-2	or	0.6E-2 < Flow < 6.1E-2.

ⁱThe INEL level probe is an experimental device and as such does not have well-documented error bands.

^jNo significant error over a 500-ms averaging interval.

^kN.A. implies not applicable.

^lFlow Technology supplies calibration constants over the ranges 6.3E-4 to 1.9E-2 m³/s and 5.0E-3 to 6.3E-2 m³/s, respectively. The uncertainty bands for these instruments should approach the quoted values for these ranges, but special care may be required. (See the section on turbine flowmeters in the critical instruments section.)

Table A.7 (continued)

Basis for steady-state and transient error bands by type code		
Type Code	Steady state	Transient
1	Critical instrument	Manufacturer's specification, OD ² scaling
2	Critical instrument	Manufacturer's specification, OD ² scaling
3	Critical instrument	Work of Carroll and Sheppard
4	Critical instrument	Work of Carroll and Sheppard
5	Critical instrument	Work of Carroll and Sheppard
6	Critical instrument	Manufacturer's specification
7	Critical instrument	Work of Carroll and Sheppard
8	Critical instrument	Work of Carroll and Sheppard
9	Critical instrument	Manufacturer's specification, OD ² scaling
10	Critical instrument	Work of Carroll and Sheppard
23	Critical instrument	Table B.2
24	Manufacturer's specification	Table B.2
25	Bench calibration + DAS	Table B.2 (inferred)
26	Critical instrument	Table B.2
27	Critical instrument	Table B.2
28	Critical instrument	Table B.2
29	Critical instrument	Table B.2 (inferred)
31	Critical instrument	Table B.2 (inferred)
32	Inferred (type code 31)	Table B.2 (inferred)
33	Critical instrument	Table B.2 (inferred)
34	Manufacturer's specification	Manufacturer's specification
35	Critical instrument	Table B.2
36	Bench calibration + DAS	Inferred (type code 34)
37	From Test 3.03.6AR	From Test 3.03.6AR
40	Critical instrument	Table B.2
43	Critical instrument	Table B.2 (inferred)
50	*****	*****
71	Bench calibration and specifications	Table B.2
75	Critical instrument	Manufacturer's specification
76	Engineering judgment	N.A.
77	Engineering judgment	N.A.
80	Inferred (type code 75)	Inferred (type code 75)
95	Inferred (type code 109)	Work of N. Chen
96	Inferred (type code 109)	Work of N. Chen
97	Critical instrument	Table B.2
98	Critical instrument	Inferred (type code 75)
99	Inferred (type code 71)	Inferred (type code 71)

Table A.7 (continued)

Basis for steady-state and transient error bands by type code		
Type Code	Steady state	Transient
105	Manufacturer's specification	Table B.2 (inferred)
106	Critical instrument	Work of R. Shipp (manufacturer's specification)
107	In situ calibration	Table B.2 (inferred)
108	Inferred (type code 107)	Table B.2 (inferred)
109	Critical instrument	Work of N. Chen
110	Bench calibrations and specifications	Table B.2
111	Inferred (type code 106)	Inferred (type code 109)

Table A.8. Worst-case instrument uncertainties

THIF instrument error bands						
Instrument description	Type code	Instrument range	Steady-state error	Transient error	Estimated response time	Assumed value of step Fn.
Rod sheath thermocouple 0.015-in. OD	1	32 F 1900 F	6.7 F < 662 F 18.5 F	1.4 F ^α	7 ms	540 F
Rod sheath thermocouple 0.020-in. OD	1	32 F 1900 F	6.7 F < 662 F 18.5 F	6.8 F ^α	12 ms	540 F
Rod middle thermocouple 0.015-in. OD	2	32 F 1900 F	6.7 F < 662 F 18.5 F	1.4 F ^α	7 ms	540 F
Rod middle thermocouple 0.020-in. OD	2	32 F 1900 F	6.7 F < 662 F 18.5 F	6.8 F ^α	12 ms	540 F
Bundle sub-channel thermocouple 0.040-in. OD	3	32 F 1900 F	6.7 F < 662 F 18.5 F	73.1 F	140 ms	270 F
Shroud box thermocouple 0.062-in. OD	4	32 F 1900 F	6.7 F < 662 F 18.5 F	143.6 F	350 ms	270 F
System thermocouple 0.125-in. OD	5	32 F 1900 F	6.7 F < 662 F 18.5 F	205.4 F	870 ms	270 F
System (Nan-mac) thermocouple 0.25-in. OD	6	32 F 1900 F	6.7 F < 662 F 18.5 F	7.2 F 2.3 F	18 ms	270 F 90 F
Spacer grid thermocouple 0.040-in. OD	7	32 F 1900 F	6.7 F < 662 F 18.5 F	73.1 F	140 ms	270 F
Array rod thermocouple 0.040-in. OD	8	32 F 1900 F	6.7 F < 662 F 18.5 F	73.1 F	140 ms	270 F
Rod sheath thermocouple 0.020-in. OD	9	32 F 1900 F	6.7 F < 662 F 18.5 F	6.8 F ^α	12 ms	540 F

Table A.8 (continued)

THIF instrument error bands						
Instrument description	Type code	Instrument range	Steady-state error	Transient error	Estimated response time	Assumed value of step Fn.
Shroud box thermocouple 0.062-in. OD	10	32 F 1900 F	6.7 F < 662 F 18.5 F	143.6 F	350 ms	270 F
Strain gage pressure cell	23	3000 psi	29 psi	N.S. ^j	0.16 ms	2.9 psi
Force balance pressure cell	24	500 psi 2500 psi	15 psi	17 psi	300 ms	35 psi
Force balance pressure cell	24	500 psi 3900 psi	23 psi	17 psi	300 ms	35 psi
Strain gage pressure cell	25	200 psi	2.5 psi	N.S.	0.32 ms	2.9 psi
Strain gage dp cell	26	±200 psi	6.2 psi	N.S.	0.32 ms	2.9 psi
Strain gage dp cell	27	±1000 psi	30 psi	N.S.	0.32 ms	2.9 psi
Strain gage ^g dp cell	28	±50 psi	1.6 psi	N.S.	0.32 ms	2.9 psi
Strain gage pressure cell	29	350 psi	3.5 psi	N.S.	0.16 ms	2.9 psi
Rod heater current	31	800 A	0.85% Reading	N.A. ^k	50 ms	N.A.
Generator current	32	1000 A	0.85% Reading	N.A.	50 ms	N.A.
Generator voltage	33	300 V	0.76% Reading	N.A.	50 ms	N.A.
Primary pump power	34	750 kW	Greater of 0.5 kW or 0.3% Reading	2.9 kW	150 ms	10 kW
Strain gage drag disk	35	±0.7E4 lb/ ft·s ² ±7.0E4 lb/ ft·s ²	56% Reading 19% Reading	70 lb/ft·s ²	16 ms	670 lb/ ft·s ²
Primary pump speed	36	100 rpm 5400 rpm	20 rpm	6 rpm	150 ms	20 rpm
Breskwire detector	37	5 V	30 ms	N.A.	20 ms	N.A.

Table A.8 (continued)

THTF instrument error bands						
Instrument description	Type code	Instrument range	Steady-state error	Transient error	Estimated response time	Assumed value of step Fn.
Strain gage drag disk	40	$\pm 1.4E4$ lb/ft \cdot s 2 $\pm 1.4E5$ lb/ft \cdot s 2	56% Reading 19% Reading	70 lb/ft \cdot s 2	16 ms	670 lb/ft \cdot s 2
Strain gage dp cell	41	± 100 in.	3.3 in.	N.S.	0.32 ms	80 in.
Strain gage dp cell	42	± 500 in.	16 in.	N.S.	0.32 ms	80 in.
Strain gage dp cell	43	± 6 psi	0.3 psi	N.S.	0.32 ms	2.9 psi
Level ⁱ indicator	50	± 10 V	***	***	***	***
RTD	71	32 F 800 F	2.0 F 4.9 F	17.8 F	10 s	18 F
Capacitive Jp cell	75	25 in.	0.4 in.	0.1 in.	131 ms	0.4 in.
Capacitive dp cell	75	150 in.	1.9 in.	0.03 in.	74 ms	0.4 in.
Position indicator	76	155 in.	0.5% Reading	N.A.	N.A.	N.A.
Position indicator	77	131 in.	0.5% Reading	N.A.	N.A.	N.A.
Capacitive dp cell	80	30 in.	0.4 in.	0.08 in.	125 ms	0.4 in.
Turbine ^f flowmeter	95	15 gpm 150 gpm	4.1% Reading	0.1 gpm	11 ms 1.2 ms	21 gpm
Turbine ^f flowmeter	96	5 gpm 50 gpm	4.1% Reading	0.1 gpm	8 ms 1 ms	1 gpm 2 gpm
Force balance dp cell	97	24 psi	0.15 psi	1.5 psi	300 ms	2.9 psi
Capacitive dp cell	98	50 psi	2.6 psi	0.2 psi	38 ms	2.9 psi
Differential temperature	99	± 50 F	6.8 F	17.8 F	10 s	18 F
Liquid level	105	150 in.	0.9 in.	6.2 in.	300 ms	7.9 in.
Liquid level	105	$5.5E4$ in.	336 in.	6.2 in.	300 ms	7.9 in.

Table A.8 (continued)

THIF instrument error bands						
Instrument description	Type code	Instrument range	Steady-state error	Transient error	Estimated response time	Assumed value of step Fn.
Gamma densitometer	106	62.4 lb/ft ³	6.5 lb/ft ³	N.A.	16 ms	N.A.
Orifice ^c flowmeter	107	1.6 gpm	4E-2 gpm	0.13 gpm	300 ms	0.16 gpm
Orifice ^c flowmeter	107	2.1 gpm	0.054 gpm	0.17 gpm	300 ms	0.22 gpm
Orifice ^c flowmeter	107	5.3 gpm	0.13 gpm	0.74 gpm	300 ms	0.94 gpm
Orifice ^c flowmeter	107	39.3 gpm	0.9 gpm	0.74 gpm	300 ms	0.94 gpm
Orifice ^c flowmeter	107	800 gpm	21 gpm	62 gpm	300 ms	80 gpm
Orifice ^d flowmeter	108	2.7 gpm	0.067 gpm	0.21 gpm	300 ms	0.27 gpm
Orifice ^e flowmeter	108	700 gpm	17.4 gpm	0.55 gpm	300 ms	70 gpm
Turbine ^{f,h} flowmeter	109	±0.5 gpm ±5.0 gpm	4.1% Reading	N.S.	8 ms 1 ms	2.5 gpm
Turbine ^{f,h,b} flowmeter	109	±1.0 gpm ±10 gpm	2.5% Reading	N.A.	8 ms 1 ms	N.A.
Turbine ^{f,h,l} flowmeter	109	±22 gpm ±225 gpm	4.1% Reading	N.S.	13 ms 2 ms	21 gpm
Turbine ^{f,h,l} flowmeter	109	±100 gpm ±1000 gpm	4.1% Reading	N.S.	18 ms 2 ms	21 gpm
RTD	110	32 F 800 F	2.0 F 4.9 F	17.8 F	10 s	18 F
In-bundle gamma densitometer	111	62.4 lb/ft ³	6.5 lb/ft ³	N.A.	16 ms	N.A.

Steady-state error bands: Two standard deviations compared to in situ standard or twice the root-sum-square of uncertainties, whichever is applicable.

Transient error bands: Assuming first-order lag function, response times (TAU), and step function ($V_f - V_0$) indicated - the average error seen by the DAS assuming the step function occurred midway between DAS samples. The averaging interval is 500 ms for thermocouples and 500 ms for all other instruments.

Total error: The total error due to steady-state error and transient error is the sum of the steady-state and transient error bands.

Table A.8 (continued)

^aError bands apply to the environment as sensed at the surface of the thermocouple sheath. Larger errors may occur when data are modeled to provide temperatures at other points. Transient response is estimated by using the response time (25 ms or less) prior to swaging the sheath (0.028 in. swaged to 0.020-in. OD) and then scaling by using the following rule: the response time is inversely proportional to the outside diameter squared (OD² scaling). An additional 7% improvement in response time was allowed for packing of the boron nitride during swaging. The smaller thermocouples (0.020-in. swaged to 0.015 in.) were estimated from the values of the larger thermocouples by first scaling the 25-ms response time to the unswaged 0.020-in. diameter using OD² scaling and then applying OD² scaling and the 7% improvement for packing to the swaged 0.015-in. OD.

^bThis instrument is fitted with Flow Technology electronics that time 10-blade passages. Averaging improves the steady-state error bands but degrades transient response.

^cRange applies specifically to instruments calibrated in subcooled liquid at a density of 62.4 lb/ft³.

^dRange applies specifically to instruments calibrated in subcooled liquid at a density of 53.7 lb/ft³.

^eRange applies specifically to instruments calibrated in subcooled liquid at a density of 46.8 lb/ft³.

^fError bands apply specifically to instruments calibrated in subcooled liquid. Extended range electronics provide readings out to 3600 gpm for the 3.5-in.-diam models and 445 gpm for the 2.0-in.-diam models, but the error bands apply only to 150% of nominal maximum range.

^gStrain gage dp cells used as pit cells are connected to different segments of the test section by long lines. These long lines induce resonant oscillations in the instrument that increase the steady-state error bands to 5 psi and the transient error bands to 60 psi in the interval immediately following blowdown.

^hThe turbine flowmeters (type code 109) have a flow range such that

-5.0 < Flow < -0.5	or	0.5 < Flow < 5.0,
-10.0 < Flow < -1.0	or	1.0 < Flow < 10.0,
-225 < Flow < -22	or	22 < Flow < 225,
-1000 < Flow < -100	or	100 < Flow < 1000.

ⁱThe INEL level probe is an experimental device and as such does not have well-documented error bands.

^jNo significant error over the averaging interval.

^kN.A. implies not applicable.

^lFlow Technology supplies calibration constants over the ranges 10-300 gpm and 80-1000 gpm, respectively. The uncertainty bands for these instruments should approach the quoted values for these ranges, but special care may be required. (See the section on turbine flowmeters in the critical instruments section.)

Table A.8 (continued)

Basis for steady-state and transient error bands by type code		
Type Code	Steady state	Transient
1	Critical instrument	Manufacturer's specification, OD ² scaling
2	Critical instrument	Manufacturer's specification, OD ² scaling
3	Critical instrument	Work of Carroll and Sheppard
4	Critical instrument	Work of Carroll and Sheppard
5	Critical instrument	Work of Carroll and Sheppard
6	Critical instrument	Manufacturer's specification
7	Critical instrument	Work of Carroll and Sheppard
8	Critical instrument	Work of Carroll and Sheppard
9	Critical instrument	Manufacturer's specification, OD ² scaling
10	Critical instrument	Work of Carroll and Sheppard
23	Critical instrument	Table B.2
24	Manufacturer's specification	Table B.2
25	Bench calibration + DAS	Table B.2 (inferred)
26	Critical instrument	Table B.2
27	Critical instrument	Table B.2
28	Critical instrument	Table B.2
29	Critical instrument	Table B.2 (inferred)
31	Critical instrument	Table B.2 (inferred)
32	Inferred (type code 31)	Table B.2 (inferred)
33	Critical instrument	Table B.2 (inferred)
34	Manufacturer's specification	Manufacturer's specification
35	Critical instrument	Table B.2
36	Bench calibration + DAS	Inferred (type code 34)
37	From Test 3.03.6AR	From Test 3.03.6AR
40	Critical instrument	Table B.2
43	Critical instrument	Table B.2 (inferred)
50	*****	*****
71	Bench calibration and specifications	Table B.2
75	Critical instrument	Manufacturer's specification
76	Engineering judgment	N.A.
77	Engineering judgment	N.A.
80	Inferred (type code 75)	Inferred (type code 75)
95	Inferred (type code 109)	Work of N. Chen
96	Inferred (type code 109)	Work of N. Chen
97	Critical instrument	Table B.2
98	Critical instrument	Inferred (type code 75)
99	Inferred (type code 71)	Inferred (type code 71)

Table A.8 (continued)

Basis for steady-state and transient error bands by type code		
Type Code	Steady state	Transient
105	Manufacturer's specification	Table B.2 (inferred)
106	Critical instrument	Work of R. Shipp (manufacturer's specification)
107	In situ calibration	Table B.2 (inferred)
108	Inferred (type code 107)	Table B.2 (inferred)
109	Critical instrument	Work of N. Chen
110	Bench calibration and specifications	Table B.2
111	Inferred (type code 106)	Inferred (type code 109)

units. Table A.5 contains nominal transient errors, and Table A.6 the worst-case transient errors. Table A.7 is the English unit version of Table A.5; Table A.8 is the English unit version of Table A.6.

The first column in each table gives a brief instrument description. The second column provides the instrument type code. (Use Table A.4 to cross reference to IANs.) The third column provides the nominal instrument range. The fourth and fifth columns give the steady-state and transient error bands, respectively. The sixth and seventh columns provide the estimated response time and step function values used to estimate the transient uncertainty value.

The English version tables are intended for reference only. Exact correspondence of entries will be limited by significant figure rounding.

The values quoted for both steady-state and transient errors are estimates based on several assumptions. It is the responsibility of the data user to ascertain the appropriateness of these assumptions when using the included error bands for THIF data analysis.

References

1. K. A. Brownlee, *Statistical Theory and Methodology in Science and Engineering*, p. 80, John Wiley and Sons, Inc., New York, 1965.
2. J. B. Scarborough, *Numerical Mathematical Analysis*, 3rd Edition, p. 429, the John Hopkins Press, Baltimore, 1955.
3. K. A. Brownlee, *Statistical Theory and Methodology in Science and Engineering*, p. 340, John Wiley and Sons, Inc., New York, 1965.
4. Unpublished report, *Summary Two and Three Dimensional Analysis of Turbine Flowmeter Response in Two-Phase Flow*, MPR Associates, Inc., October 11, 1977.
5. Internal memo from R. L. Anderson, I&C Division ORNL, to B. J. Veazie, *Error in BDHT Thermocouple*, June 18, 1980.

Appendix B

CALCULATED MASS FLOWS

This appendix describes the method of calculating mass flows at the THTF test section boundaries and the estimated uncertainties in these calculations. The calculated mass flows at the inlet and outlet of the test section for the reflood, boiloff, and uncovered bundle Tests 3.09.10I-X and 3.09.10AA-HH are included.

Methodology and Instrumentation

In general, mass flow calculations are made by combining a volumetric flow measurement Q with a measured or calculated fluid density ρ

$$\dot{m} = \rho Q . \quad (B.1)$$

Where conditions permit, in subcooled or superheated flows, the density is deduced from fluid properties based on temperature and pressure measurements. In two-phase flow, the density is measured by a gamma densitometer (when available). For the small break test series, the inlet conditions were always subcooled.

The steady-state inlet volumetric flows were measured using an orifice flowmeter (FE-18A) or the 1/2-in. turbine meters (FE-250 and FE-260). (See Fig. 1 for instrument locations.) When in range [$<1.7 \times 10^{-4} \text{ m}^3/\text{s}$ (2.7 gpm)], the orifice flowmeter is the preferred instrument in terms of accuracy and reliability. The transient inlet volumetric flow was measured by a 2-in. turbine meter (FE-3) for all of the reflood tests. One of the 1/2-in. turbine meters (FE-250) was also used in the early portion of Test 3.09.10Q until it was overranged. This was the only reflood test that used only the 1/2-in. steady-state line (Fig. 1). The other tests were reflooded through the 3/4-in. reflood line. Reflood through the 3/4-in. line resulted in meaningless flow measurement for FE-18A, FE-250, and FE-260 once the valve at the inlet flow manifold was opened and reflood was initiated.

The outlet volumetric flow was measured by a 2-in. turbine meter (FE-202) or one of the orifice flowmeters in the outlet orifice flow manifold (FE-282 or FE-283). Flow was also monitored in the shroud leakage bypass line by an orifice flowmeter (FE-927) and a 1/2-in. turbine meter (FE-280). (FE-927 indicated a substantial and nonrepeatable offset when under-ranged. As a result, it was not always possible to determine when the instrument reading was valid. Accordingly, FE-927 was not used in mass flow calculations.) It should be noted that measurement in the outlet orifice flow manifold includes flow through the shroud bypass line, whereas flow at the test section outlet spool piece (FE-202) does not. The shroud bypass line was open only for the transient reflood and boil-off tests. The line was valved off for the uncovered bundle tests once steady-state equilibrium conditions in the bundle were obtained.

Mass flows for the transient tests were calculated from transient instrument data by the mass flow code AMICON.¹ Logic in the AMICON and water properties codes determines whether a temperature- and pressure-deduced density or a densitometer-measured density (if available) is appropriate (based on a comparison of measurements by these same instruments). For indicated subcooled or superheated conditions, temperature- and pressure-deduced densities were used. If saturated conditions were indicated by temperature and pressure measurements (within thermocouple and pressure transducer uncertainty bands) and the densitometer-measured density was less than the saturated vapor density, then the densitometer reading was replaced by the temperature- and pressure-deduced density (the saturated vapor density).

For later reference, a comparison of outlet fluid thermocouple measurements (TE-208, TE-281, TE-282, and TE-927 indicated in Fig. 1) is made with the saturation temperature based on a pressure measurement made in the test section upper plenum (PE-201). The comparisons for the five reflood tests and the five boiloff tests are shown in Figs. B.1-B.10. For most of the tests the temperature in the shroud bypass line appears to follow the saturation temperature. Since a densitometer is not available on this line, however, a pressure- and temperature-deduced density is always used. For the reflood tests, the indicated outlet conditions were superheated during most of the time of interest. The fluid temperatures for the boiloff tests, however, appeared to follow the saturation temperature over significant time periods. Except for the boiloff test 3.09.10X, densitometer measurements indicated densities lower than saturated vapor

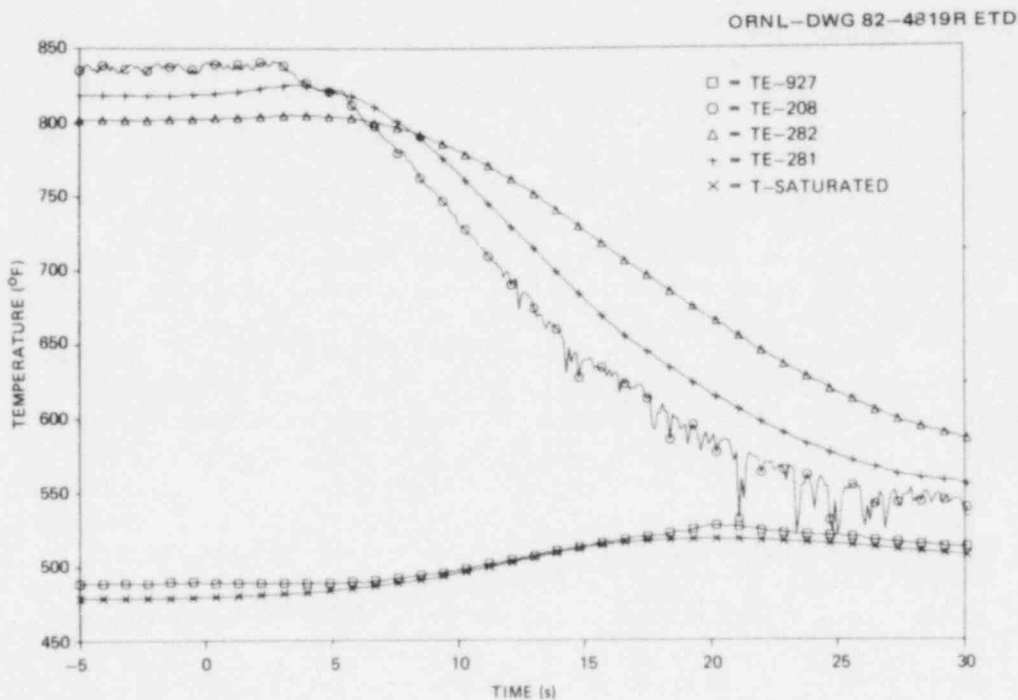


Fig. B.1. Temperature histories for Test 3.09.100.

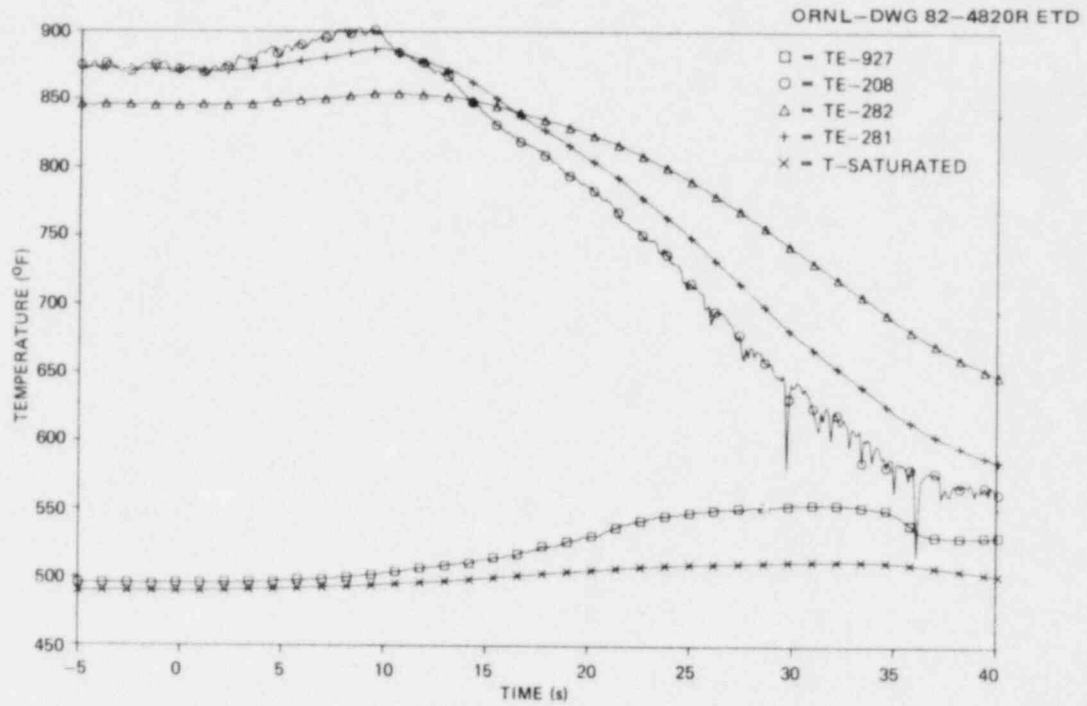


Fig. B.2. Temperature histories for Test 3.09.10P.

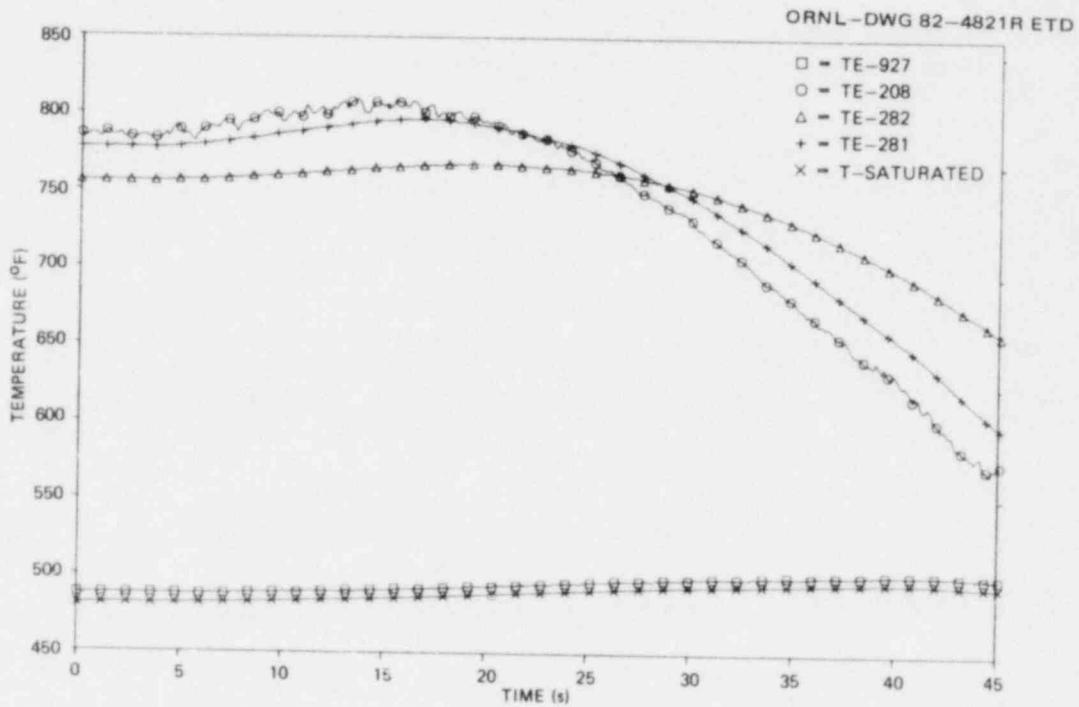


Fig. B.3. Temperature histories for Test 3.09.10Q.

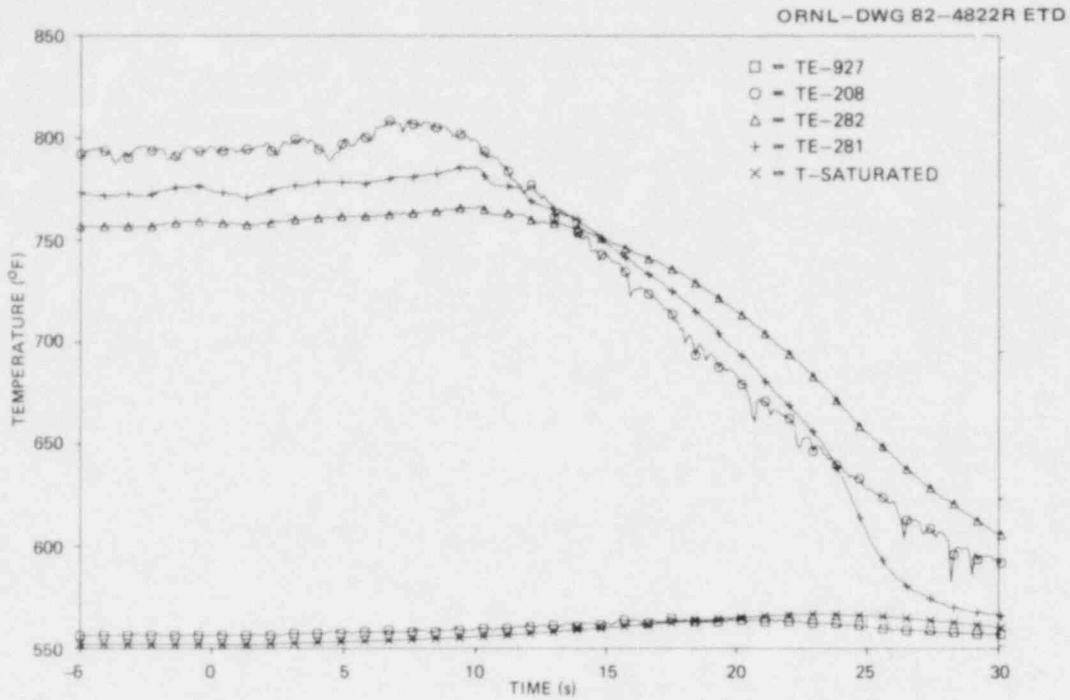


Fig. B.4. Temperature histories for Test 3.09.10R.

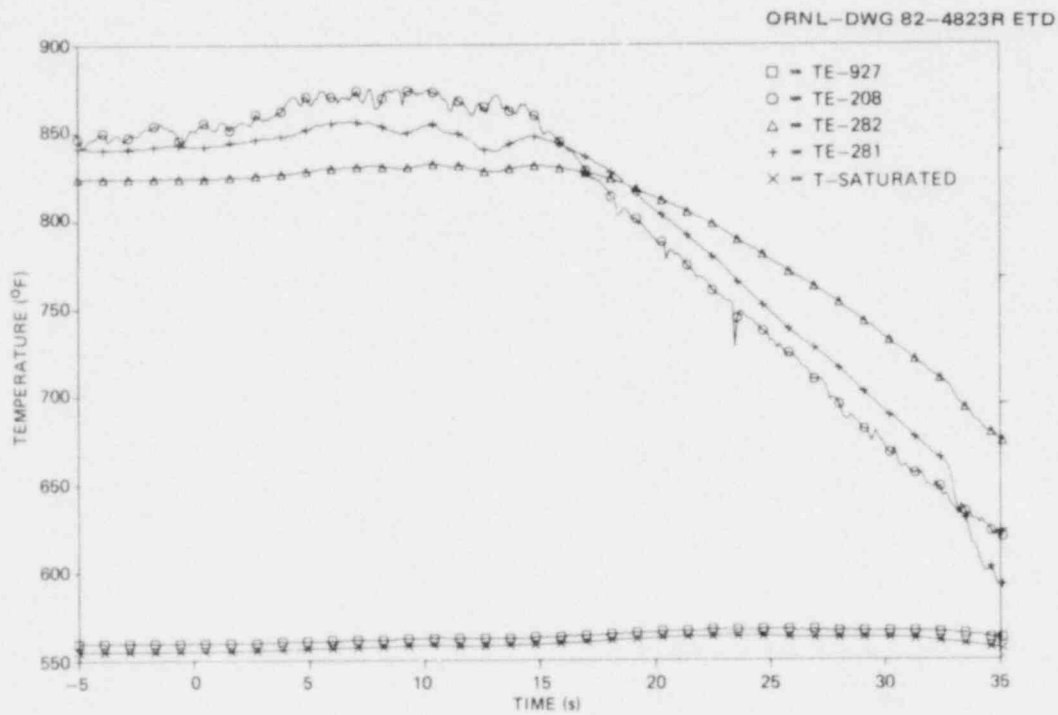


Fig. B.5. Temperature histories for Test 3.09.10S.

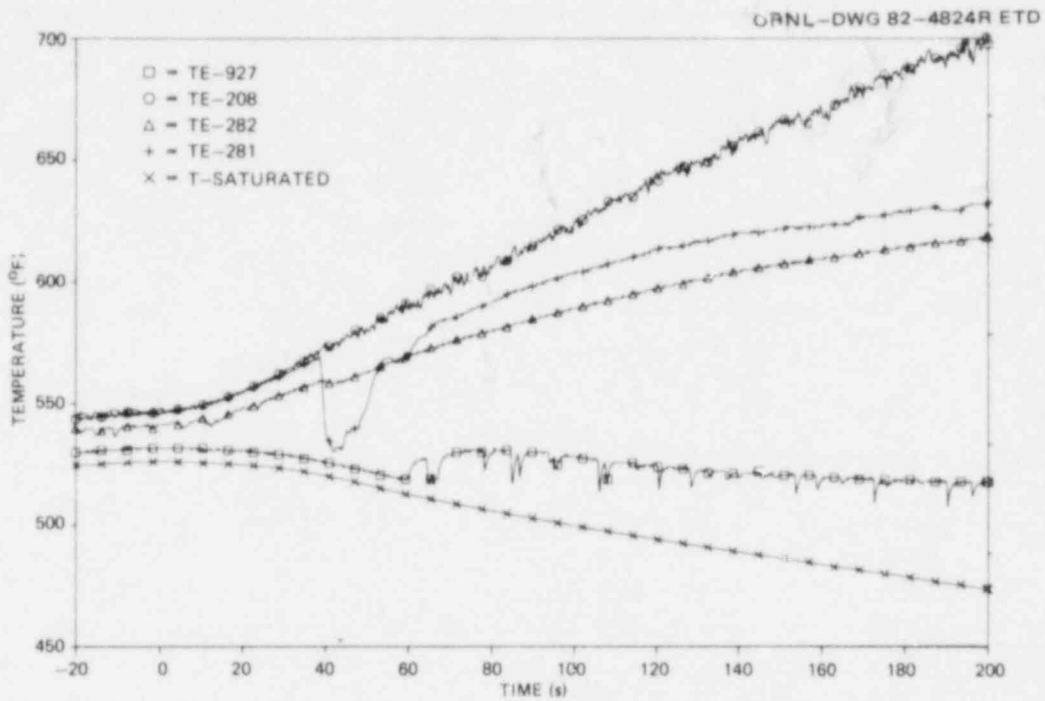


Fig. B.6. Temperature histories for Test 3.09.10T.

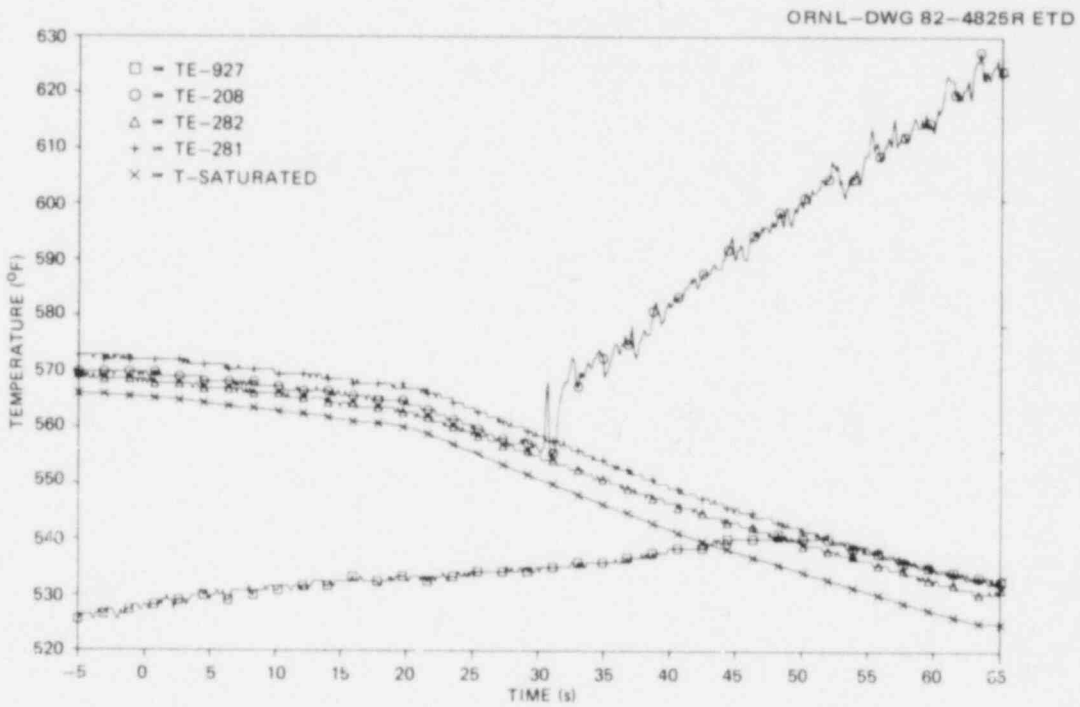


Fig. B.7. Temperature histories for Test 3.09.10U.

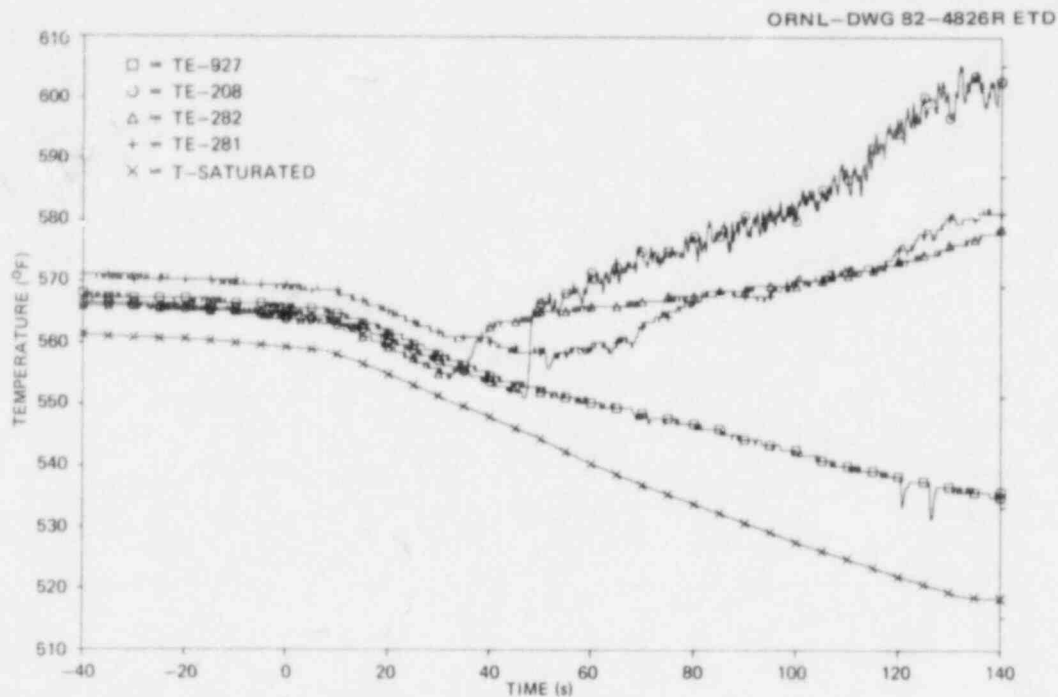


Fig. B.8. Temperature histories for Test 3.09.10V.

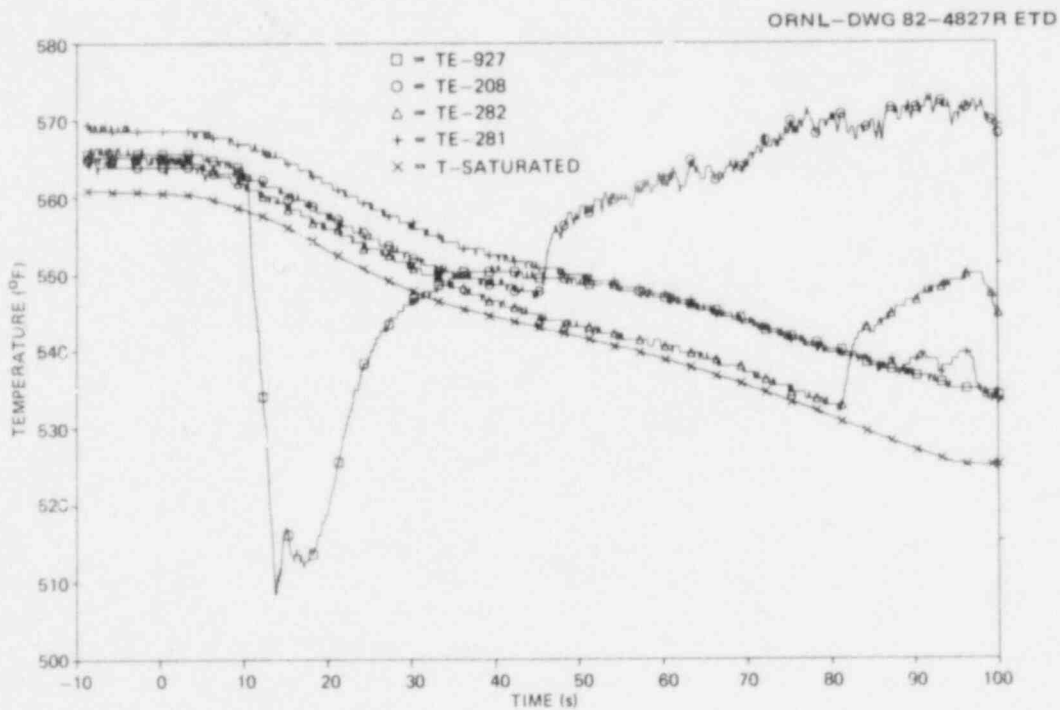


Fig. B.9. Temperature histories for Test 3.09.10W.

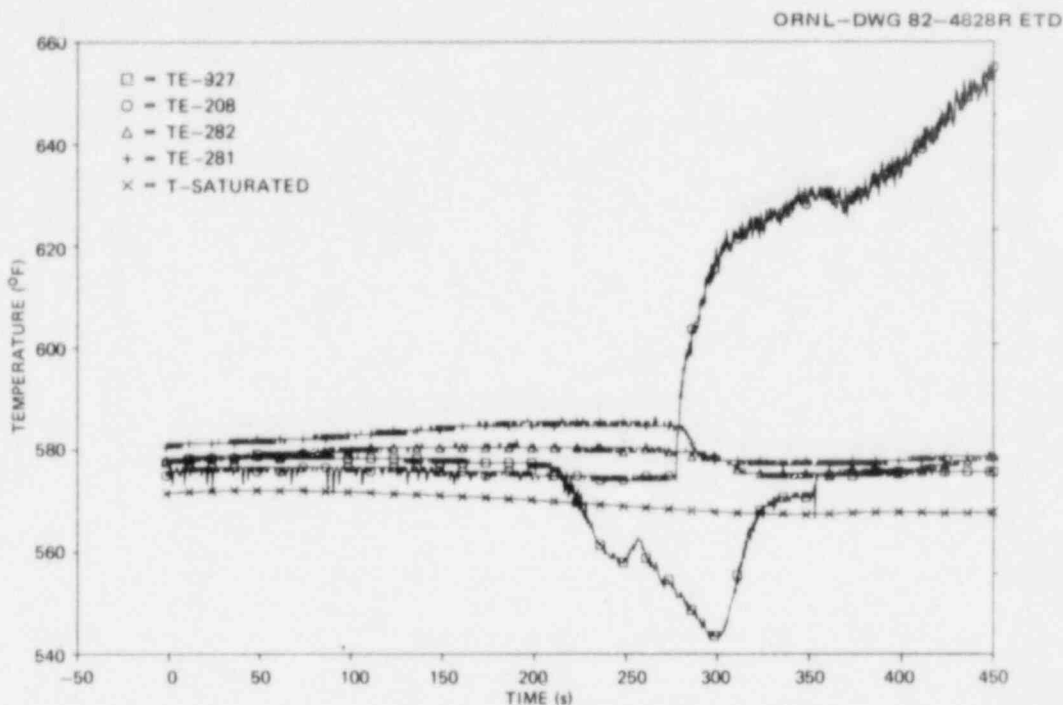


Fig. B.10. Temperature histories for Test 3.09.10X.

densities, and, as a result, the density was determined from temperature and pressure measurements over all times indicated. The very high-quality or saturated steam at the outlet was not unexpected, because the boiloff tests were generally initiated with the upper level of the bundle already uncovered to some extent.

Calculated Reflood Mass Flow Rates

Mass flows of interest for the transient reflood test 3.09.100 are shown in Figs. B.11-B.15. Mass flow is shown for FE-250 in Fig. B.11 and indicates the pre-reflood inlet mass flow rate. This flow is valid until the initiation of reflood at ~ 1.3 s. FE-18A was overranged and is not shown. The 1/2-in. turbine meter, FE-260, failed and is not shown. Figure B.12 shows the inlet reflood mass flow rate once the flow exceeds the deadband of the 2-in. turbine meter, FE-3. Figure B.13 shows the mass flow calculated at the outlet turbine meter, FE-202; Fig. B.14 shows results from the high range outlet orifice flowmeter, FE-282. The outlet orifice flow manifold bypass line was open for this test, invalidating measurements made by FE-283. Mass flow calculated in the shroud bypass line is shown in Fig. B.15.

Mass flows of interest for the transient reflood test 3.09.10P are shown in Figs. B.16-B.21. Mass flows are shown for FE-250 and FE-18A in Figs. B.16 and B.17, indicating the pre-reflood inlet mass flow rates.

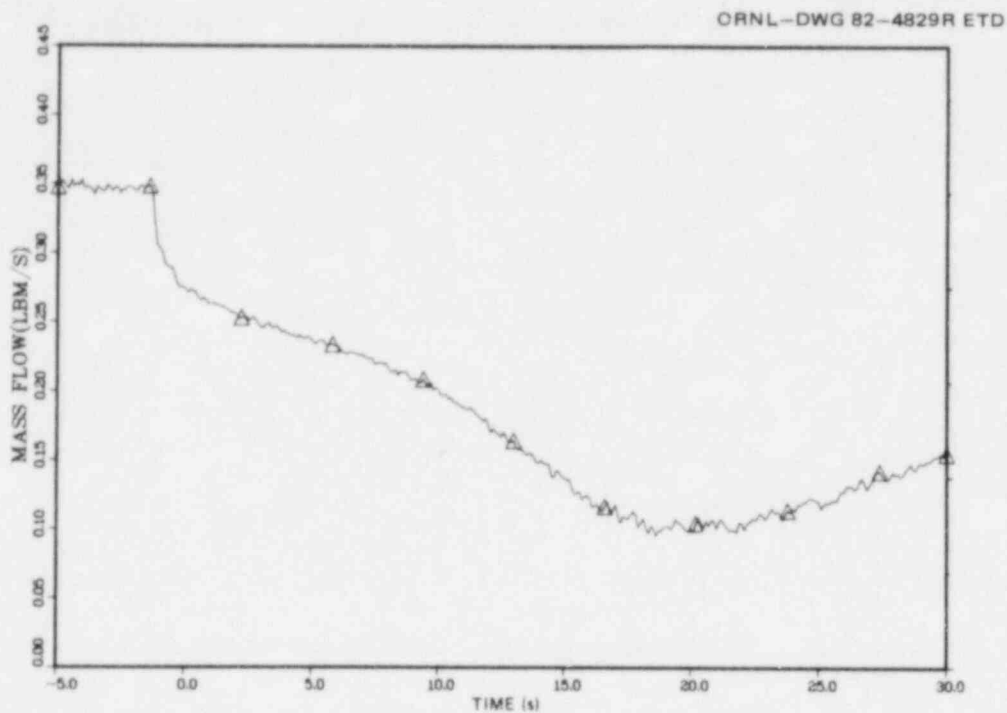


Fig. B.11. Test section inlet mass flow rate for Test 3.09.100; based on FE-250.

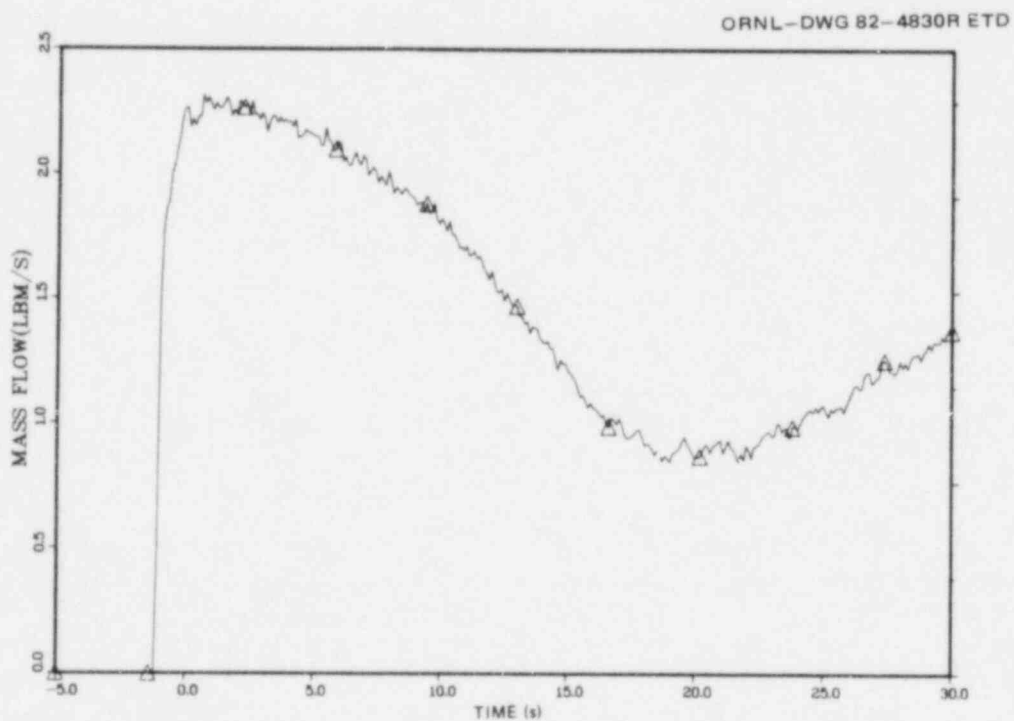


Fig. B.12. Test section inlet mass flow rate for Test 3.09.100; based on FE-3.

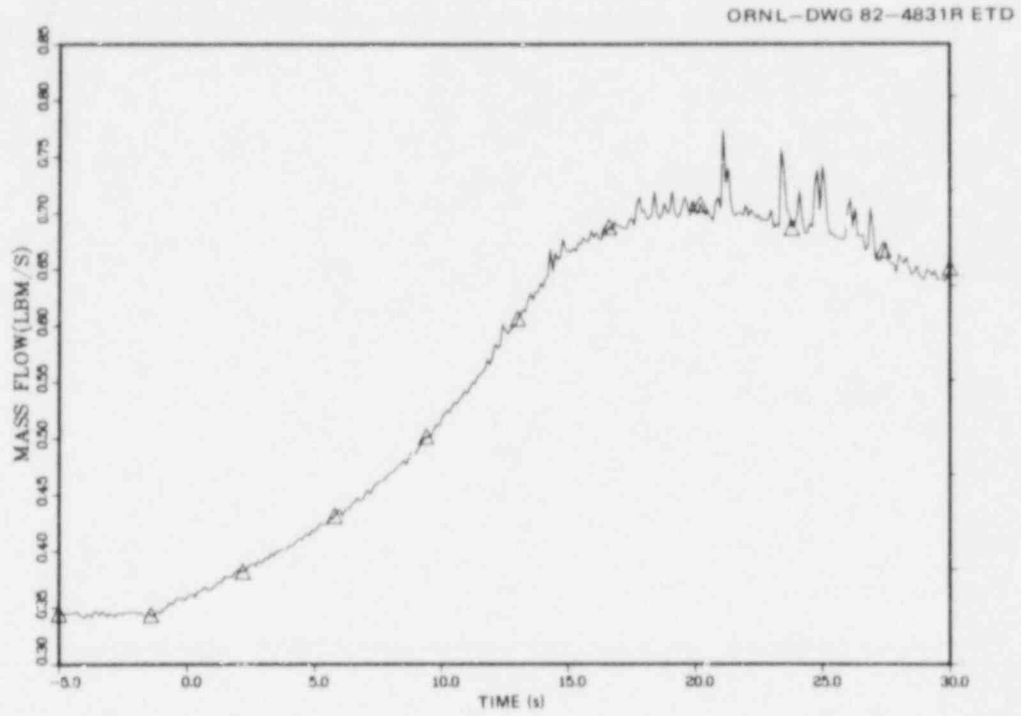


Fig. B.13. Test section outlet mass flow rate for Test 3.09.100; based on FE-202.

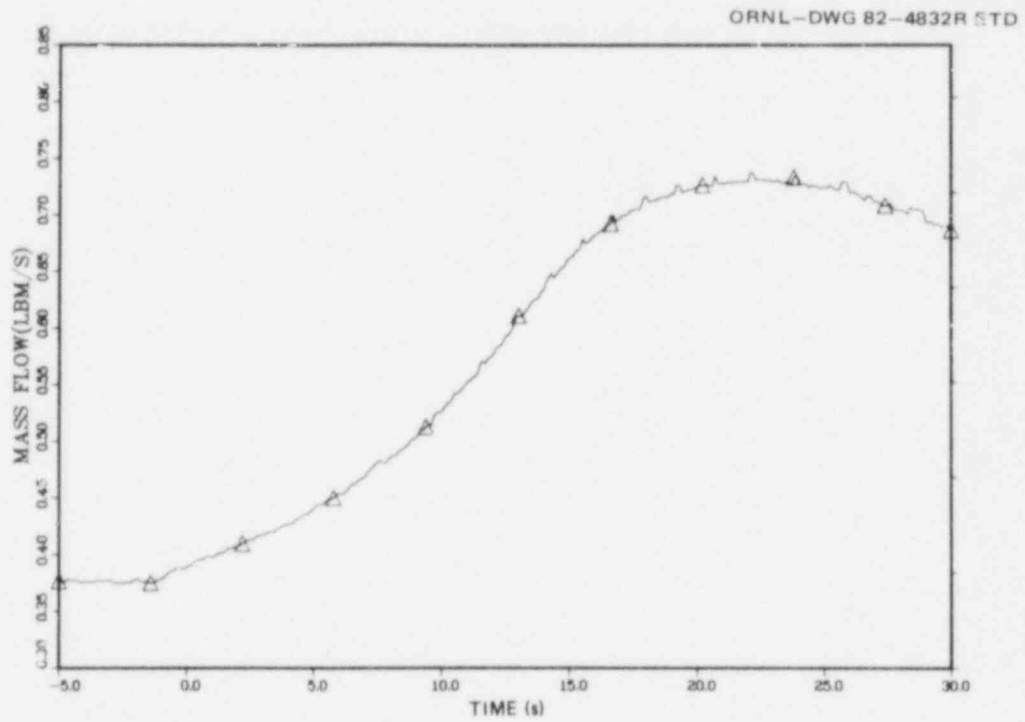


Fig. B.14. Test section outlet mass flow rate for Test 3.09.100; based on FE-282.

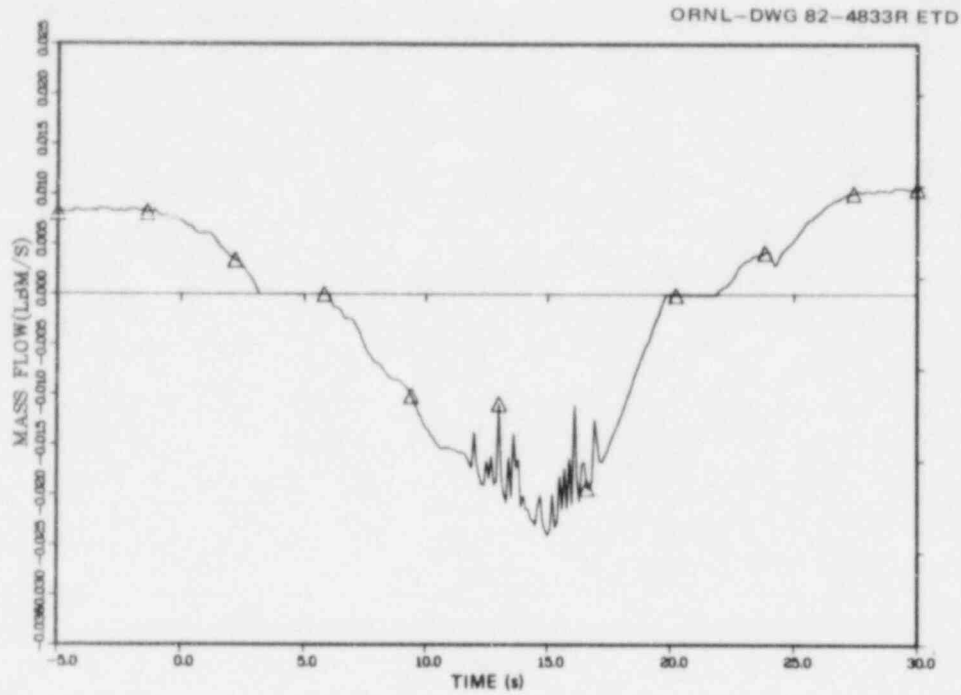


Fig. B.15. Shroud bypass line flow rate for Test 3.09.100; based on FE-280.

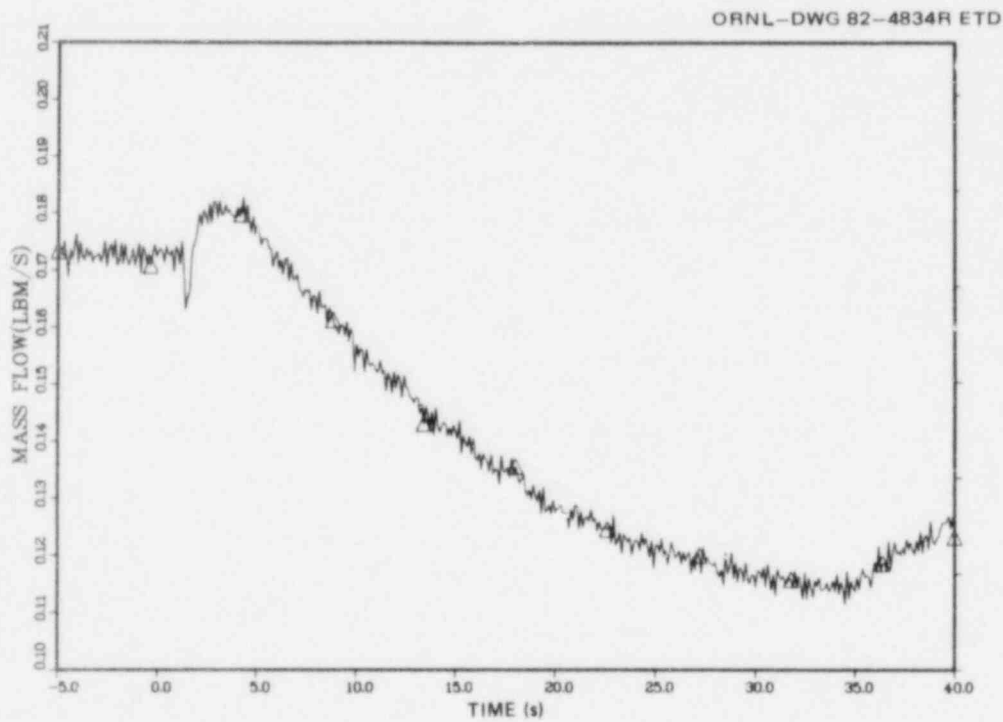


Fig. B.16. Test section inlet mass flow rate for Test 3.09.10P; based on FE-250.

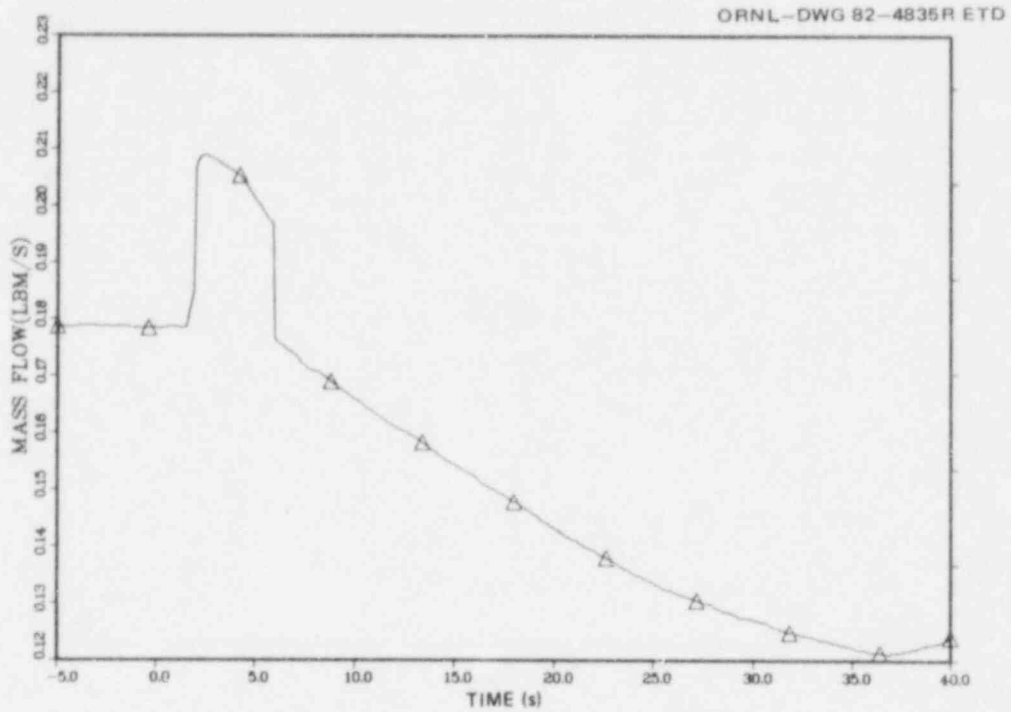


Fig. B.17. Test section inlet mass flow rate for Test 3.09.10P; based on FE-18A.

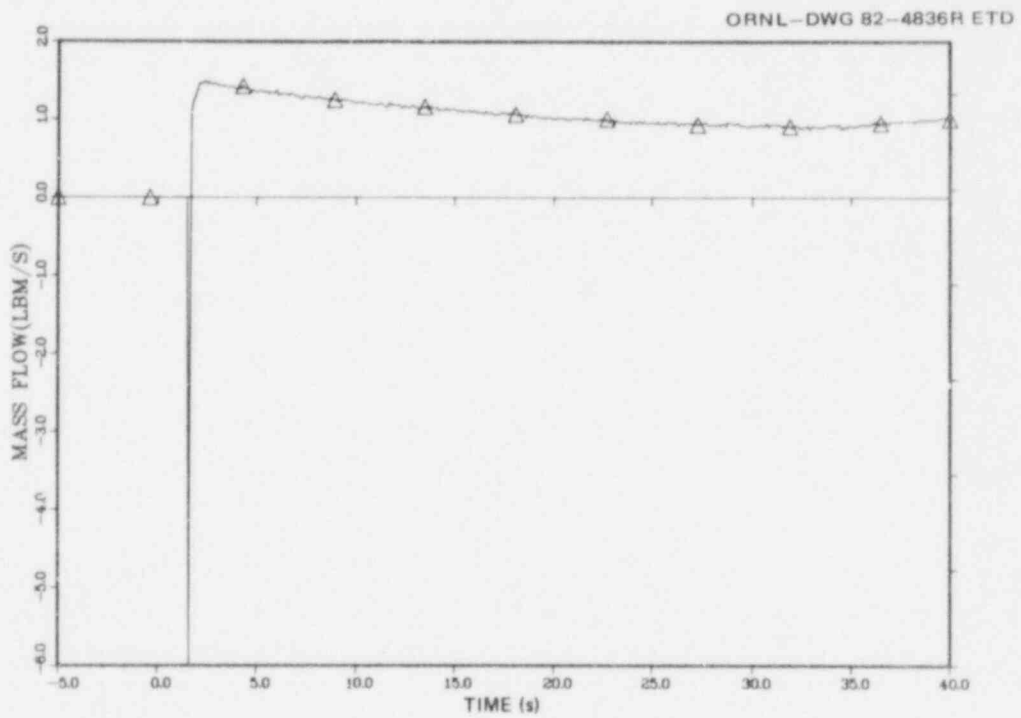


Fig. B.18. Test section inlet mass flow rate for Test 3.09.10P; based on FE-3.

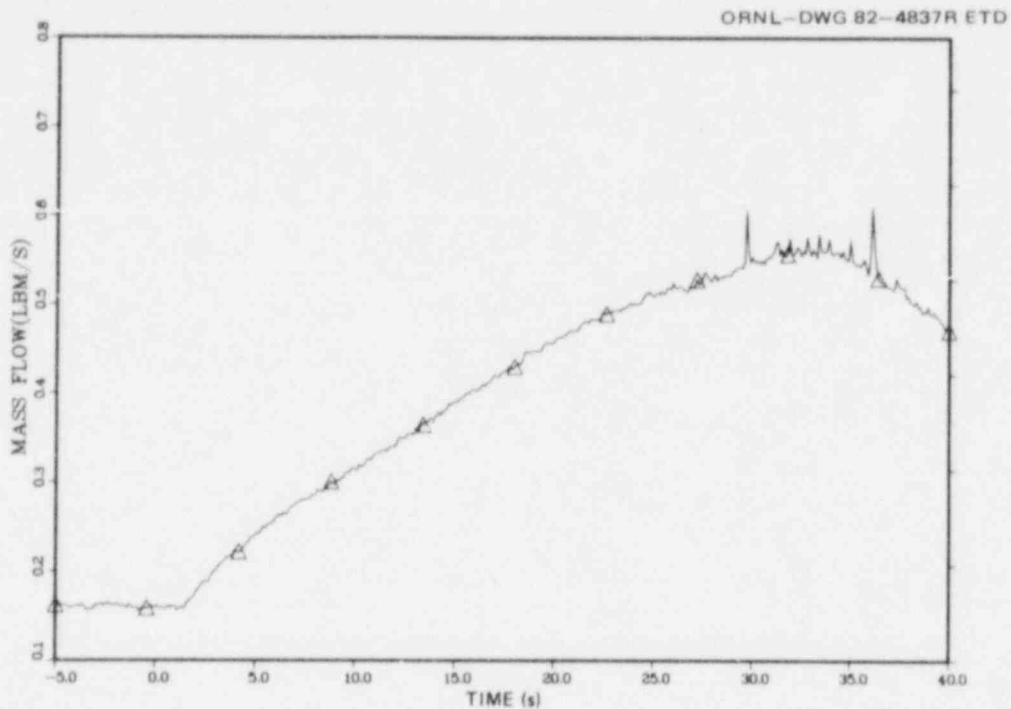


Fig. B.19. Test section outlet mass flow rate for Test 3.09.10P; based on FE-202.

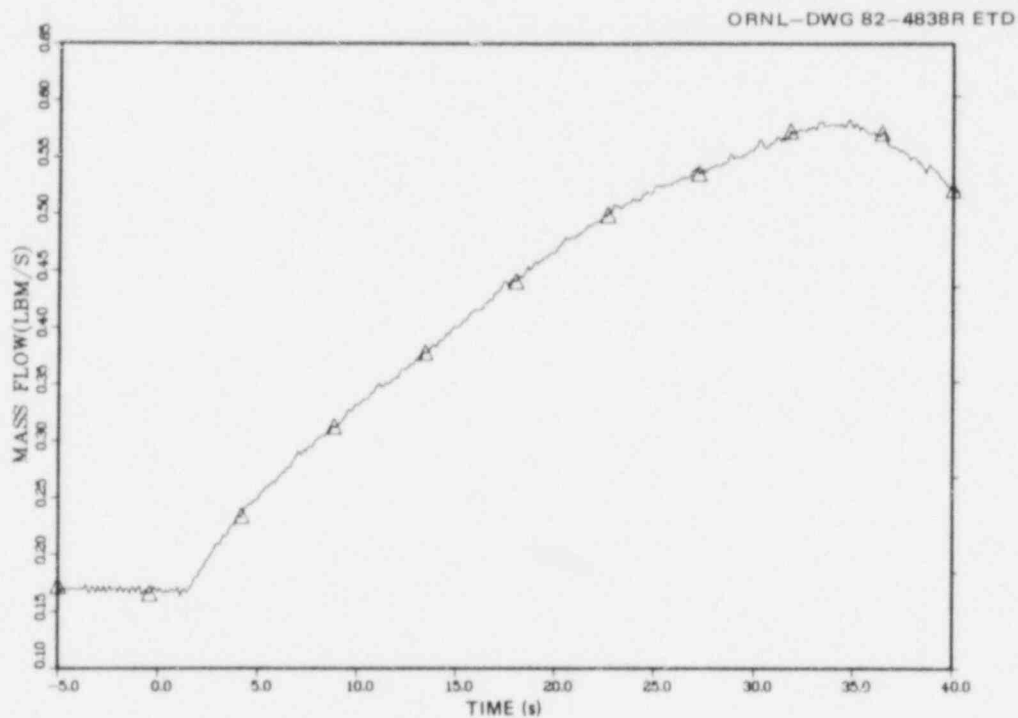


Fig. B.20. Test section outlet mass flow rate for Test 3.09.10P; based on FE-282.

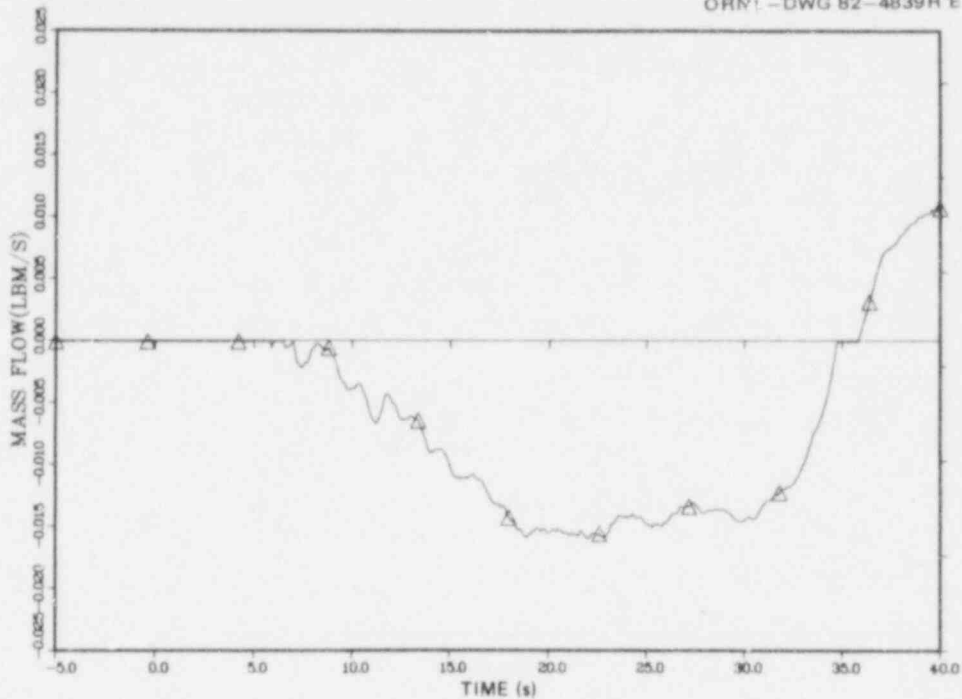


Fig. B.21. Shroud bypass line flow rate for Test 3.09.10P; based on FE-280.

These flows are valid until the initiation of reflod at ~1.6 s. The 1/2-in. turbine meter, FE-260, failed and is not shown. Figure B.18 shows the inlet reflod mass flow rate once the flow exceeds the deadband of the 2-in. turbine meter, FE-3. Figure B.19 shows the mass flow calculated at the outlet turbine meter, FE-202; Fig. B.20 shows results from the high range outlet orifice flowmeter, FE-282. The outlet orifice flow manifold bypass line was open for this test and thus invalidates measurements made by FE-283. Mass flow calculated in the shroud bypass line is shown in Fig. B.21.

Mass flows of interest for the transient reflod Test 3.09.10Q are shown in Figs. B.22-B.27. Mass flows are shown for FE-250 and FE-18A in Figs. B.22 and B.23, indicating the pre-reflod inlet mass flow rates. Reflod for this test was through the 1/2-in. steady-state line, and so measurements from FE-18A and FE-250 are valid until they are overranged at ~4.3 and 4.5 s, respectively. The 1/2-in. turbine meter, FE-260, failed and is not shown. Figure B.24 shows the inlet reflod mass flow rate once the flow exceeds the deadband of the 2-in. turbine meter, FE-3. Figure B.25 shows the mass flow calculated at the outlet turbine meter, FE-202; Fig. B.26 shows results from the high range outlet orifice flowmeter, FE-282. The outlet orifice flow manifold bypass line was open for this test and thus invalidates measurements made by FE-283. Mass flow calculated in the shroud bypass line is shown in Fig. B.27.

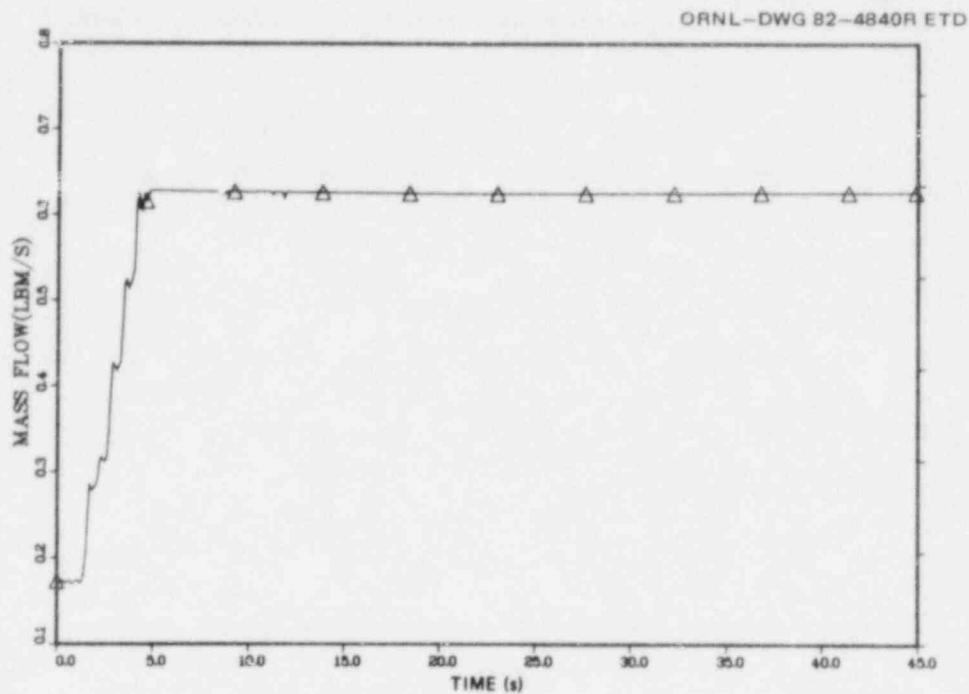


Fig. B.22. Test section inlet mass flow rate for Test 3.09.10Q; based on FE-250.

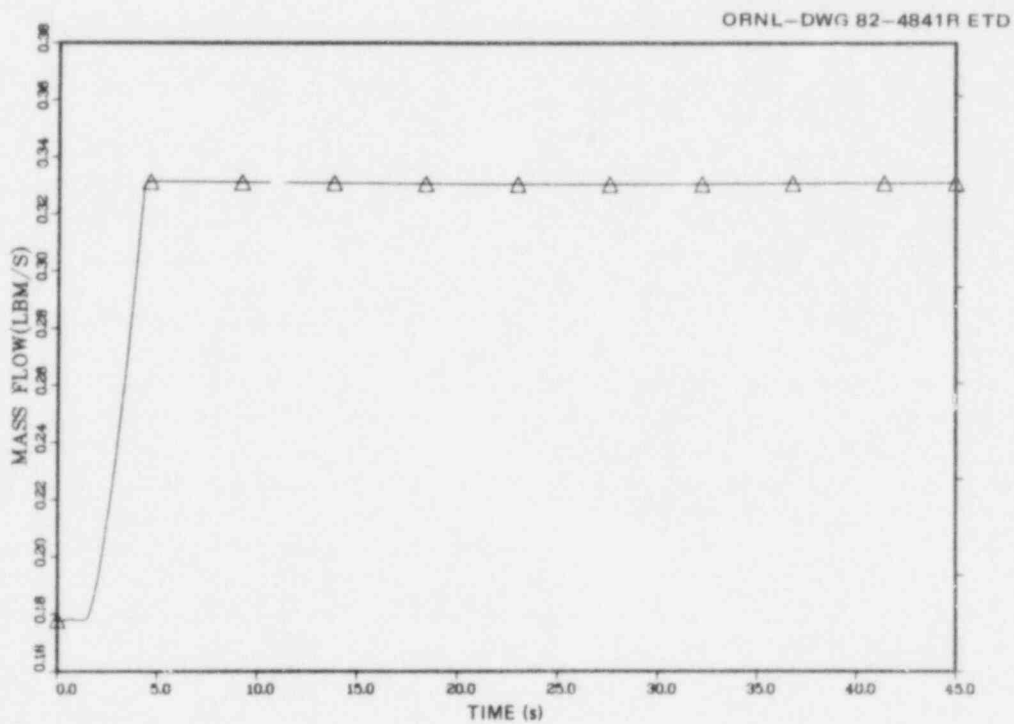


Fig. B.23. Test section inlet mass flow rate for Test 3.09.10Q; based on FE-18A.

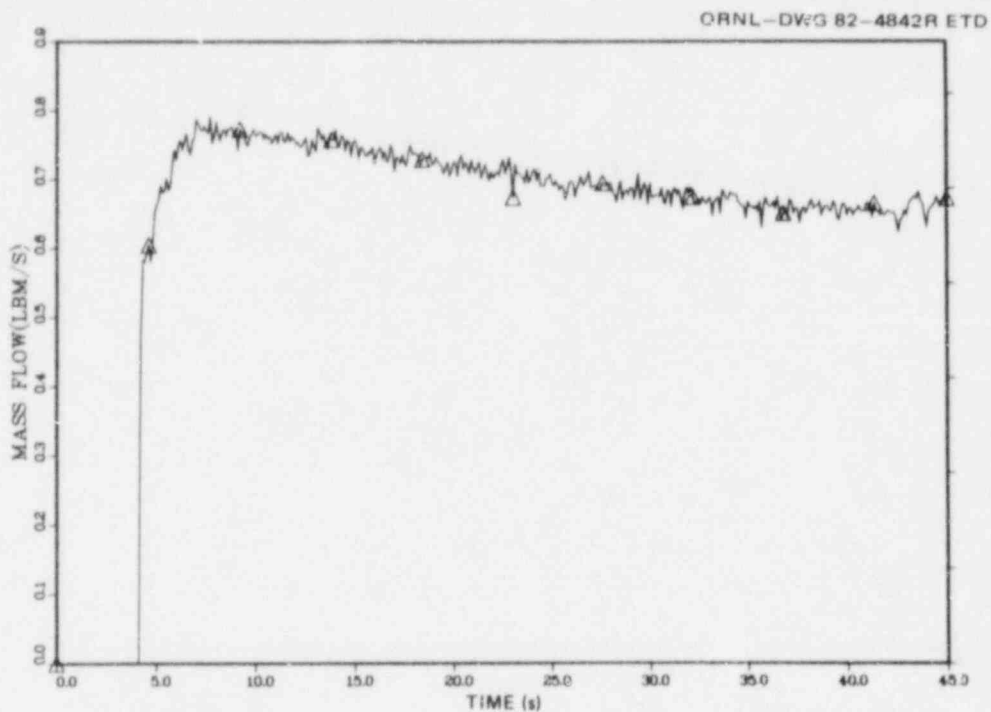


Fig. B.24. Test section inlet mass flow rate for Test 3.09.10Q; based on FE-3.

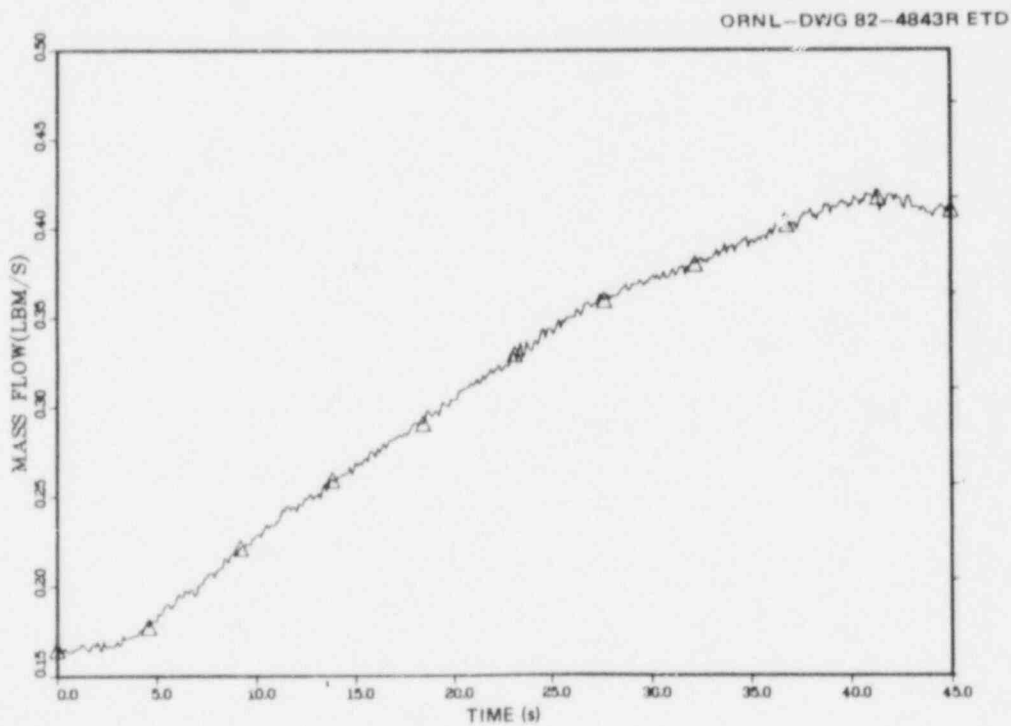


Fig. B.25. Test section outlet mass flow rate for Test 3.09.10Q; based on FE-202.

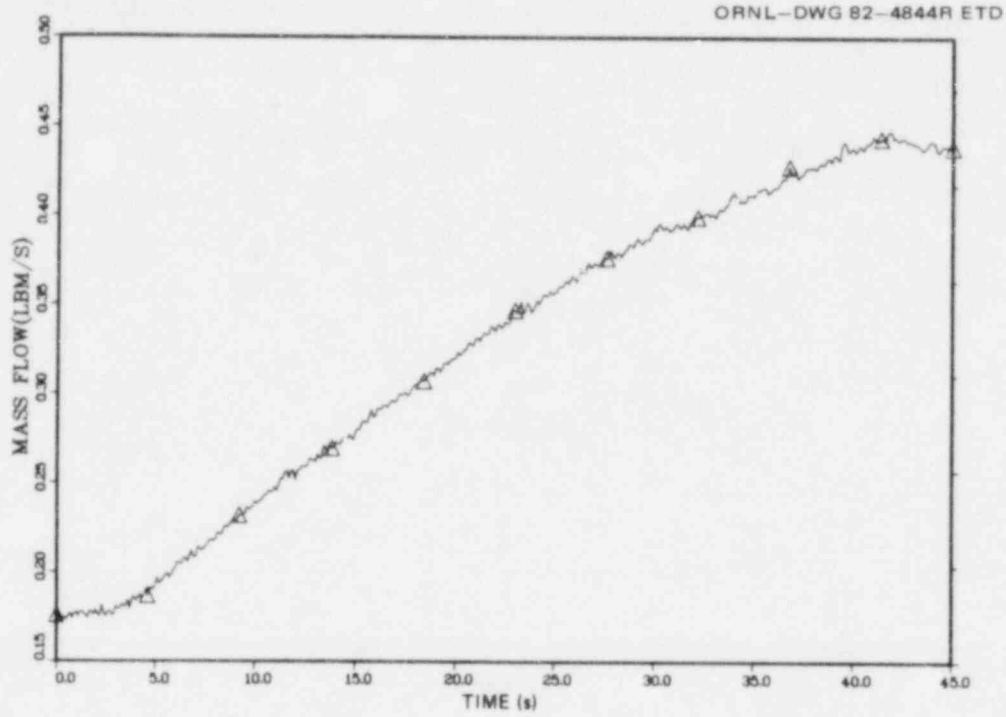


Fig. B.26. Test section outlet mass flow rate for Test 3.09.10Q; based on FE-282.

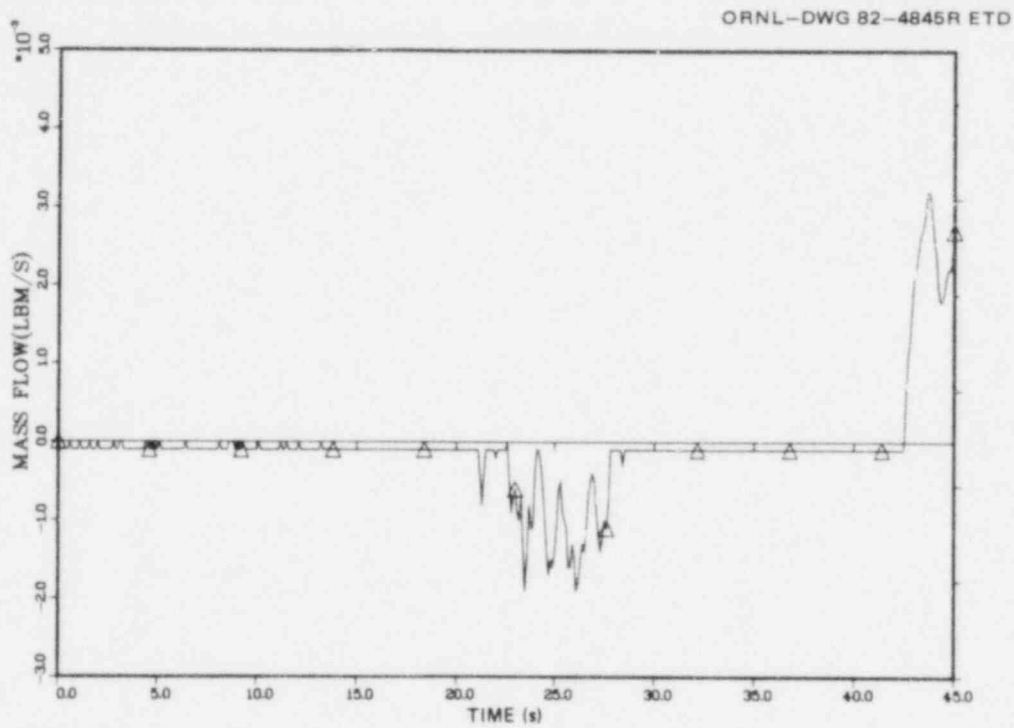


Fig. B.27. Shroud bypass line flow rate for Test 3.09.10Q; based on FE-280.

Mass flows of interest for the transient reflood Test 3.09.10R are shown in Figs. B.28-B.32. Mass flow is shown for FE-250 in Fig. B.28 indicating the pre-reflood inlet mass flow rate. This flow is valid until the initiation of reflood at ~ 1.7 s. FE-18A was overranged and is not shown. The 1/2-in. turbine meter, FE-260, failed and is not shown. Figure B.29 shows the inlet reflood mass flow rate once the flow exceeds the deadband of the 2-in. turbine meter, FE-3. Figure B.30 shows the mass flow calculated at the outlet turbine meter, FE-202; Fig. B.31 shows results from the high range outlet orifice flowmeter, FE-282. The outlet orifice flow manifold bypass line was open for this test, invalidating measurements made by FE-283. Mass flow calculated in the shroud bypass line is shown in Fig. B.32.

Mass flows of interest for the transient reflood Test 3.09.10S are shown in Figs. B.33-B.38. Mass flows are shown for FE-250 and FE-18A in Figs. B.33 and B.34, indicating the pre-reflood inlet mass flow rates. These flows are valid until the initiation of reflood at 1.4 s. The 1/2-in. turbine meter, FE-260, failed and is not shown. Figure B.35 shows the inlet reflood mass flow rate once the flow exceeds the deadband of the 2-in. turbine meter, FE-3. Figure B.36 shows the mass flow calculated at the outlet turbine meter, FE-202; Fig. B.37 shows results from the high range outlet orifice flowmeter, FE-282. The outlet orifice flow manifold bypass line was open for this test invalidating measurements made by FE-283. Mass flow calculated in the shroud bypass line is shown in Fig. B.38.

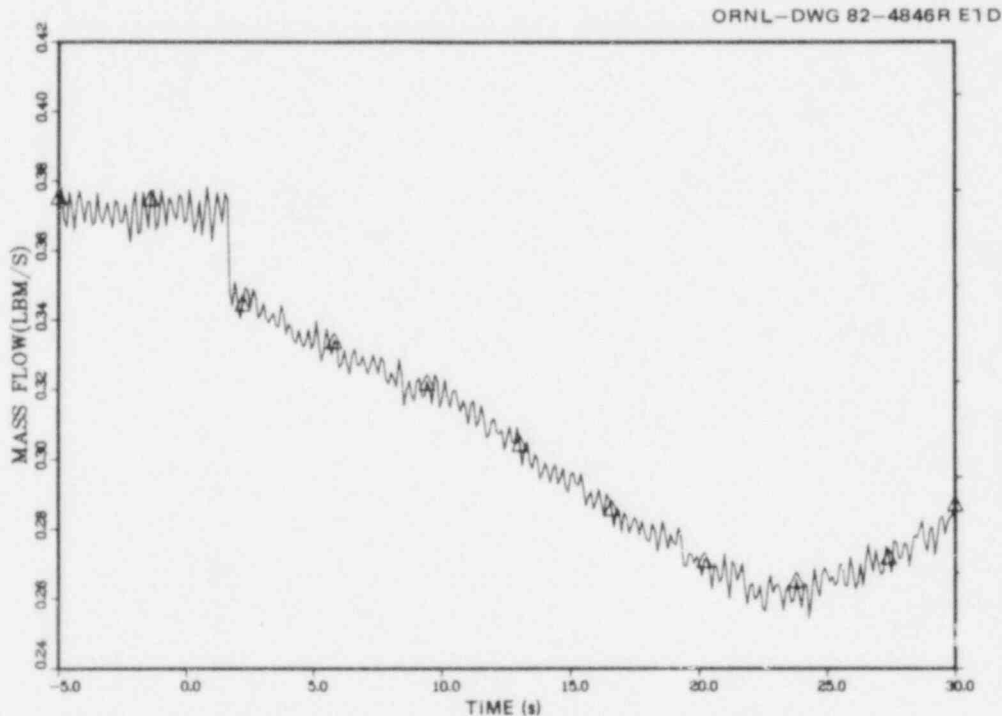


Fig. B.28. Test section inlet mass flow rate for Test 3.09.10R; based on FE-250.

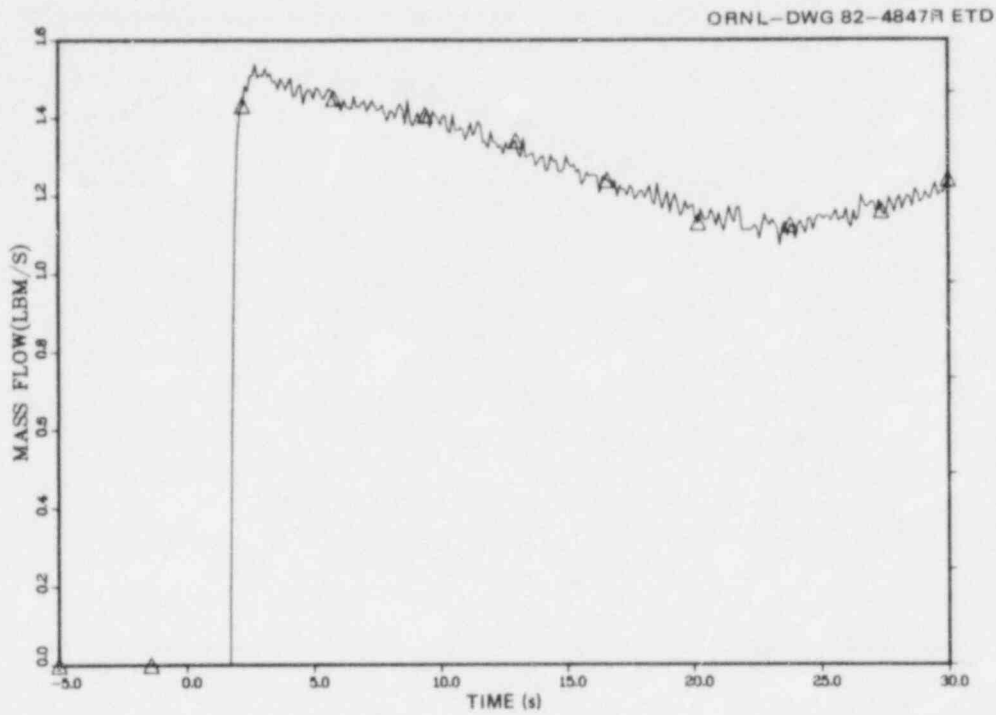


Fig. B.29. Test section inlet mass flow rate for Test 3.09.10R; based on FE-3.

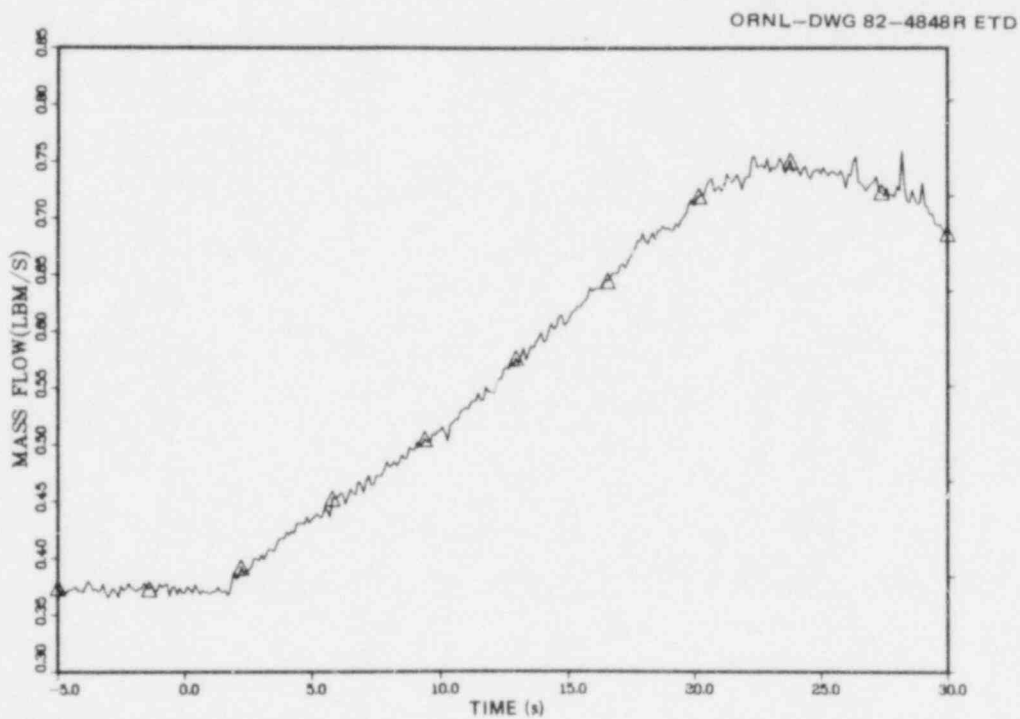


Fig. B.30. Test section outlet mass flow rate for Test 3.09.10R; based on FE-202.

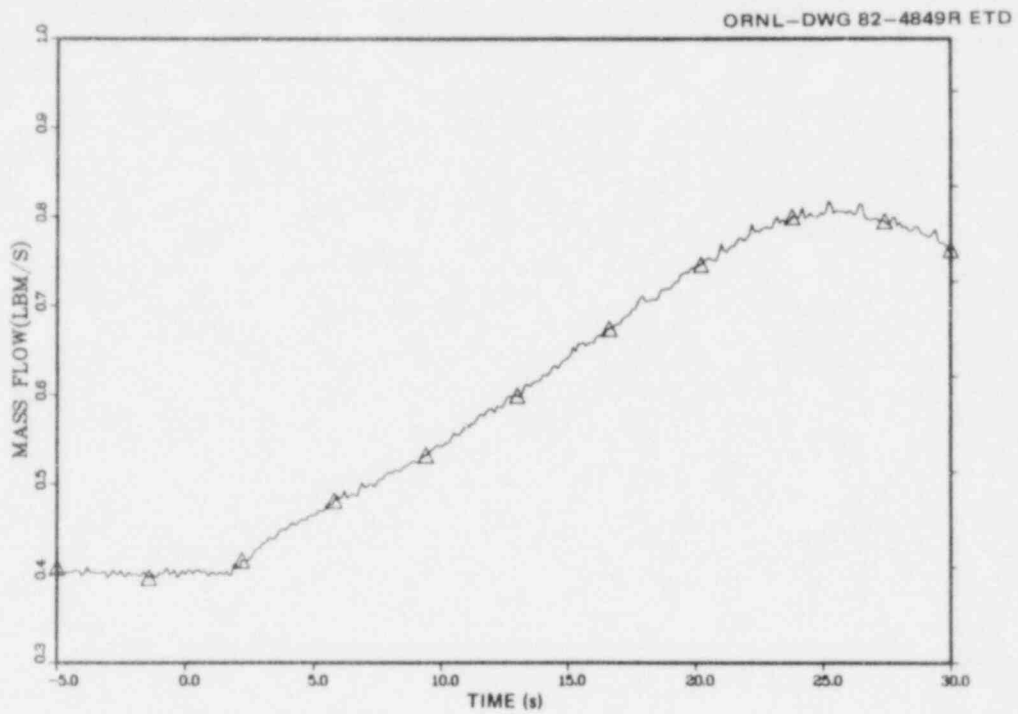


Fig. B.31. Test section outlet mass flow rate for Test 3.09.10R; based on FE-282.

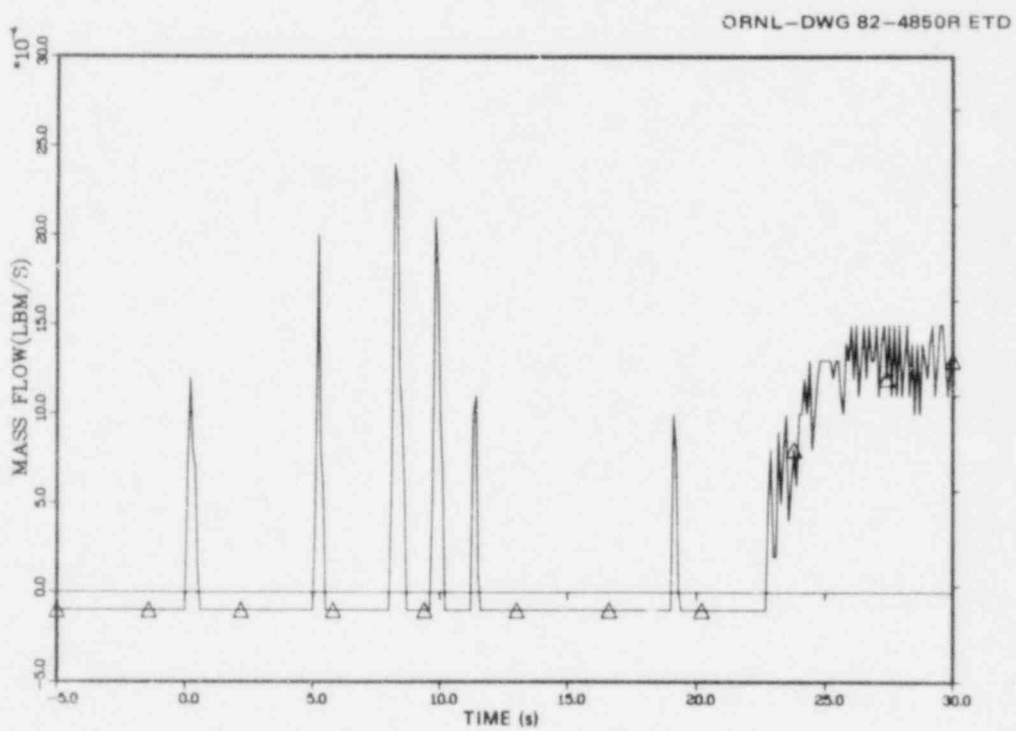


Fig. B.32. Shroud bypass line flow rate for Test 3.09.10R; based on FE-280.

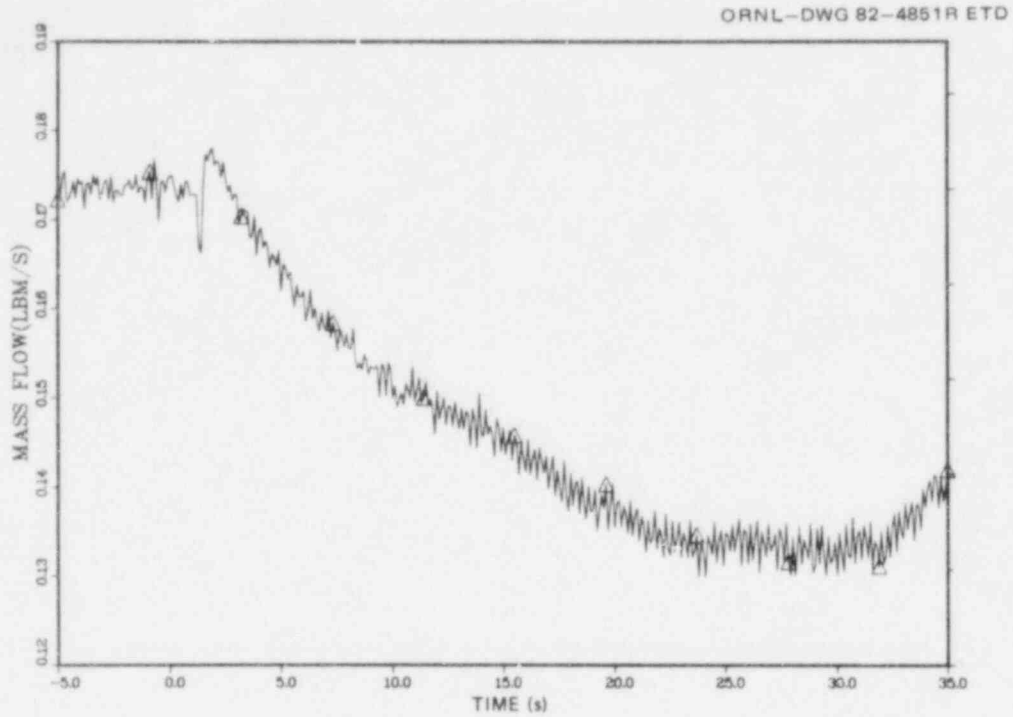


Fig. B.33. Test section inlet mass flow rate for Test 3.09.10S; based on FE-250.

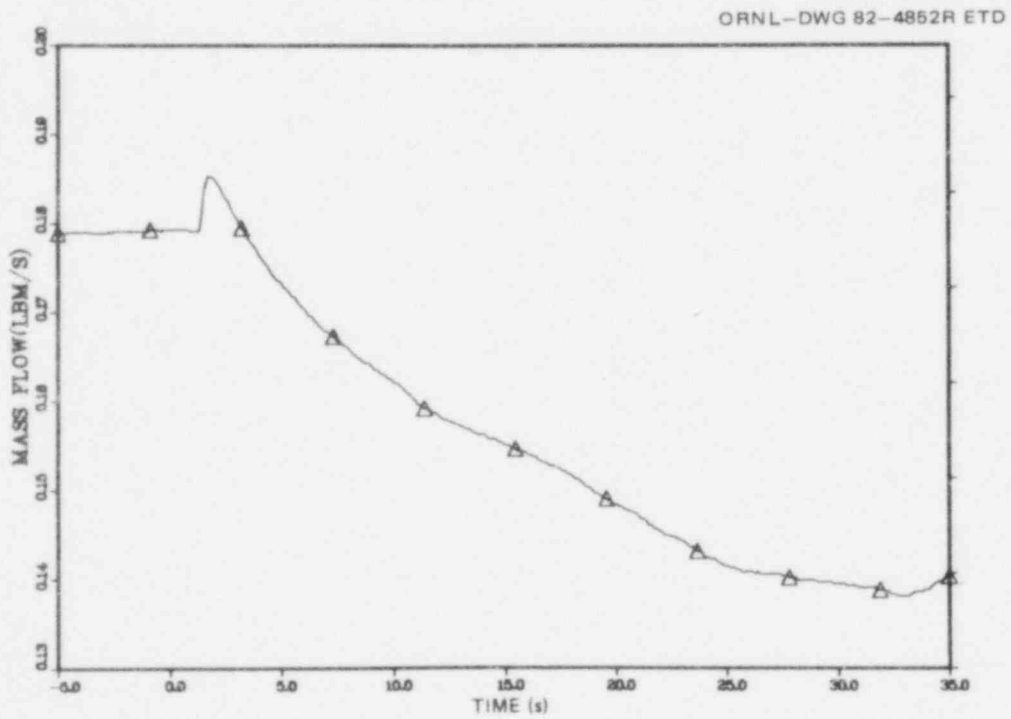


Fig. B.34. Test section inlet mass flow rate for Test 3.09.10S; based on FE-18A.

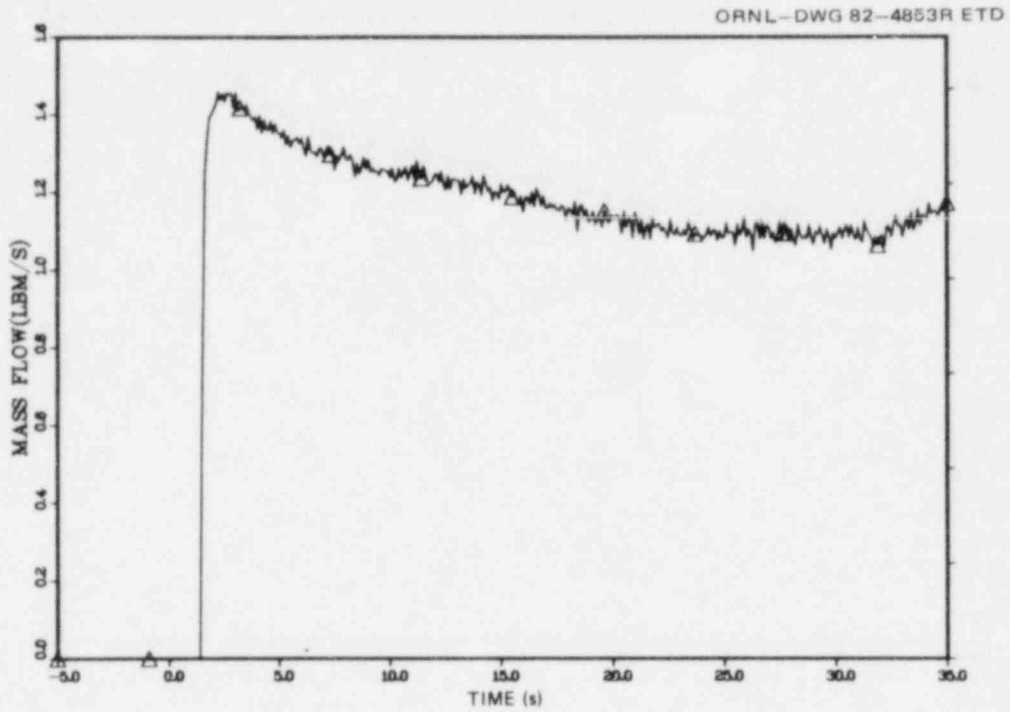


Fig. B.35. Test section inlet mass flow rate for Test 3.09.10S; based on FE-3.

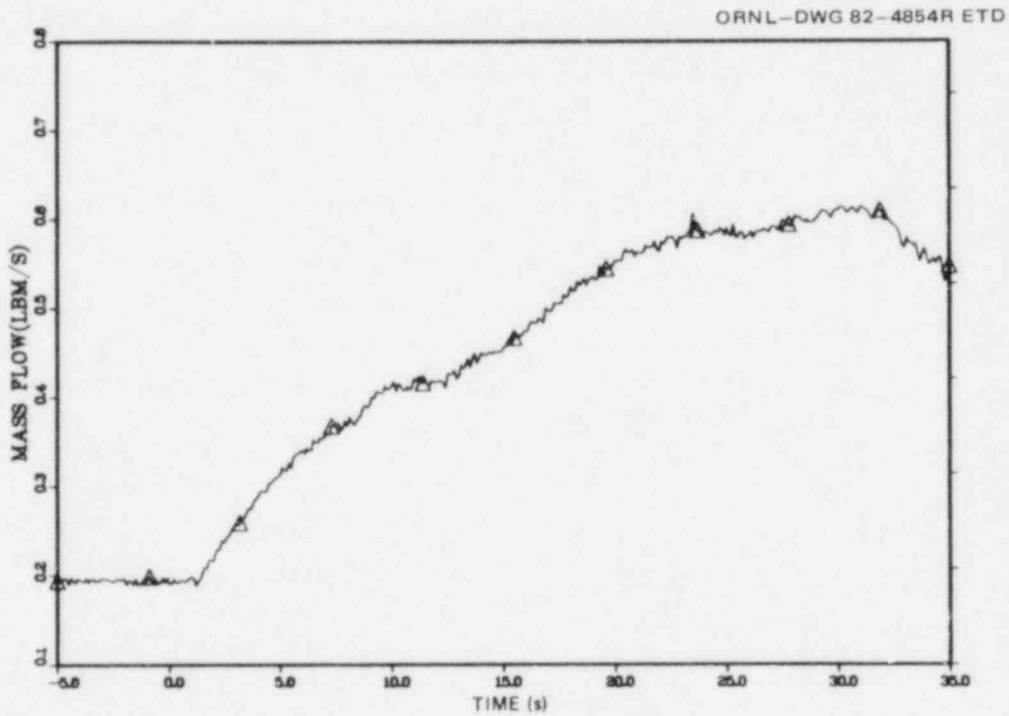


Fig. B.36. Test section outlet mass flow rate for Test 3.09.10S; based on FE-202.

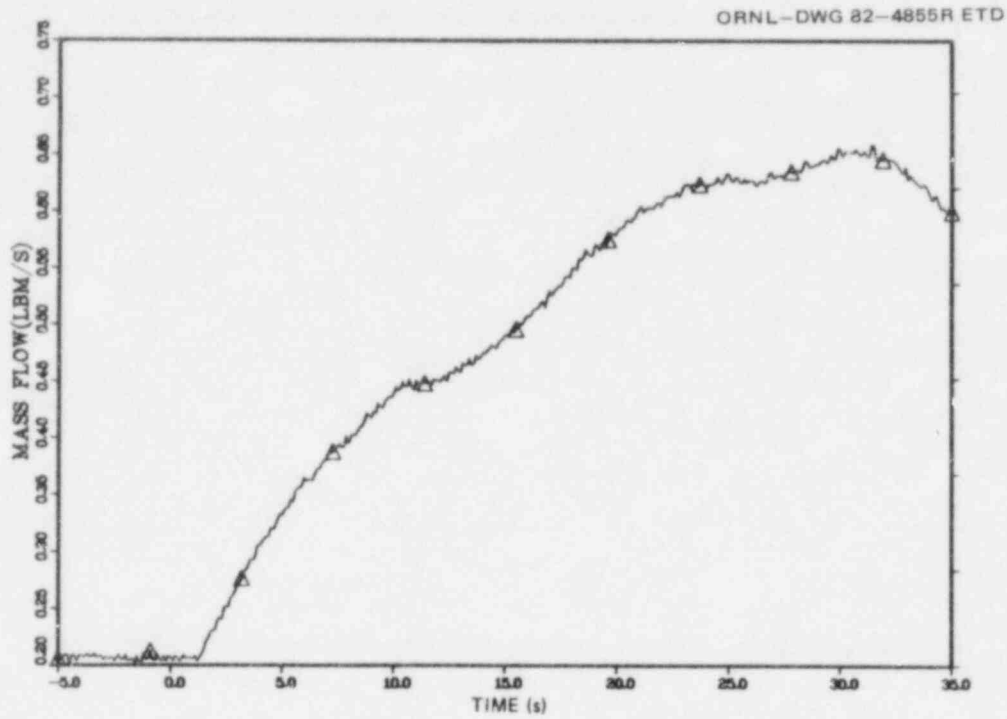


Fig. B.37. Test section outlet mass flow rate for Test 3.09.10S; based on FE-282.

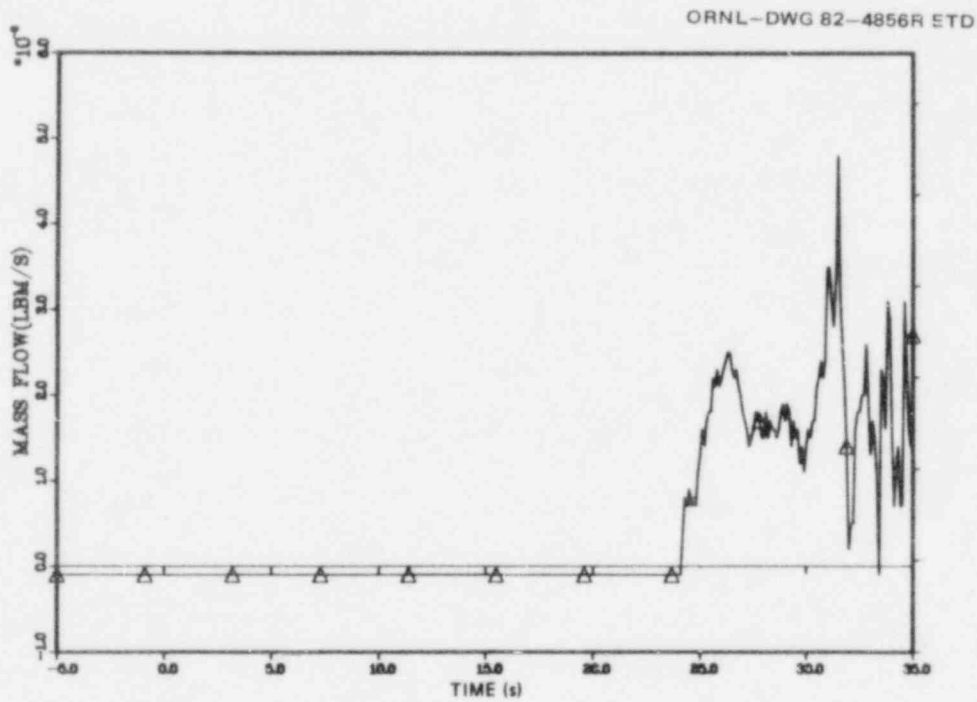


Fig. B.38. Shroud bypass line flow rate for Test 3.09.10S; based on FE-280.

Mass flows for the boiloff tests are shown only for the outlet instrumentation, because inlet flow was shut off to initiate these tests.

The mass flows for Test 3.09.10T are shown in Figs. B.39-B.41. Flows at FE-202 and FE-282 are shown in Figs. B.39 and B.40, respectively. Since the bypass leg in the outlet orifice manifold was open, FE-283 measurements are not shown. The shroud bypass flow is shown in Fig. B.41, where positive flow is out of the shroud plenum annulus.

The mass flows for boiloff Test 3.09.10U are shown in Figs. B.42-B.44. The outlet orifice manifold bypass line was again open so that mass flows at FE-283 are not shown.

The mass flows for boiloff Test 3.09.10V are shown in Figs. B.45-B.48. The outlet orifice manifold bypass line was closed for this test, so all of the outlet flow does pass through the line containing FE-283.

The mass flows for boiloff Test 3.09.10W are shown in Figs. B.49-B.52. The turbine meter, FE-202, in Fig. B.49 appears to be in the deadband for the low initial flows (~ 3 s). The bypass line in the outlet orifice manifold is closed for this test, so all of the outlet flow passes through the line containing FE-283.

The mass flows for boiloff test 3.09.10X are shown in Figs. B.53-B.56. The turbine meter, FE-202, is apparently in the deadband over most of the transient. The bypass line in the outlet orifice manifold is again closed for this test, so all of the outlet flow passes through the line containing FE-283.

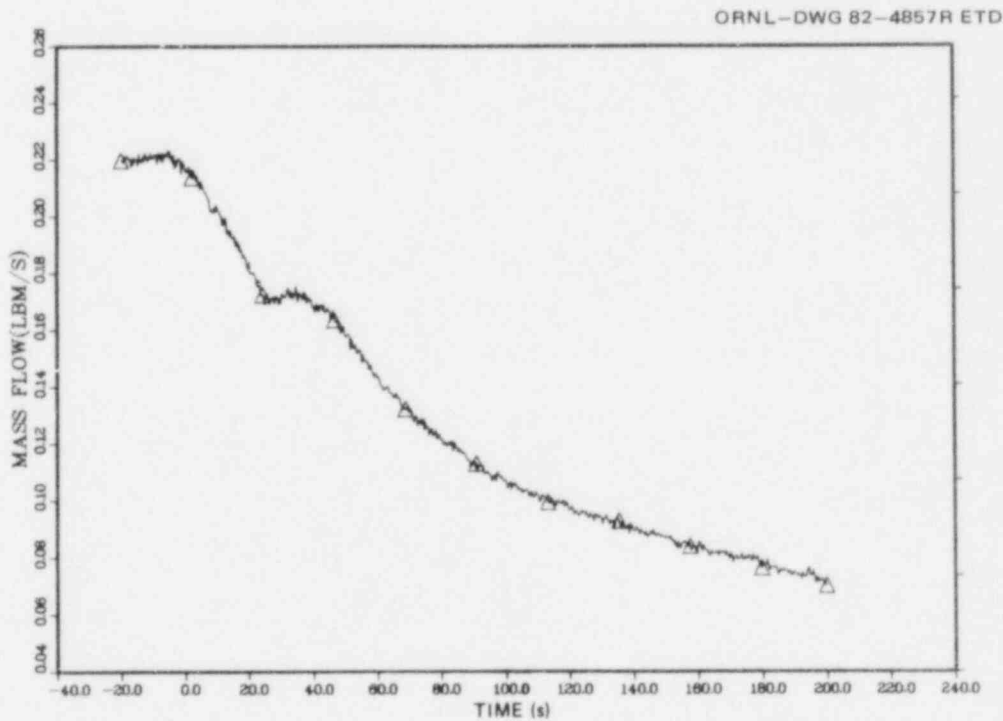


Fig. B.39. Test section outlet mass flow rate for Test 3.09.10T; based on FE-202.

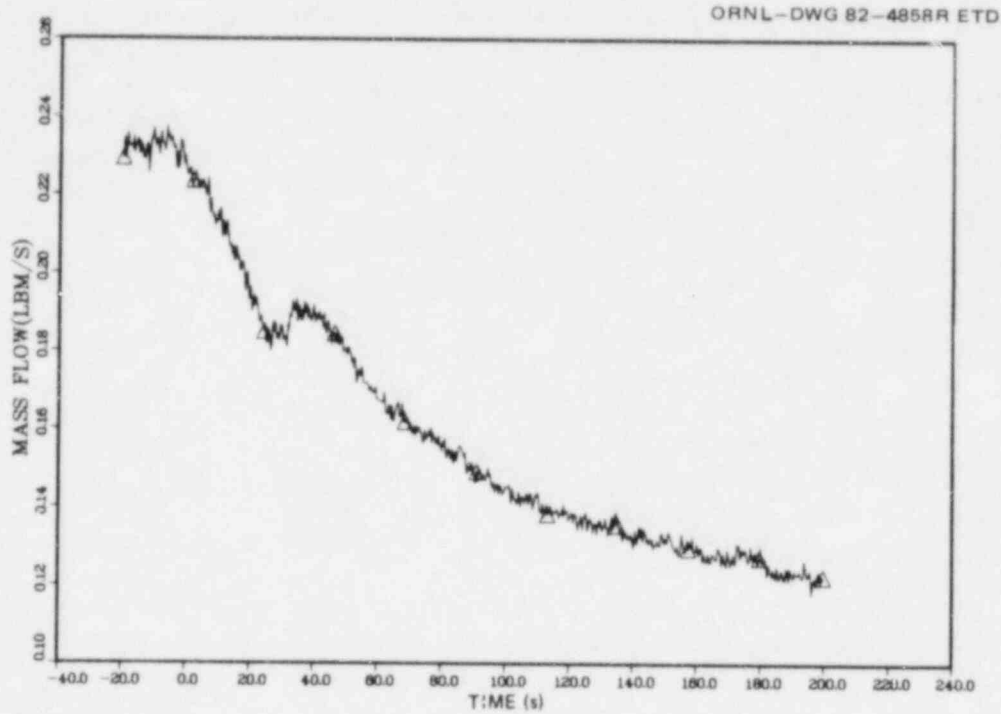


Fig. B.40. Test section outlet mass flow rate for Test 3.09.10T; based on FE-282.

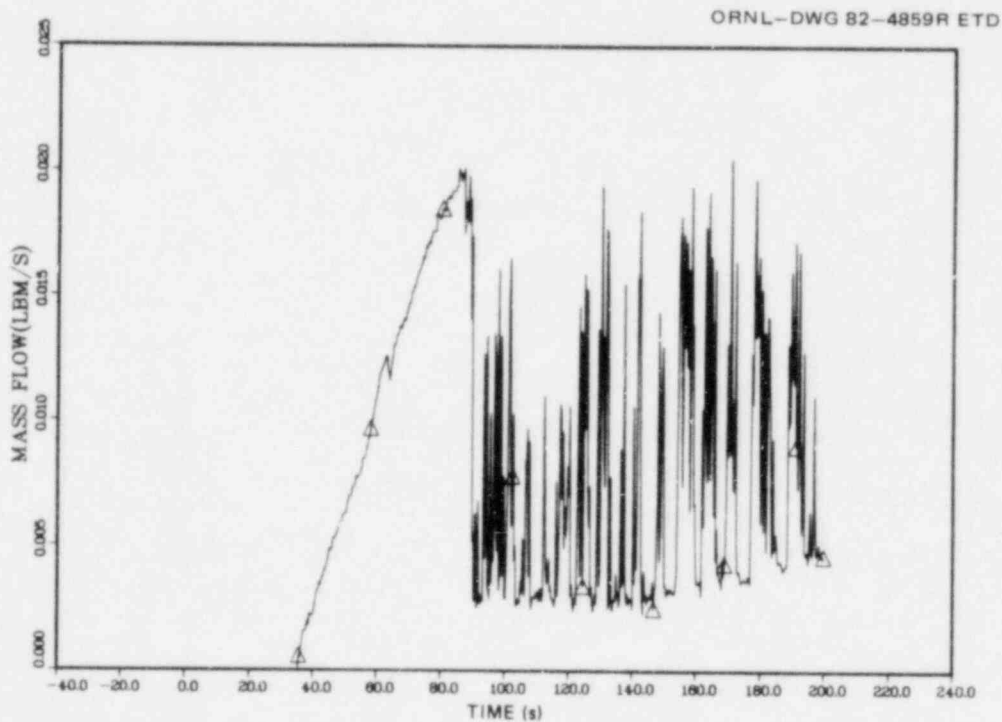


Fig. B.41. Shroud bypass line flow rate for Test 3.09.10T; based on FE-280.

ORNL-DWG 82-4860R ETD

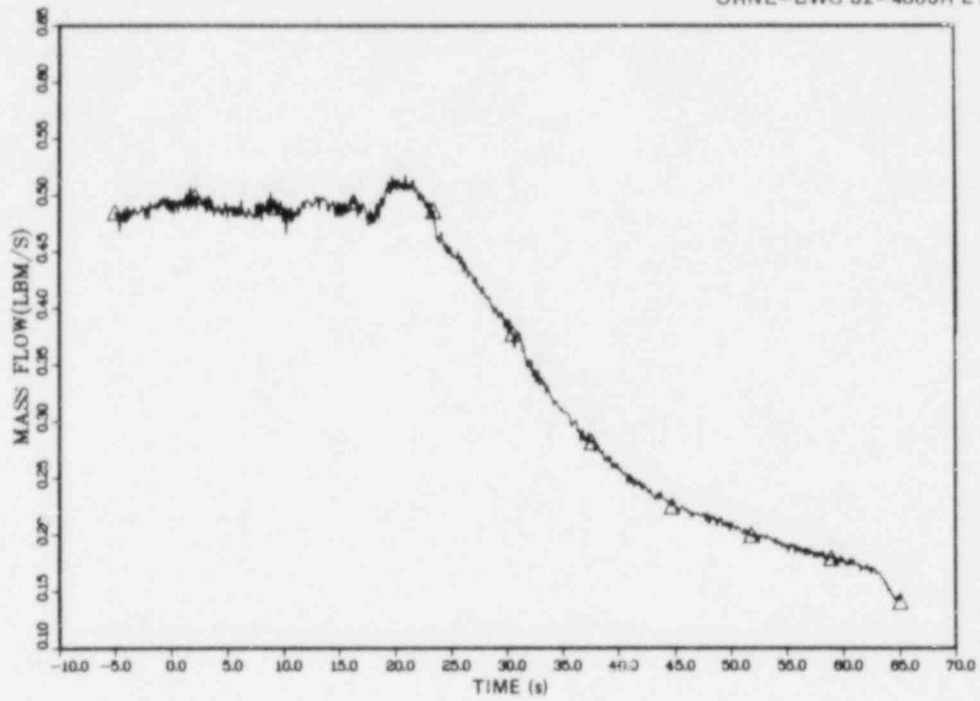


Fig. B.42. Test section outlet mass flow rate for Test 3.09.10U; based on FE-202.

ORNL-DWG 82-4861R ETD

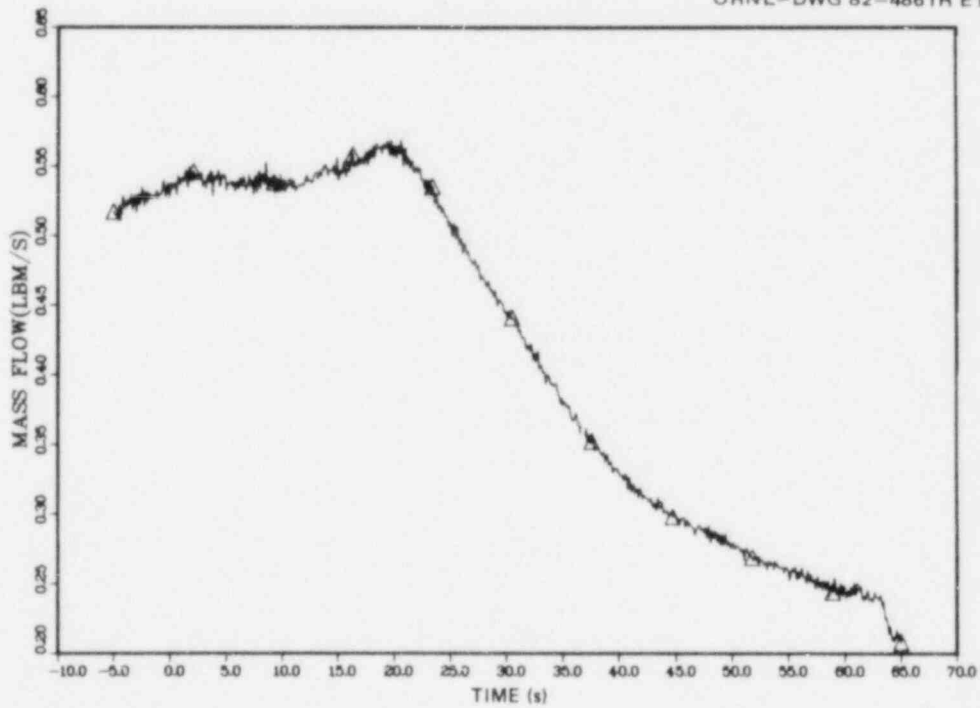


Fig. B.43. Test section outlet mass flow rate for Test 3.09.10U; based on FE-282.

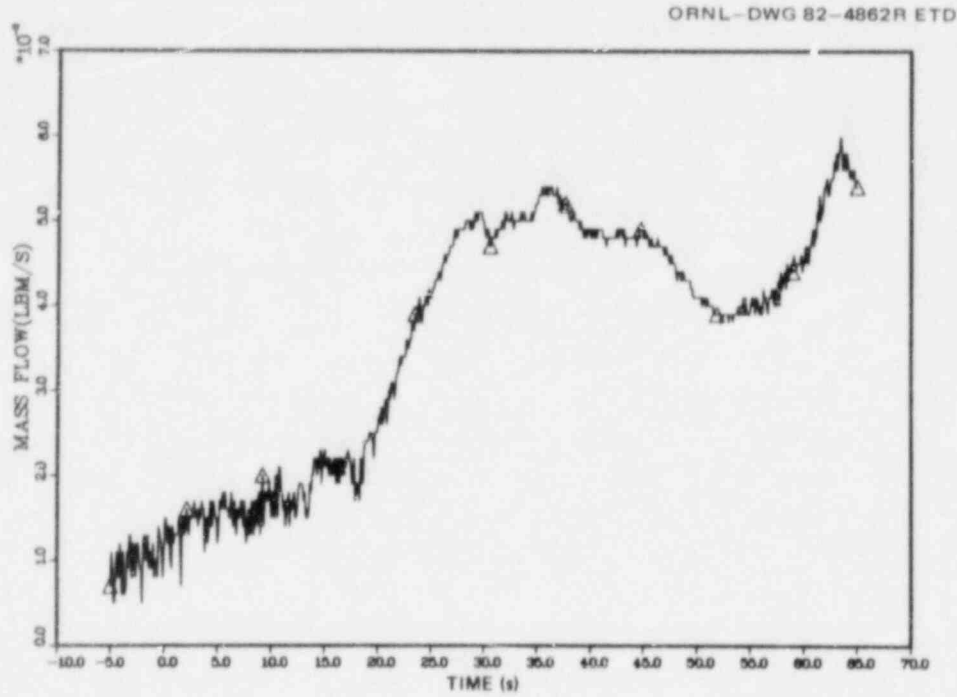


Fig. B.44. Shroud bypass line flow rate for Test 3.09.10U; based on FE-280.

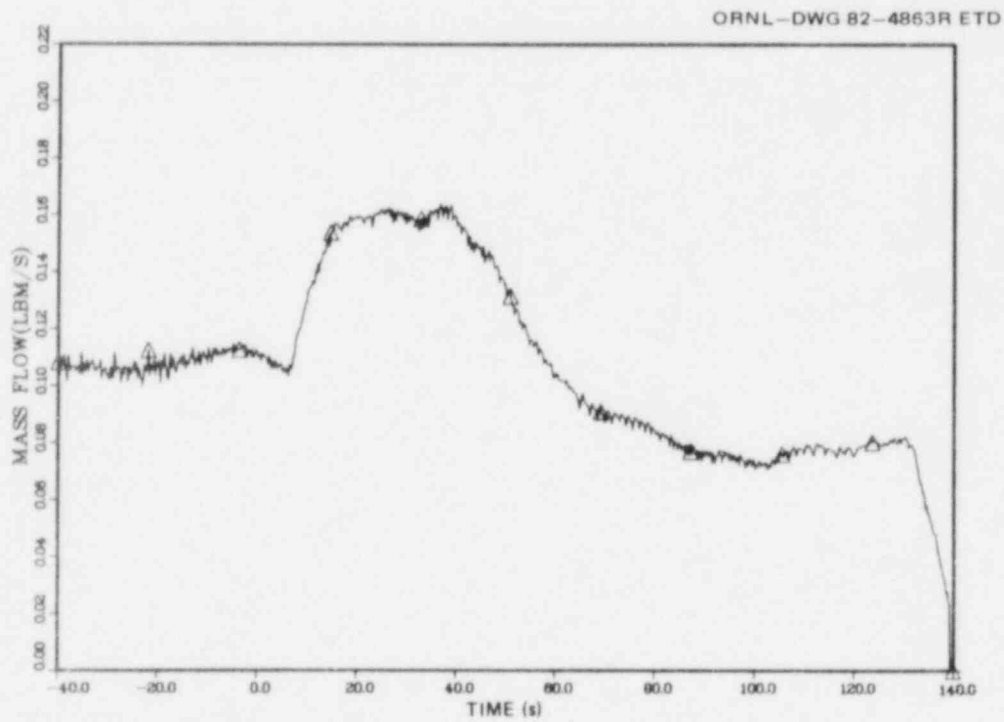


Fig. B.45. Test section outlet mass flow rate for Test 3.09.10V; based on FE-202.

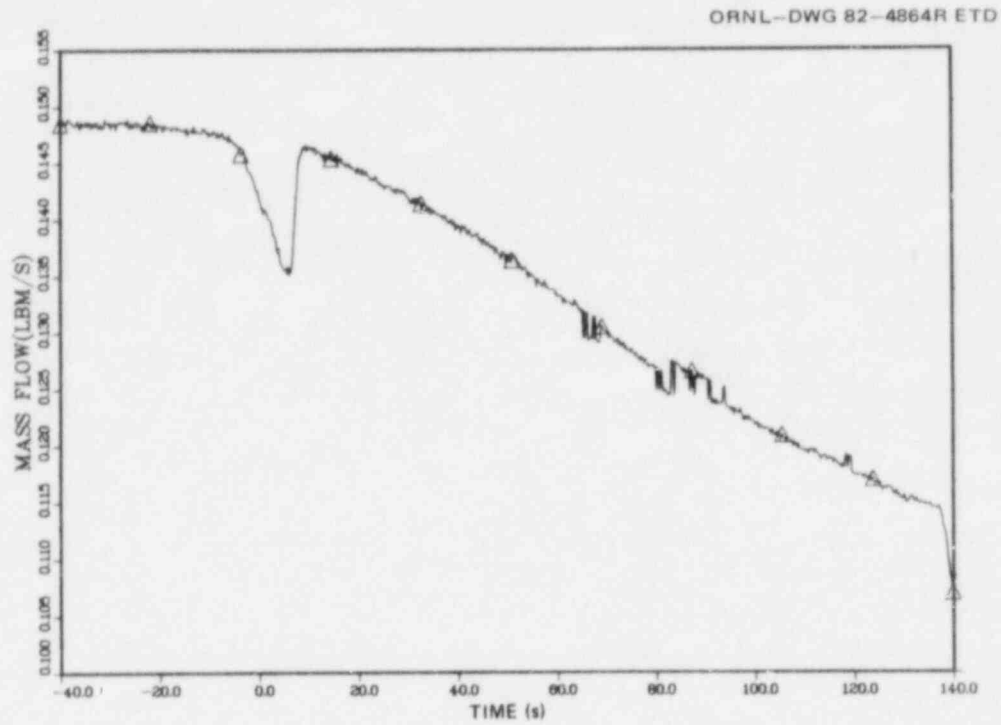


Fig. B.46. Test section outlet mass flow rate for Test 3.09.10V; based on FE-283.

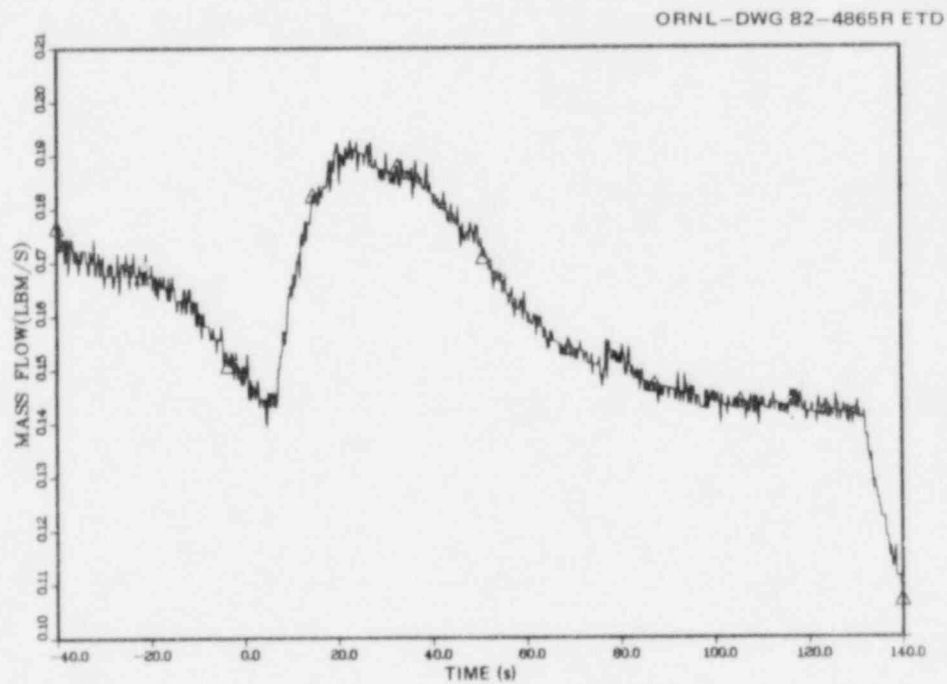


Fig. B.47. Test section outlet mass flow rate for Test 3.09.10V; based on FE-282.

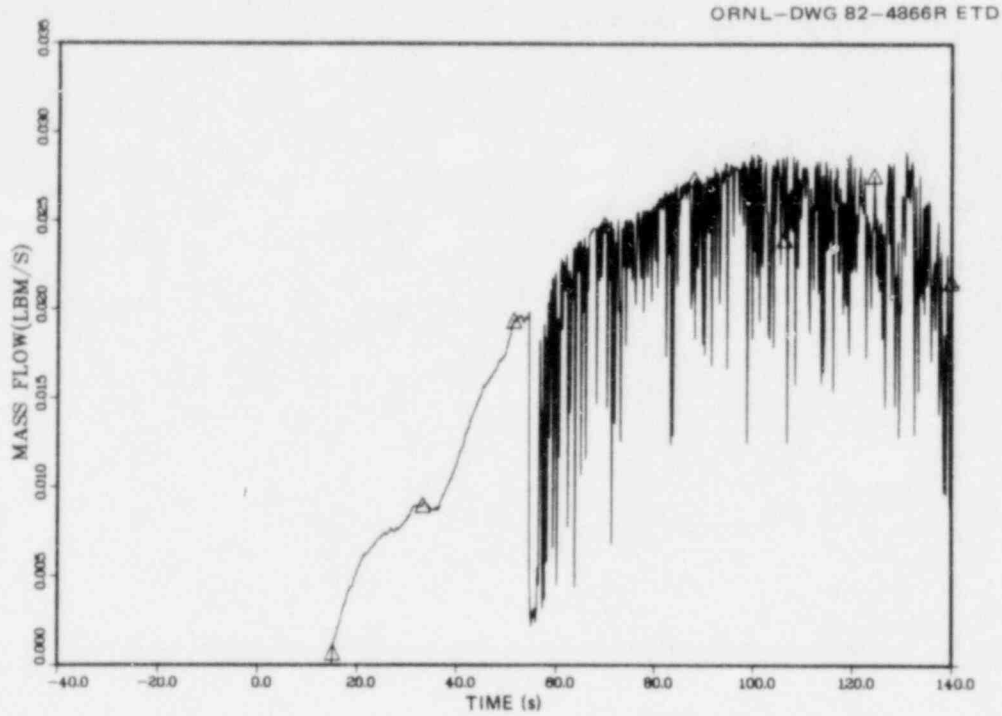


Fig. B.48. Shroud bypass line flow rate for Test 3.09.10V; based on FE-280.

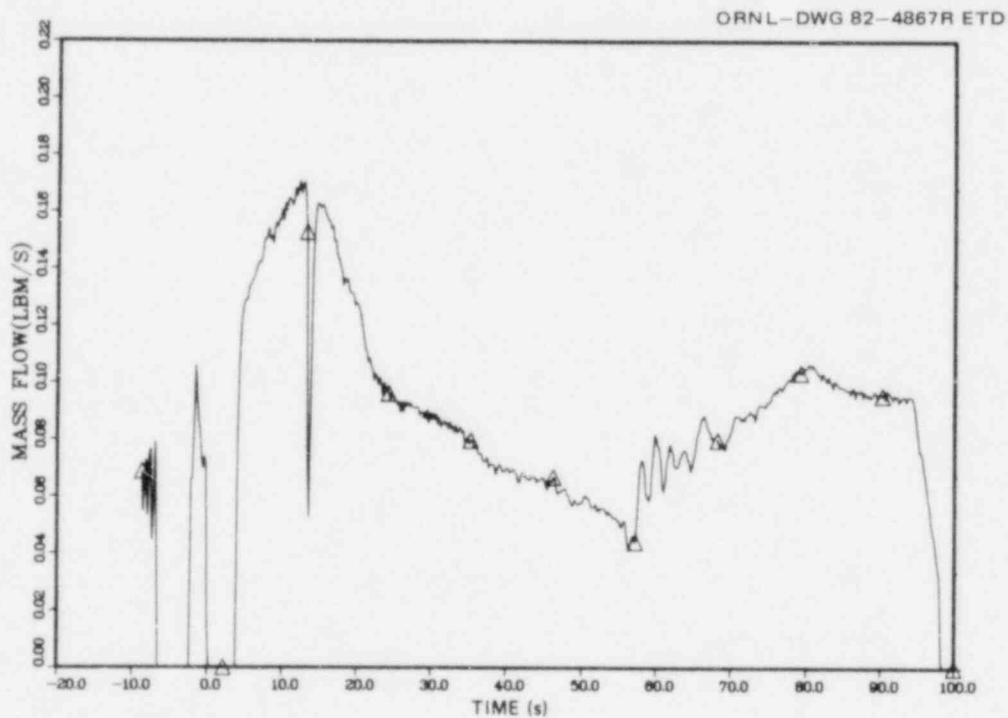


Fig. B.49. Test section outlet mass flow rate for Test 3.09.10W; based on FE-202.

ORNL-DWG 82-4868R ETD

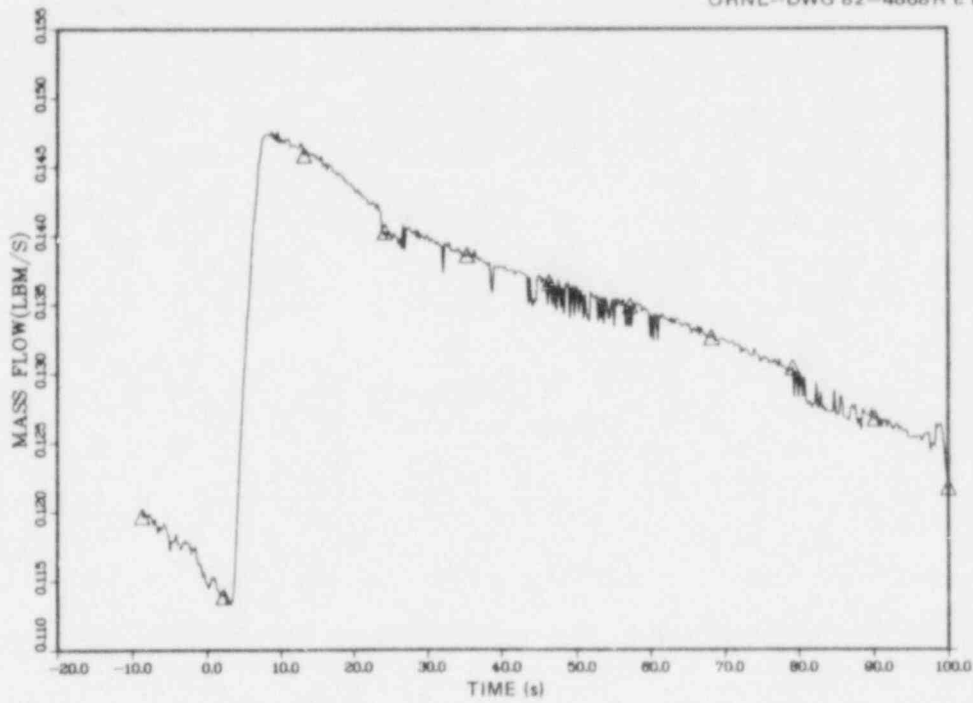


Fig. B.50. Test section outlet mass flow rate for Test 3.09.10W; based on FE-283.

ORNL-DWG 82-4869R ETD

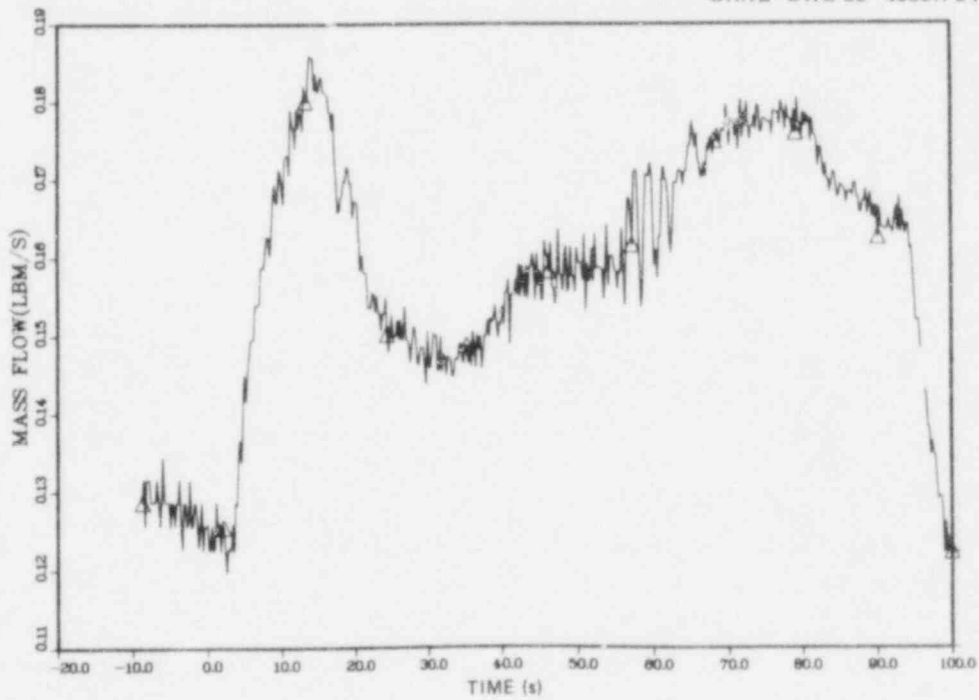


Fig. B.51. Test section outlet mass flow rate for Test 3.09.10W; based on FE-282.

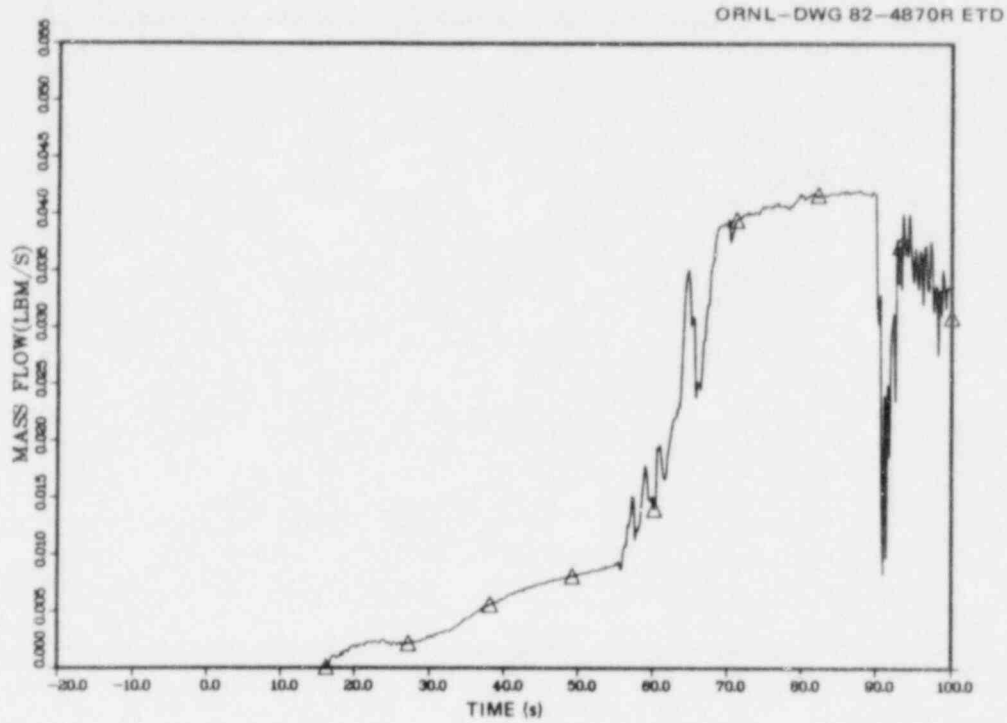


Fig. B.52. Shroud bypass line flow rate for Test 3.09.10W; based on FE-280.

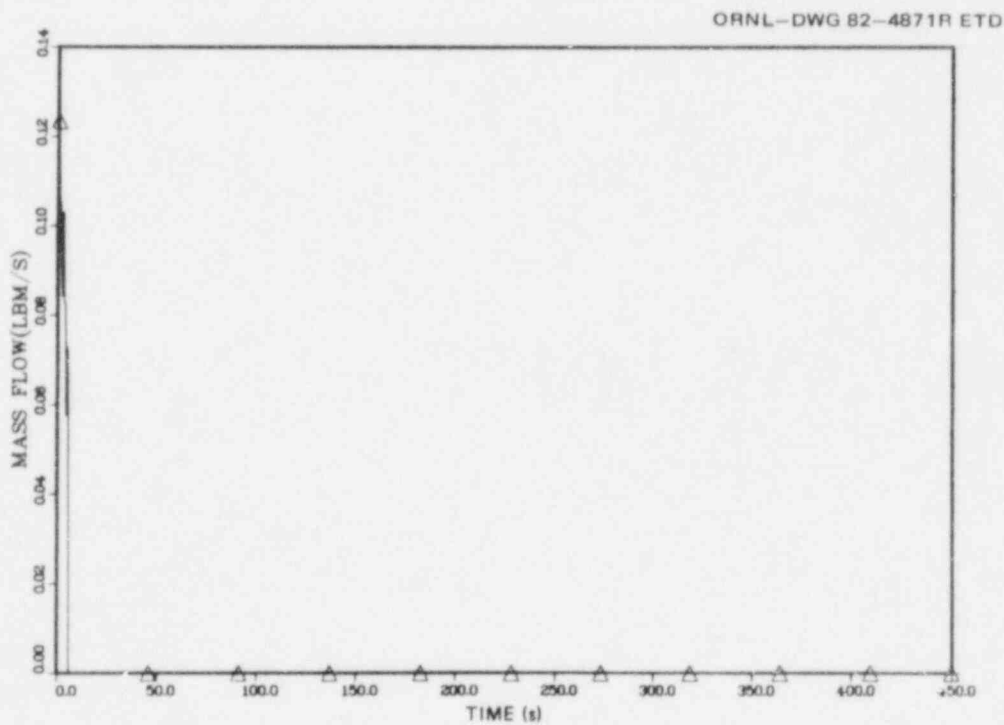


Fig. B.53. Test section outlet mass flow rate for Test 3.09.10X; based on FE-202.

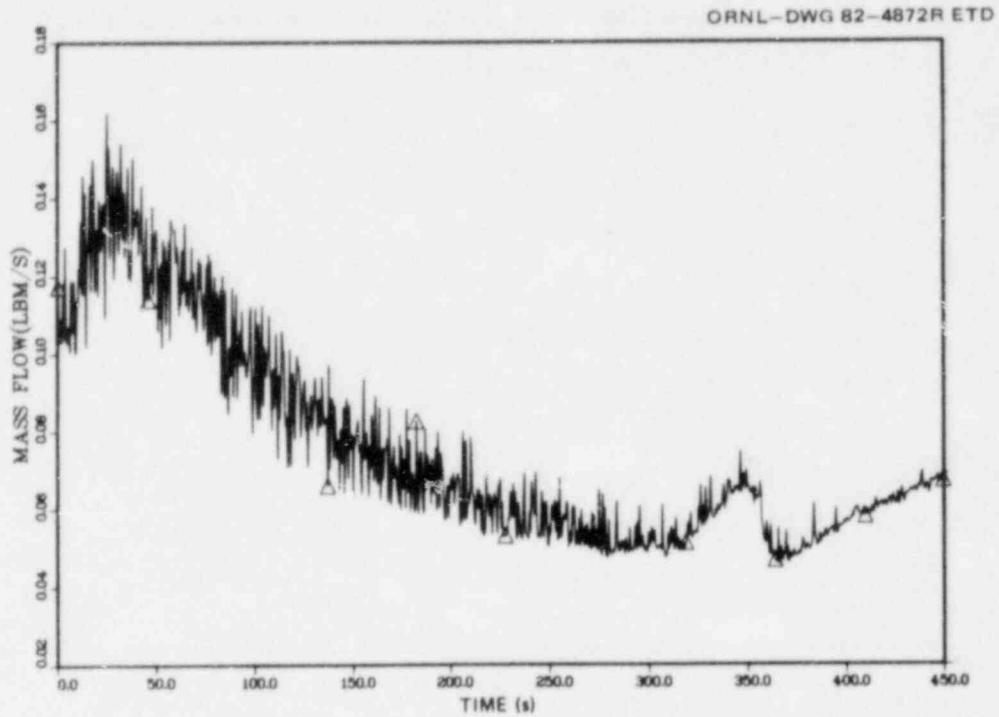


Fig. B.54. Test section outlet mass flow rate for Test 3.09.10X;
based on FE-283.

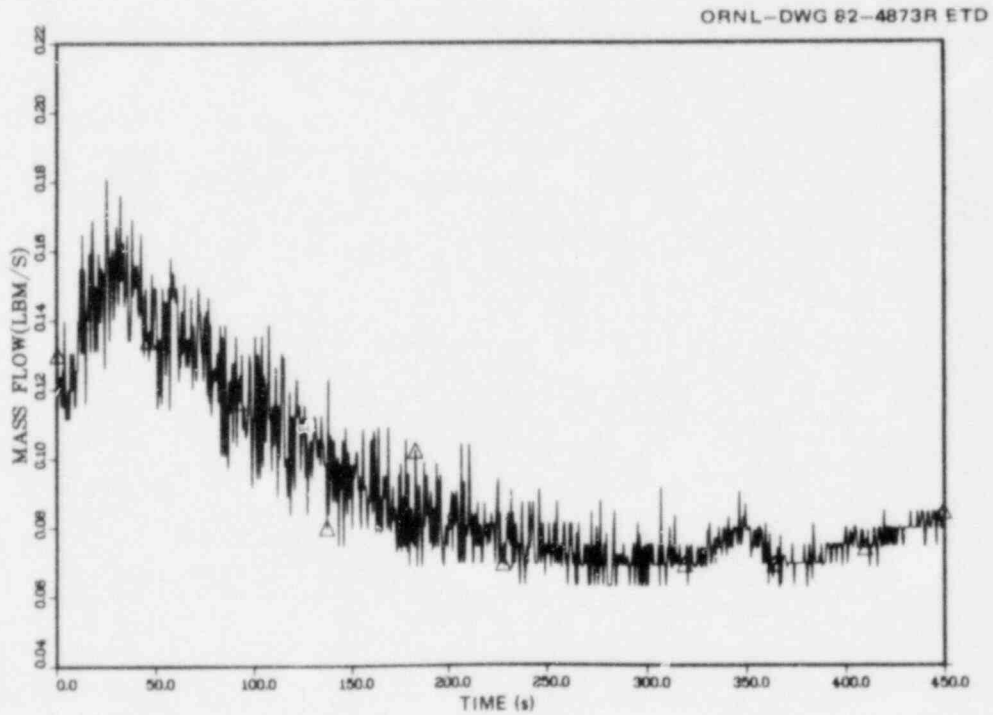


Fig. B.55. Test section outlet mass flow rate for Test 3.09.10X;
based on FE-282.

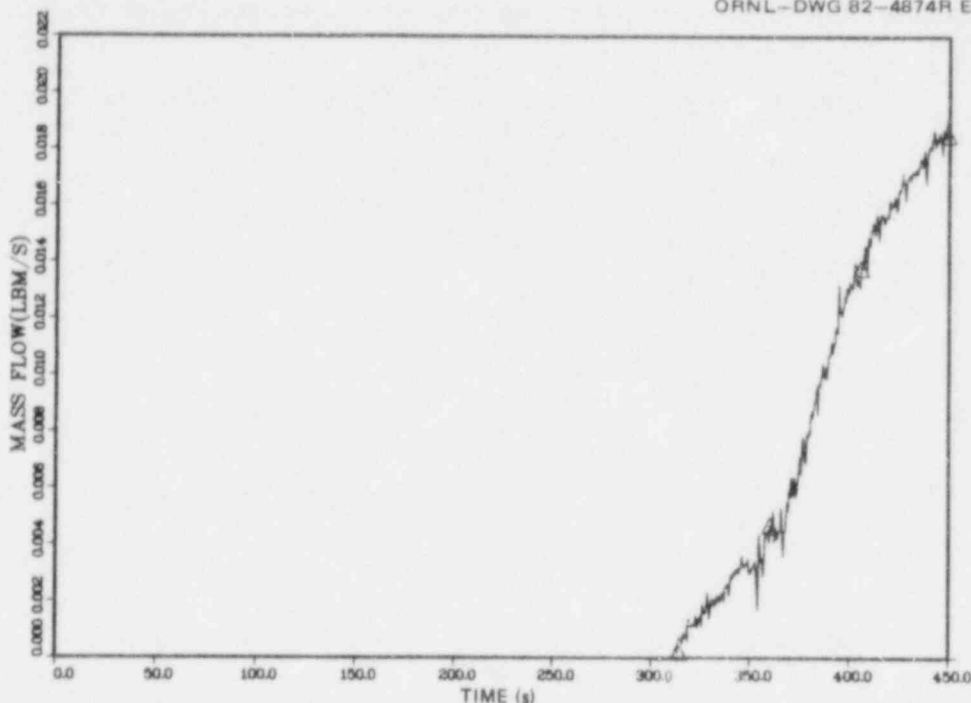


Fig. B.56. Shroud bypass line flow rate for Test 3.09.10X; based on FE-280.

Mass Flow Uncertainties

For the test section inlet, conditions were always subcooled, and the mass flow uncertainty may be estimated by the standard propagation of errors method (Appendix A) using individual instrument uncertainties as stated in Table 27 in the main text.

The variance of the mass flow $V(\dot{m})$ is given by

$$V(\dot{m}) = \sigma_{\dot{m}}^2 = \left(\frac{\partial \dot{m}}{\partial \rho}\right)^2 V(\rho)^2 + \left(\frac{\partial \dot{m}}{\partial Q}\right)^2 V(Q)^2 . \quad (\text{B.2})$$

Expressed in terms of the standard deviation σ of the individual instrument, the equation becomes

$$\sigma_{\dot{m}} = \sqrt{(Q\sigma_{\rho})^2 + (\rho\sigma_Q)^2} , \quad (\text{B.3})$$

where σ_{ρ} = density measurement uncertainty and σ_Q = volumetric flow measurement uncertainty. The density in the calculation of the inlet mass flow rate is based on measured inlet pressure and temperature. A 2σ error band for the density is estimated from water properties assuming 2σ deviations in temperature and pressure from the measured values. This results

in a 2σ density uncertainty estimate of $\pm 4.8 \text{ kg/m}^3$ ($\pm 0.30 \text{ lb}_m/\text{ft}^3$) for the range of inlet temperatures and pressure observed. For the steady-state inlet orifice meter, the 2σ uncertainty is $\pm 4.2 \times 10^{-6} \text{ m}^3/\text{s}$ ($\pm 0.07 \text{ gpm}$). Substituting into E_{ρ} , (B.3), assuming a nominal density of 860 kg/m^3 ($53.7 \text{ lb}_m/\text{ft}^3$) and a range of volumetric flows from $3.1 \times 10^{-5} \text{ m}^3/\text{s}$ (0.5 gpm) to $1.7 \times 10^{-4} \text{ m}^3/\text{s}$ (2.7 gpm), yields a corresponding 2σ mass flow uncertainty of $3.9 \times 10^{-3} \text{ kg/s}$ ($8.6 \times 10^{-3} \text{ lb}_m/\text{s}$).

For the transient reflood tests, the 2-in. inlet turbine meter (FE-3) and the 1/2-in. inlet turbine meter (FE-250) were the primary inlet volumetric flow measurement instruments. (The 1/2-in. inlet turbine meters were also used for some of the uncovered bundle tests.) The 1/2-in. turbine meter was overranged for all of the reflood tests except the early portions of 3.02.10Q. The 2σ steady-state uncertainty bands for both types of turbine meters in subcooled flow is 4.1% of reading. Although the uncertainty band is stated over a range of $1.3 \times 10^{-3} \text{ m}^3/\text{s}$ (22 gpm) to $1.4 \times 10^{-2} \text{ m}^3/\text{s}$ (222 gpm), for the 2-in. turbine meter, the calibration data on the specific turbine meter used extends down to approximately $6.3 \times 10^{-5} \text{ m}^3/\text{s}$ (10 gpm). It is believed that the stated uncertainty bands should still reasonably represent the instrument output at the lower calibrated levels. Measurement of lower initial flow rates occurring as the reflood valve is opened may have significantly higher uncertainties due to bearing friction and rotor inertia effects on the turbine meter. Transient errors are not expected to be significant once the flow rates reach calibrated levels since the transients are comparatively slow.

In order to facilitate the calculation of the mass flow uncertainty for this case, the uncertainty in the deduced density is stated as a percent of reading of the nominal inlet density [860 kg/m^3 ($53.7 \text{ lb}_m/\text{ft}^3$)]. Equation (B.3) expressed in percent of reading results in a 2σ mass flow uncertainty of $\pm 4.14\%$ of reading.

The outlet mass flow is calculated from measured volumetric flows and densities. The volumetric flows are measured by either turbine meters or orifice flowmeters. Densities are determined by either a single-beam gamma densitometer measurement on the outlet spool piece or a temperature- and pressure-deduced density. For all of the steady-state data scans, for most of the transient reflood time periods of interest, and for portions of the boiloff time periods of interest, the outlet flow is superheated steam, and a pressure- and temperature-deduced density is used. An estimate of the uncertainties in the determination of the superheated steam density, assuming a 2σ deviation in temperature and pressure measurements, was made. The results are shown in Table B.1 for the range of temperatures and pressures of interest.

The results of propagating these uncertainties through the mass flow calculation for the turbine meters are shown in Table B.2. The 2σ uncertainty for the 1/2- and 2-in. turbine meters as stated in Table 27 for subcooled conditions is used (4.1% of reading) in the calculation. In an effort to determine the validity of using the subcooled uncertainty estimate for the 2-in. turbine meter, a comparison of inlet and outlet flow rates from a number of steady-state data scans over a range of pressures was made. Scans were chosen where the inlet orifice meter, FE-18A, was in

Table B.1. Superheated steam density uncertainty based on 2σ error in pressure and temperature measurements

Temperature	522 K (480°F)	560 K (550°F)	590 K (600°F)	672 K (750°F)	755 K (900°F)	895 K (1150°F)
Pressure	$2\sigma_p$ (% of reading)					
2.76 MPa (400 psi)	10.1	9.3	9.0	9.9	9.4	9.1
5.5 MPa (800 psi)		6.5	5.9	6.4	5.7	5.2
8.27 MPa (1200 psi)			5.9	5.6	4.9	4.0

Table B.2. Mass flow uncertainty based on superheated steam density 2σ uncertainty and subcooled turbine meter 2σ uncertainty (4.1% reading)

Temperature	522 K (480°F)	560 K (550°F)	590 K (600°F)	672 K (750°F)	755 K (900°F)	895 K (1150°F)
Pressure	$2\sigma_m$ (% of reading)					
2.76 MPa (400 psi)	10.9	10.2	9.9	10.7	10.3	10.0
5.5 MPa (800 psi)		7.7	7.2	7.6	7.0	6.6
8.27 MPa (1200 psi)			7.2	6.9	6.4	5.7

range in order to provide a low uncertainty reference flow [2σ of $\pm 3.0 \times 10^{-3}$ kg/s (8.6×10^{-3} lb_m/h)]. The ratio of the calculated outlet flow to the calculated inlet flow for these scans is shown in Fig. B.57. It should be noted that the mass flows are obtained from the product of the average density and average volumetric flow over the scan interval rather than by averaging the product over the scan interval. Data points which deviate significantly from 1.0 may be the result of an actual imbalance in flow due to energy and mass storage effects in the test section. For a majority of the scans, the inlet and outlet mass flows agree within approximately 7-8%.

Uncertainties in mass flows for the outlet orifice flowmeters are based on uncertainties associated with the flowmeters and on uncertainties in density (Table B.1). Mass flow for an orifice meter is calculated as

$$\dot{m} = C(\rho\Delta P)^{1/2}, \quad (\text{B.4})$$

where C is the calibration coefficient, ρ is the fluid density, and ΔP is the pressure drop across the orifice. Uncertainties for the orifice flowmeters are presented in Table 27 and can be conveniently expressed as percent of full-scale volumetric flow at the calibration density (ρ_{CAL}) of

ORNL-DWG 81-22693 ETD

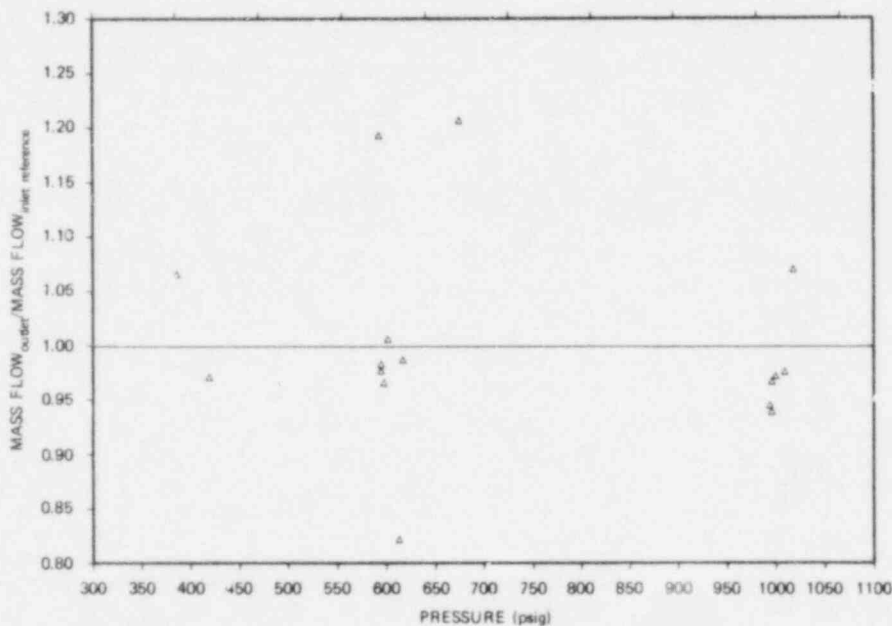


Fig. B.57. Comparison calculated outlet mass flows to reference inlet mass flows.

1000 kg/m³ (62.4 lb_m/ft³). Accordingly, it simplifies matters to rewrite Eq. (B.4) in terms of volumetric flow at the calibration density \dot{Q}_{CAL} ,

$$\dot{m} = \sqrt{\rho \rho_{CAL}} \dot{Q}_{CAL} \quad (B.5)$$

Relative uncertainty in mass can now be written as

$$\frac{\sigma_{\dot{m}}}{\dot{m}} = \sqrt{\left(\frac{\sigma_{\rho}}{2\rho}\right)^2 + \left(\frac{\sigma_{\dot{Q}_{CAL}}}{\dot{Q}_{CAL}}\right)^2} \quad (B.6)$$

As noted, the uncertainty in density is tabulated in Table B.1. The steady-state uncertainty associated with the orifice flowmeters is 2.5% of the full-scale reading. Therefore,

$$\frac{\sigma_{\dot{m}}}{\dot{m}} = \sqrt{\left(\frac{\sigma_{\rho}}{2\rho}\right)^2 + \left[\frac{0.025}{(\dot{Q}_{CAL}/\dot{Q}_{CAL_{FS}})}\right]^2} \quad (B.7)$$

Relative uncertainty in mass flow is tabulated for values of $\dot{Q}_{CAL}/\dot{Q}_{CAL_{FS}}$ of 0.1, 0.25, and 1.0 in Tables B.3, B.4, and B.5, respectively.

Although the test section outlet flow was superheated for the uncovered bundle tests and the time periods of interest for the reflood tests, saturated steam and two-phase flow conditions existed during portions of the boiloff tests. Mass flow uncertainties in two-phase flow may be considerably higher than those expected in single-phase flow. For the outlet turbine meters, the effects of void fraction, flow regime, slip, and rotor inertia on the interpretation of the turbine meter output may be considerable. In addition, the stated 2σ uncertainty for the gamma densitometers [104 kg/m³ (6.5 lb_m/ft³)] is a significant uncertainty for high-quality mass flows. A detailed study of two-phase mass flux uncertainties in THTF instrumented spool pieces is presented in Ref. 2. In-place experimental estimates of mass flow uncertainties from steady-state tests described in Ref. 2 using larger 3.5-in. turbine meters (although geometrically similar) indicate 2σ uncertainties of approximately $\pm 80\%$ for the turbine meter single-beam densitometer mass flow model. Since data are not available for the smaller 2-in. turbine meter used for these tests, this result is the best available two-phase mass flow uncertainty estimate.

Quasi-Steady-State Mass Flow Rates

Table B.6 summarizes the inlet and outlet mass flow rates for each of the 14 quasi-steady-state tests. In all tests except 3.09.10GG and HH,

Table B.3. Estimated 2σ mass flow uncertainty for the orifice flowmeters at 10% of the full-scale range

Temperature	522 K (480°F)	560 K (550°F)	590 K (600°F)	672 K (750°F)	755 K (900°F)	895 K (1150°F)
Pressure	$2\sigma_m$ (% of reading)					
2.76 MPa (400 psi)	13.5	13.3	13.3	13.4	13.4	13.3
5.5 MPa (800 psi)		12.9	12.8	12.9	12.8	12.8
8.27 MPa (1200 psi)			12.8	12.8	12.7	12.7

Table B.4. Estimated 2σ mass flow uncertainty for the orifice flowmeters at 25% of the full-scale range

Temperature	522 K (480°F)	560 K (550°F)	590 K (600°F)	672 K (750°F)	755 K (900°F)	895 K (1150°F)
Pressure	$2\sigma_m$ (% of reading)					
2.76 MPa (400 psi)	7.1	6.8	6.7	7.0	6.9	6.8
5.5 MPa (800 psi)		6.0	5.8	5.9	5.8	5.6
8.27 MPa (1200 psi)			5.8	5.7	5.6	5.4

Table B.5. Estimated 2σ mass flow uncertainty for the orifice flowmeters
at 100% of the full-scale range

Temperature	522 K (480°F)	560 K (550°F)	590 K (600°F)	672 K (750°F)	755 K (900°F)	895 K (1150°F)
Pressure	2σ (% of reading)					
2.76 MPa (400 psi)	5.2	4.8	4.7	5.1	4.9	4.7
5.5 MPa (800 psi)		3.5	3.2	3.4	3.1	2.9
8.27 MPa (1200 psi)			3.2	3.1	2.8	2.4

Table B.6. Quasi-steady-state mass flows for Tests
3.09.10I-N and 3.09.10AA-HH^a

Test	Inlet mass flow [kg/s (lb _m /h)]	Outlet mass flow [kg/s (lb _m /h)]
3.09.10I ^b		0.1840 ± 0.0124 (1460 ± 98)
3.09.10J	0.0799 ± 0.0038 (634 ± 30)	0.0782 ± 0.0054 (621 ± 43)
3.09.10K ^b		0.0193 ± 0.0016 (153 ± 13)
3.09.10L ^b		0.1800 ± 0.0101 (1428 ± 80)
3.09.10M	0.0827 ± 0.0038 (656 ± 30)	0.0781 ± 0.0044 (620 ± 35)
3.09.10N	0.0268 ± 0.0038 (213 ± 31)	0.0285 ± 0.0017 (226 ± 13.4)
3.09.10AA	0.1307 ± 0.0039 (1037 ± 31)	0.1252 ± 0.0104 (994 ± 83)
3.09.10BB	0.0584 ± 0.0039 (463 ± 31)	0.0595 ± 0.0051 (472 ± 40)
3.09.10CC	0.0446 ± 0.0039 (354 ± 31)	0.0311 ± 0.0030 (247 ± 24)
3.09.10DD	0.1225 ± 0.0039 (972 ± 31)	0.1204 ± 0.0085 (956 ± 67)
3.09.10EE	0.0680 ± 0.0039 (540 ± 31)	0.594 ± 0.0041 (472 ± 33)
3.09.10FF	0.0299 ± 0.0040 (237 ± 31)	0.0238 ± 0.0023 (189 ± 18)
3.09.10GG ^{b,c}		0.2010 ± 0.0124 (1595 ± 99)
3.09.10HH ^{b,c}		0.2032 ± 0.0167 (1613 ± 132)

^aNumbers in table have been rounded off. Accordingly, unit conversions may not appear to be exact.

^bAll reliable test section inlet flow instrumentation out of range.

^cMass flows based on saturated vapor density. Conditions at outlet may have been two-phase. Accordingly, mass flows for tests GG and HH should be used with caution.

both test section inlet and outlet instrumentation indicated single-phase conditions. Accordingly, mass flow was calculated from a measured volumetric flow rate and a density derived from measured temperature and pressure. Uncertainty in mass flow was estimated using the methodology described in the previous section. In Tests 3.09.10GG and HH, the test section outlet fluid thermocouple indicated saturated conditions. However, the outlet densitometer did not indicate liquid. As a result, outlet mass flow was based on the saturated vapor density. However, it should be noted that high void fraction dispersed two-phase flow at the test section outlet would not be detected by the densitometer. Thus, caution should be exercised when using mass flows for Tests 3.09.10GG and HH because two-phase conditions may have existed.

References

1. J. W. Teague, II, *AMICON - A Multi-Model Interpretive Code for 2- ϕ Flow Instrumentation with Uncertainty Analysis*, K/CSD/TM-38.
2. N. C. Chen and D. K. Felde, *Two-Phase Mass Flux Uncertainty Analysis for the Thermal Hydraulic Test Facility (THTF) Instrumented Spool Pieces*, ORNL/TM-7859 (to be published).

NUREG/CR-2525, Vol. 4
 ORNL/NUREG/TM-407/V4
 Dist. Category R2

Internal Distribution

- | | | | |
|--------|----------------|--------|-------------------------------|
| 1-5. | T. M. Anklam | 26. | L. J. Ott |
| 6-7. | W. G. Craddick | 27. | T. W. Robinson, Jr. |
| 8. | D. K. Felde | 28. | A. G. Sutton |
| 9. | S. S. Gould | 29. | M. S. Thompson |
| 10. | J. E. Hardy | 30. | H. E. Trammell |
| 11. | H. W. Hoffman | 31. | ORNL Patent Office |
| 12-16. | D. F. Hunt | 32. | Central Research Library |
| 17-19. | C. R. Hyman | 33. | Document Reference Section |
| 20. | A. L. Lotts | 34-35. | Laboratory Records Department |
| 21-25. | C. B. Mullins | 36. | Laboratory Records, RC |

External Distribution

- 37-41. Director, Division of Reactor Safety Research, Nuclear Regulatory Commission, Washington, DC 20555
42. Office of Assistant Manager for Energy Research and Development, Department of Energy, ORO, Oak Ridge, TN 37830
- 43-44. Technical Information Center, Department of Energy, Oak Ridge, TN 37830
- 45-389. Given distribution as shown under category R2 (10-NTIS)